

International PhD program in Cardiovascular  
Pathophysiology and Therapeutics - CardioPaTh

Advantages of 3D Echocardiography over 2D  
Echocardiography in the evaluation of different  
cardiac structures

PhD thesis

Gianpiero Pagnano MD

02/09/1986 Naples (Italy)

# Table of contents

Chapter 1.	General introduction and outline of the thesis	pag. 5
Part I.	Comparison of 2D and 3D Echocardiography in the assessment of different cardiac structures	
Chapter 2.	Definition of the role of 3D Transtoracic echocardiography (TTE) in the evaluation of the diameter of the ascending aorta in comparison with 2D TTE. <b>Pagnano G</b> , Papitsas M, Theodoropoulos K, Papachristidis A, Monaghan MJ <i>Draft</i>	pag. 10
Chapter 3.	Sizing of Wachman device: 2D vs 3D Transesophageal Echocardiography <b>Pagnano G</b> , Eskandari M, Monaghan MJ <i>Draft</i>	pag. 22
Chapter 4.	The impact of vendor-specific ultrasound beam-forming and processing techniques on the visualisation of in-vitro experimental “scar”: implications for myocardial scar imaging using 2D and 3D echocardiography. Papachristidis A, Queirós S, Theodoropoulos KC, D’hoogec J, Rafter P, Masoero G, Zidros S, <b>Pagnano G</b> , Huang M, Dancy L, Sado D, Shah AM, Murgatroyd FD, and Monaghan MJ <i>Under Review - J Am Soc Echocardiogr</i>	pag. 38
Part II.	Echocardiographic and other cardiac findings in COVID-19	

Chapter 5. Right Ventricular-Arterial Uncoupling Independently Predicts Survival in COVID-19 ARDS pag. 78  
D'Alto M, Marra A, Severino S, Salzano A, Romeo E, De Rosa RC, Stagnaro F, **Pagnano G**, Verde R, Murino P, Farro A, Ciccarelli G, Vargas M, Fiorentino G, Servillo G, Gentile I, Corcione A, Cittadini A, Naeije R, Golino P  
*Published in Crit Care 2020 Nov 30;24(1):670.*

Chapter 6. Clinical characteristics and prognosis of hospitalized COVID-19 patients with incident sustained tachyarrhythmias: A multicenter observational study. pag. 97  
Russo V, Di Maio M, Mottola FF, **Pagnano G**, Attena E, Verde N, Di Micco P, Silverio A, Scudiero F, Nunziata L, Fele N, D'Andrea A, Parodi G, Albani S, Scacciatella P, Nigro G, Severino S.  
*Published in Eur J Clin Invest. 2020 Aug 19:e13387.*

### Part III. Unusual echocardiographic findings

Chapter 7. Mitral pseudostenosis due to a large left atrial myxoma. pag.105  
Theodoropoulos KC, Masoero G, **Pagnano G**, Walker N, Papachristidis A, Monaghan MJ.  
*Published in J Geriatr Cardiol. 2018 Mar;15(3):244-245.*

Chapter 8. Unexpected Thrombus in a previously closed left atrial appendage pag.107  
Papitsas M, **Pagnano G**, Monaghan MJ  
*Draft*

Chapter 9. Differential diagnosis of a mass attached to mechanical mitral valve. Papitsas M, **Pagnano G**, Monaghan MJ, Papachristidis A pag.109  
*Submitted*

## Part IV. Discussion and Conclusions

Discussion and Conclusions	pag.112
Bibliography	pag.117
Curriculum Vitae	pag.134
List of publications	pag.136
Acknowledgements	pag.138

## **CHAPTER 1**

### **General introduction and outline of the thesis**

Since its introduction in clinical practice, Echocardiography has been an extremely useful tool for clinicians. In the past few decades Echocardiography went from providing few limited morphological information to full anatomical and functional details of the heart. During the evolution of Echocardiography several important improvements were provided by technical upgrades such as the introduction of B-Mode and Color-Doppler.

One of the latest major innovations is represented by Three-dimensional (3D) echocardiographic imaging. Initially requiring an offline analysis of the 3D datasets acquired during a standard study, nowadays advancements in computer and transducer technologies allow real-time 3D echocardiographic acquisition and analysis of cardiac structures from any spatial point of view.

3D Echocardiography can have different applications:

1. Evaluation of cardiac chamber volumes and masses, avoiding geometric assumptions and allowing a measurement that is closer to gold standards as Magnetic Resonance (MR) (1-6);
2. Assessment of regional left ventricular (LV) and right ventricular (RV) wall motion (7, 8);
3. High definition of the cardiac valves associated with diagnostic images that can also help surgical planning (9);

4. By using 3D color-Doppler it allows volumetric evaluation of regurgitant jets of native and prosthetic valves and also shunts.

3D Echocardiography has been successfully applied to both Transthoracic and Transoesophageal studies. 3D Transthoracic Echocardiography (TTE) can be routinely used to assess LV and RV systolic function and valve anatomy. In particular, 3D TTE echocardiography is a useful tool for the LV assessment allowing a precise definition of the volumes of the LV (10). The limitation of intra-operator variability may be overcome through the definition of standardized parameters for the execution of the echocardiograms (10). 3D Transoesophageal Echocardiography allows to acquire images with higher frame rate with a better definition of the cardiac structures especially cardiac valves. This feature has had great impact in the development of the structural cardiac intervention and has been successfully used during procedures that now are part of the routine structural heart intervention such as Transcatheter Aortic Valve Implantation (TAVI) (11), Mitraclip (12), paravalvular leak closure. 3D Echocardiography is also becoming part of the standard approach to new structural heart intervention that are being developed such as multiple techniques of tricuspid valve repair or mitral valve repair (13, 14). The multiple advantages offered by 3D Transoesophageal Echocardiography supports its use in several clinical applications where previously 2D Echocardiography has been considered the gold standard.

Echocardiography is in general a fast and low-cost method that can offer important information in different disease settings. In the recent pandemic COVID-19 outbreak echocardiography played a pivotal role in characterizing the myocardial involvement in SARS-CoV2 infection. Italy was one of the first European countries to be reached by the SARS-CoV-2 pandemic outbreak starting from the end of February 2020.

SARS-CoV2 virus has a binding domain for ACE receptor expressed on human cells. Alveolar epithelial type II cells represent 83% of all ACE2-expressing cells but ACE2 receptor is present in a variety of human cells including the myocardial and endothelial cells (15). SARS-CoV2 induces lung damage through its cytopathic effect, but it is also able to downregulate ACE2 expression. ACE2 regulates renin-angiotensin system, whose dysfunction results in impaired blood pressure and fluid/electrolyte balance, enhanced airways inflammation and vascular permeability.

The main clinical feature of COVID-19 is a severe interstitial pneumonia that may quickly degenerate in acute respiratory distress syndrome (ARDS) requiring Intensive Care admission. Mortality related to SARS-CoV-2 infection is still debated, however is reported around 2-3% (16). Severity of clinical manifestations of this disease is very variable across the ages, ranging from completely asymptomatic patients to ARDS. Comorbidities including hypertension, diabetes and coronary artery disease also seem to play a role in defining the severity of the onset and progression of the disease. Lung is

the mainly affected organ, however the progression of the disease other organs maybe involved, culminating in a multi-organ failure in the most severe cases. ICU patients have different clinical characteristics from other hospitalized patients.

Myocardial involvement has been suspected due to the finding of increased levels of the high sensitivity cardiac Troponine I that are even higher in non-survivors (16). However, it remains unknown whether the increase Troponine I levels are associated with alteration of imaging findings of myocardial damage. Cardiac characteristics of the COVID-19 disease are currently being evaluated and their impact on mortality is still not completely understood.

This thesis is divided in 3 main parts. The leitmotiv of this research project is the application of 2D and 3D Echocardiography to different disease settings and the comparison between the two techniques in the definition of different cardiac structures. In particular, the first part is focused on the comparison between 3D and 2D echocardiography in the definition of the diameter of the dilatation of the ascending aorta, during the sizing of Watchman device for left atrial appendage closure and in the evaluation of myocardial scar. The second part is focused on the characterization of the Echocardiographic features of COVID-19. Finally, the third part shows few specific cases where the association of 2D and 3D Echocardiography was important for the identification and characterization of peculiar and unusual cardiac masses.



## Part I

### Comparison of 2D and 3D Echocardiography in the assessment of different cardiac structures

## **CHAPTER 2**

### **Definition of the role of 3D Transthoracic Echocardiography (TTE) in the evaluation of the diameter of the ascending aorta in comparison with 2D TTE**

**Gianpiero Pagnano**, Micheal Papitsas, Konstantinos Theodoropoulos,  
Alexandros Papachristidis, Mark Monaghan

#### **Background**

Multiple non-invasive tests can be used to evaluate the diameter of the ascending aorta (17). The most accurate tests are the Computed Tomography (CT) and the Magnetic Resonance (MR) thanks to their capability of acquiring a 3D dataset of the aorta (17). However, CT and MR are not routinely used for the evaluation of the ascending aorta because of the costs, the limited availability, and the exposure to ionizing radiations. The Transthoracic Echocardiogram (TTE) is routinely used for the evaluation of the ascending aorta because is fast, low cost and safe (17). 3D Echocardiography could be a more reliable technique than 2D Echocardiography for the measurement of the aorta, thanks to its ability to acquire 3D datasets of the vessel (18, 19). The role of 3D Echocardiography in the evaluation of the ascending aorta is not yet defined. The aim of the study is to define the role of 3D TTE in the evaluation of the diameter of the

ascending aorta by comparing it with 2D TTE. The study also aims to demonstrate that the 3D TTE can be used routinely for monitoring of patients with dilatation of the ascending aorta.

## **Methods**

### *Inclusion Criteria:*

This is a perspective monocentric study. We enrolled patients with dilatation of the ascending aorta defined in presence, at the 2D standard TTE, of a diameter > 37 mm, in agreement with "American Society of Echocardiography" and "European Association of Cardiovascular Imaging" guidelines (17). Clinical information, including age, sex, comorbidities and reason for performing the Echo was collected for all patients from clinical records.

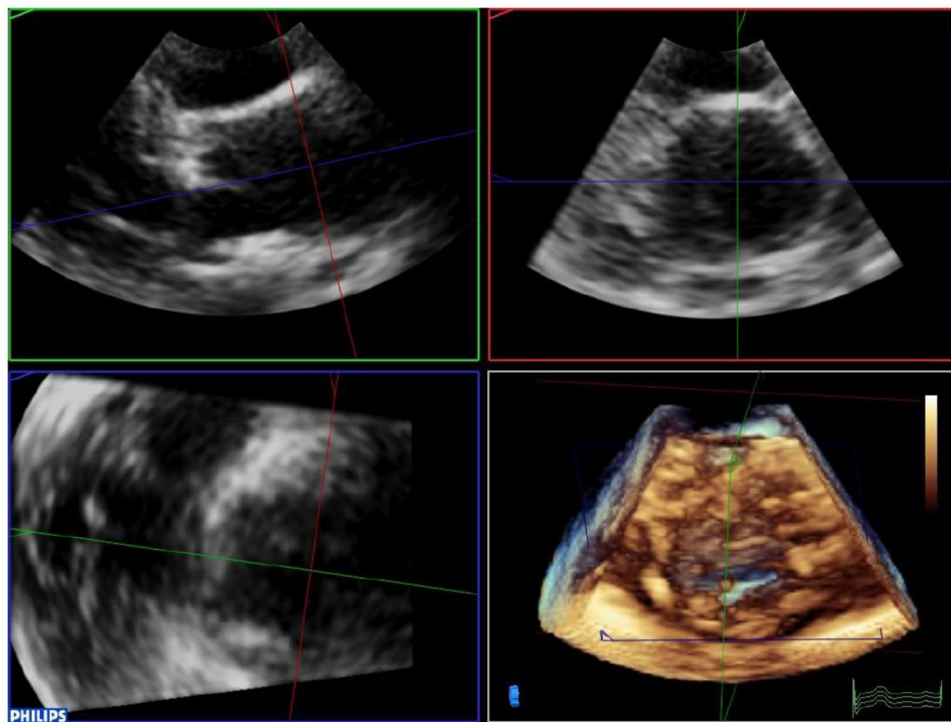
### *Definition of the sample size:*

Sample size was calculated using the statistics program SPSS. A sample size of 24 was calculated based on a standard deviation of the value of the difference between 2D and 3D of 1.49, and effect size of 0.95, an  $\alpha$  error of 0.050 and a  $\beta$  error of 0.20.

### *Study protocol and analysis of the images:*

Patients underwent a standard complete 2D Echocardiography followed by the acquisition of 3D images of the ascending aorta. All the echocardiograms were performed using Vivid E95 (GE) or Epiq 7 (Philips Ultrasound System). The acquisition of the ascending aorta images was performed by expert sonographers. 2D images were acquired in long axis parasternal projection, using standardized protocols to obtain the largest and most accurate visualization of the ascending aorta. 3D datasets were acquired from the parasternal long axis view of the ascending aorta with probes having a frequency between 1 MHz and 4 MHz. Real-time 3D-zoom volume rendered images or Full-volume gated acquisition volume rendered images were used to obtain the highest frame rate. 3D images have been analysed and processed offline (Figure 1) to best visualize the edges of the ascending aorta using EchoPaC (GE healthcare; QLAB Philips Medical Systems). Evaluation of the anteroposterior (AP) diameter of the ascending aorta in the 2D and of the largest diameter in the 3D images was performed by two blind operators. All the evaluations were performed by the 2 blind operators using the same images. The operators performed an offline measurement of the telediastolic diameters of the aorta using the “inner edge to inner edge” technique. This technique was chosen since it is commonly used for the analysis of the multiplanar images (CT and MRI).

Figure 1: Offline analysis of aortic 3D dataset.



### *Statistical analysis*

The measures of the diameters are shown as mean  $\pm$  standard deviation (SD). The means were compared using Paired T Test using the statistical software Graph Pad. Values of  $p < 0.05$  were considered statistically significant. Bland-Altman and scatter plot were used to compare 2D and 3D data and were created using the statistical software GraphPad Prism. In Bland-Altman plot data are expressed as mean  $\pm$  95% confidence interval (CI). Alpha Cronbach coefficient was used to calculate the interobserver agreement and the analysis was performed using the statistical software SPSS. Cronbach's alpha coefficient was interpreted as follows:

Cronbach's alpha	Internal consistency
$\alpha \geq 0.9$	Excellent
$0.9 > \alpha \geq 0.8$	Good
$0.8 > \alpha \geq 0.7$	Acceptable
$0.7 > \alpha \geq 0.6$	Questionable
$0.6 > \alpha \geq 0.5$	Poor
$0.5 > \alpha$	Unacceptable

## Results

### *Demographic features*

Thirty patients in follow up at the Department of non-invasive cardiology at London King's College Hospital were included into the study. Mean age was  $68.1 \pm 11.2$  years. Male to female ratio was 2.7:1 (Table 1).

Table 1. Demographic features and measures of the diameters evaluated with 2D and 3D Echocardiography.

Age (years)	Sex	2D diameter (mm)	3D diameter (mm)
79	M	43	44
65	M	38	39
62	F	43	44
43	F	37	38
61	M	36	37
45	F	46	45
70	F	43	44
70	M	37	40
79	F	40	41
59	M	52	53
77	M	37	41
81	F	51	52
81	M	40	41
57	M	44	46
51	M	40	42
75	M	40	40
81	M	43	43
66	M	41	42
71	F	45	48
85	M	51	53
70	M	41	41
56	M	55	54
66	F	42	42
69	F	43	43
84	M	41	41
64	M	38	40
72	M	45	46
70	F	39	39
56	M	37	38
78	F	46	45

### *Comparison between 2D and 3D diameters*

The mean of the 3D anteroposterior diameters was higher compared to the 2D diameters. Table 2 summarizes mean values of the 2D and 3D diameters, differences between 2D and 3D diameter, confidence intervals, Pearson's and Cronbach's alpha coefficient for the interobserver agreement.

Table 2: Synoptic table of the comparison between 2D and 3D diameters and of the interobserver agreement.

	AP diameter (mm)
3D Ecocardiography	42.47 ± 4.84
2D Ecocardiography	43.4 ± 4.62
Mean of the differences	0.93 ± 1.17
95% CI	-1.36 a 3.23
Pearson's coefficient	0.94
Cronbach's α coefficient 2D	0.98
Cronbach's α coefficient 3D	0.97

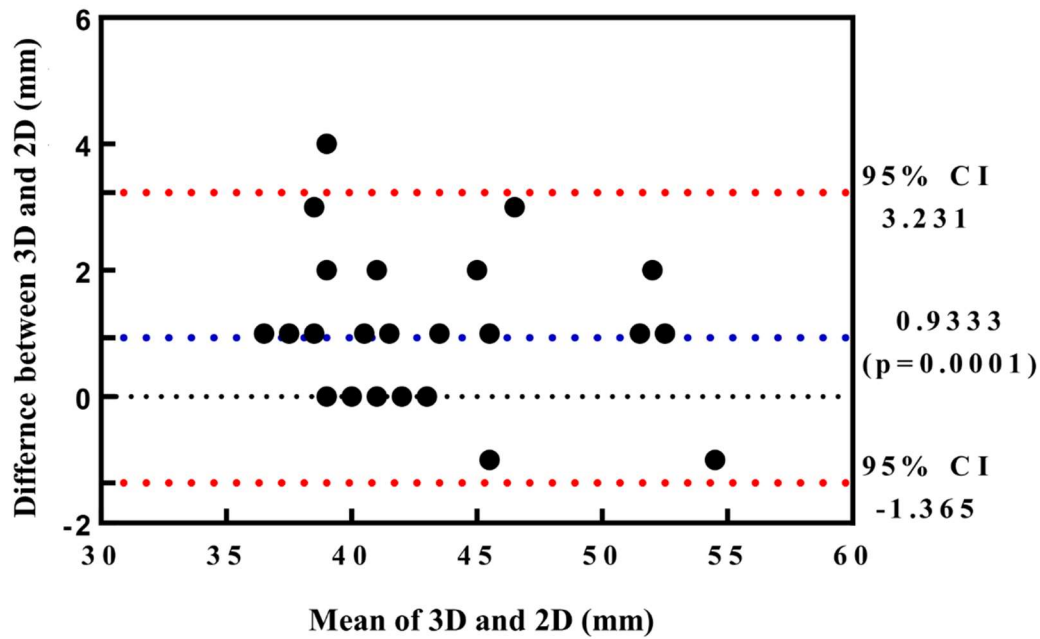
AP, anteroposterior; CI, confidence interval

In particular, the diameters obtained with 3D Echocardiography were  $0.93 \pm 1.17$  mm higher than those obtained with 2D Echocardiography ( $p=0.0001$ ).

Figure 2 shows the Bland-Altman plot comparing the anteroposterior diameters obtained with 2D and 3D Echocardiography. In particular, Bland-Altman plot shows a confidence interval that ranges from -1.36 to 3.23.

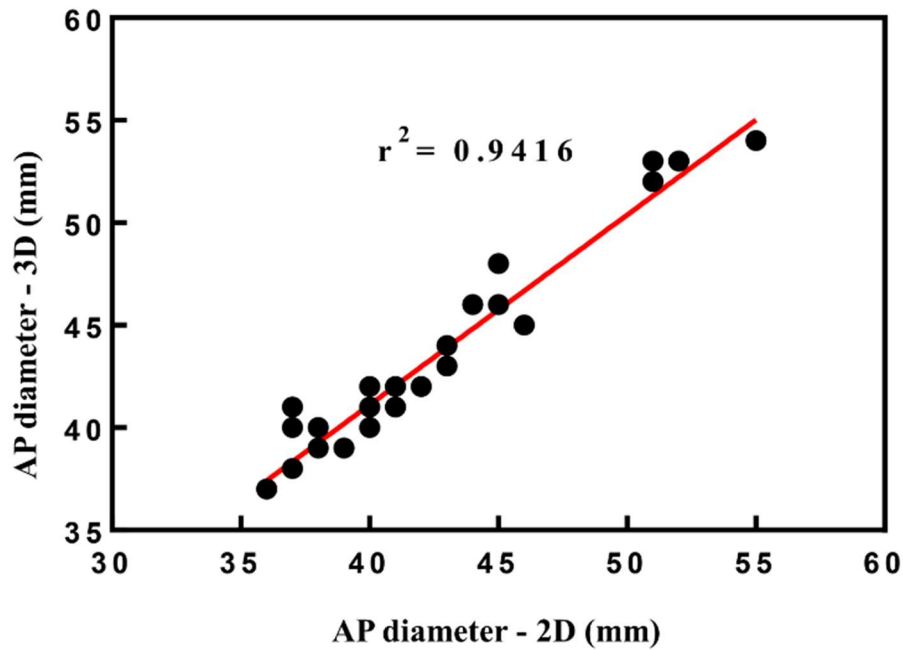


Figure 2: Bland-Altman plot comparing the AP ascending aorta diameters obtained with 2D and 3D Echocardiography.



In figure 3 the scatterplot shows a high degree of correlation between the diameters measured with 3D and 2D Ecocardiography ( $r^2=0.94$ ).

Figure 3: Scatterplot showing the correlation between 2D and 3D diameters.



#### *Interobserver agreement*

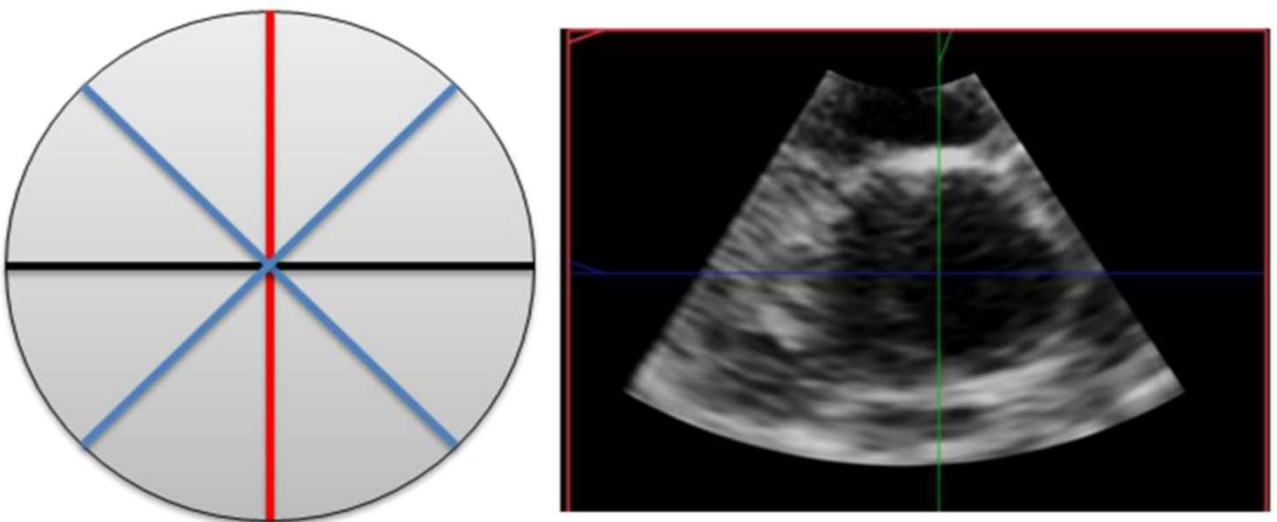
Interobserver agreement was measured for both the 2D and 3D Echocardiography and showed in 21 out of 30 patients, showing an excellent degree of correlation for both the techniques (Cronbach's alpha coefficient 0.98 and 0.96, respectively).

#### *Evaluation of the maximum diameter with 3D Echocardiography*

The evaluation of the maximum 3D diameter of the ascending aorta in transversal section of the 3D datasets was not possible in all the cases since, as shown in figure 3 the measurement of the transversal diameter in the short axis may be affected by the loss of resolution of the edge of the aorta. For

this reason, during the 3D datasets analysis the measurements of the diameters and comparisons between them were performed using the anteroposterior diameter of the ascending aorta (Figure 4).

Figure 4: Left panel shows a schematic representation of the transversal section of the aorta and some of the possible measurable diameters. The right panel shows an example of the transvers section obtained from the analysis of the 3D datasets where there is a loss of the ascending aorta edge resolution corresponding to the latero-lateral diameter.



## Discussion

The present study shows that the AP diameter measured with 3D Echocardiography is higher when compared to the one measured with 2D Echocardiography. The reason for this difference is that, similarly to MR and CT, 3D Echocardiography can offer multiplanar views of the ascending aorta, allowing a better definition of the AP diameter. In particular, this is possible since 3D analysis allows the perpendicular alignment the 3 spatial planes. In the traditional 2D analysis the measurement of the ascending aorta diameter in the long axis parasternal projection may be underestimated since the section used to calculate the diameter may be oblique (19). For this reason, even though currently 3D Echocardiography is not a standardized technique for the evaluation of the diameters of the ascending aorta, it should be performed, when possible, together with the 2D Echocardiography, in order to promptly identify dilatations or aneurisms of the vessel. Moreover, when compared with the other multiplanar techniques, 3D Echocardiography is more largely available, has limited costs, is easy to perform and does not expose the patient to ionizing radiations. Recent evidences suggest that 3D Echocardiography has several advantages compared with 2D in the study of the aortic root, especially in the pre-surgical evaluation of the aortic transcatheter valve replacement (20). However, differently from the evaluation of the aortic root, this study shows how the measurement of the diameter of the ascending aorta in adult patients may be affected by the non-

complete visualization in the short axis of the latero-lateral diameter in some patients. This may also be explained by the conformation of the ascending aorta that can lead to a loss of resolution in the 3D dataset.

As previously shown, the dilatations of the aortic root and of the ascending aorta may be asymmetric (21-23) and thus might be missed when the diameter obtained from the 2D images is not the real maximum diameter of the vessel.

The 3D evaluation is a useful tool in the diagnosis of asymmetric dilatations of the aorta since it allows a better definition of the maximum diameter among those visible in 3D short axis. This feature prevents the underestimation of the diameter that may derive from a complex geometry of the dilatation.

## CHAPTER 3

### **Sizing of Watchman device: 2D vs 3D Transesophageal Echocardiography**

#### **Background**

Atrial fibrillation (AF) is the most common arrhythmia whose incidence is increasing worldwide due to aging of the population and longer survival of patients with chronic heart disease. Other risk factors for AF include smoking habit, sedentary lifestyle, salt intake, excess calorie consumption, and high blood pressure. One of the most serious complication of AF is cardiac embolism (24). Cardioembolic thrombi in non-valvular AF (NVAF) mainly originate from the left atrial appendage (LAA) (25). The standard prophylaxis to reduce stroke risk patients with NVAF is based on the use of oral anticoagulants (OACs). However, the use of OACs may be limited in a substantial number of patients with relative or absolute contraindications to OACs, mainly due to concerns of major bleeding risk and other adverse events while using OACs. LAA closure (LAAC) represents an alternative to reduce the risk of stroke in patients with contraindication to long-term OACs. Exclusion of the LAA for this reason has become part of cardiothoracic procedures such a valvular surgery or MAZE surgery. Watchman device has been demonstrated to be efficacious for transcatheter LAA occlusion (LAAO). Studies have shown that the use of Watchman device is able to reduce the

stroke risk in patients with atrial fibrillation who are not suitable for long-term OACs. The Watchman device consists of three main components: the WATCHMAN LAAC device, the WATCHMAN delivery system, and the WATCHMAN access system and is available in five sizes: 21, 24, 27, 30, and 33 mm. Different imaging modalities can be used for the periprocedural assessment of LAA including magnetic resonance imaging (MRI), computed tomography (CT), and Echocardiography (26, 27). A precise assessment of the LAA morphology is crucial in order to prevent intra-procedural device changes, recapture manoeuvres and to reduce procedure time.

The size of the device is usually predicted using 2D Echocardiography. 3D Echocardiography being a multi-planar technique presents a number of advantages when compared to 2D analysis (28). For example, 3D Echo allows within a single acquisition to obtain all the 4 views (0, 45, 90 and 135 degrees) required to measure the LAA orifice and to predict the device size. Moreover, the measurement of the maximum diameter could be more accurate and less operator dependent, potentially leading to smaller risk of residual leaks after implantation and complications. Residual leaks are frequently encountered following LAAO procedures and their clinical implications and optimal management remain controversial.

This is prospective study to evaluate the efficacy of the 3D vs 2D evaluation of the dimensions of the left atrial appendage before Watchman Device implantation.

## **Methods**

### *Study population*

Patients in follow-up at King's College Hospital Cardiology Department for AF and contraindication to OACs were enrolled into the study after informed consent. A history of major bleeding (e.g. gastrointestinal or intracranial bleeding) was considered as contraindication for OACs. The study was approved by the institution Ethical board. All the patient underwent implantation of a Watchman device. At the time of the enrolment information was collected from the clinical records regarding Age, Sex and past medical history. In particular we collected information regarding cardiovascular risk factors including history of hypertension, Diabetes Mellitus, Hyperlipidemia and smoking habit. Thromboembolic risk was assessed through CHA2DS2-VASc score while bleeding risk was assessed through HAS-BLED score. Only patients with CHA2DS2-VASc  $\geq 2$  were included in the study.

### *Watchman device implantation manufacturer's protocol*

Following the manufacturer indications, watchman device implant procedure consists of several different steps. Before starting the procedure, it is necessary to assess LAA anatomy by measuring the ostium size and determining the shape of the LAA using Transoesophageal Echocardiography. After the femoral venous puncture, the operator needs to cross the interatrial septum and bring the device to the LAA. Then, the correct



device for the patient's LAA size is deployed if all the following criteria are met: device is at the ostium of the LAA, fixation anchors are engaged and the device is stable, the device is compressed by 8-20% of the original size and the device covers completely the ostium and all the lobes of the appendage are covered. All discharged patients were prescribed 100 mg aspirin and warfarin therapy for 45 days. A follow-up Transoesophageal Echocardiogram (TOE) 45 days after the procedure was performed to assess if there is any residual flow through and/or around the WATCHMAN device. Anticoagulation therapy was stopped if there was a peri-device flow  $\leq 5$ mm.

Table 1: Watchman device sizing and after implantation compression range according to manufacturer protocol.

<b>Maximum LAA Ostium</b>	<b>Device Size</b> <i>(uncompressed diameter)</i>	<b>Maximum (20%)</b> Compression Measured Diameter	<b>Minimum (8%)</b> Compression Measured Diameter
17-19 mm	21 mm	16.8 mm	19.3 mm
20-22 mm	24 mm	19.2 mm	22.1 mm
23-25 mm	27 mm	21.6 mm	24.8 mm
26-28 mm	30 mm	24.0 mm	27.6 mm
29-31 mm	33 mm	26.4 mm	30.4 mm

### *Study protocol and analysis of the images:*

Patients enrolled underwent a periprocedural TOE aimed at establishing the device size. To this scope LAA orifice diameter and LAA depth were measured through 2D images acquired at standard 0, 45, 90 and 135 degrees mid-oesophageal views, following manufacturer's protocol for acquisition. In parallel 3D datasets of LAA were acquired to perform a measurement of 3D derived area, perimeter, maximum and minimum diameter and depth of LAA. Different shapes of the LAA appendage were evaluated and divided in 4 categories: 1) Windssock, 2) Broccoli, 3) Chicken Wing, 4) Cactus. After the deployment of the Watchman device compression was calculated both with 2D and 3D measurements and the presence of a residual peri-device leak was evaluated. A TOE was performed 6 weeks after the successful implantation of the device. Device compression, residual leak, and the development of complications at the time of the procedure and after 6 weeks, were evaluated to determine the outcome of the procedure. As per manufacturer indications normal compression of the device in the LAA has been considered between 8 and 20% of the device size. Successful implantation of the device was defined according to the EHRA/EAPCI expert consensus demonstrating the stability of the Watchman device in the LAA after the release and the absence of a significant peri-device leak (29).

## *Statistical analysis*

The measures of the diameters are shown as mean  $\pm$  standard deviation (SD). The means were compared using Paired T Test using the statistical software Graph Pad. Values of  $p < 0.05$  were considered statistically significant. Bland-Altman and scatter plot were used to compare 2D and 3D data and were created using the statistical software GraphPad Prism. In Bland-Altman plot data are expressed as mean  $\pm$  95% CI. Alpha Cronbach coefficient was used to calculate the interobserver agreement and the analysis was performed using the statistical software SPSS.

## **Results**

### *Clinical features*

40 patients were initially selected for the study matching the Echocardiographic criteria. 2 patients were excluded because the procedure was not successful, and 1 patient was excluded because the ostium of LAA could not accommodate the size of the largest device. 37 patients were included into the study. Mean age was  $73.7 \pm 7.6$  years. Male to female ratio was 2.46:1. Mean CHA<sub>2</sub>DS<sub>2</sub>-VASc score was  $3.6 \pm 1.4$ ; HAS-BLED score was  $3.4 \pm 1.0$ . 51.4% of the patients had a previous history of stroke. The most common contraindication for OACs was previous intracranial bleeding, observed in 56.8% of the patients. The most common risk factors were hypertension and hyperlipidemia, observed in 73% and 51.4% of the patients

respectively. Table 2 summarizes the clinical features of the patients enrolled in the study.

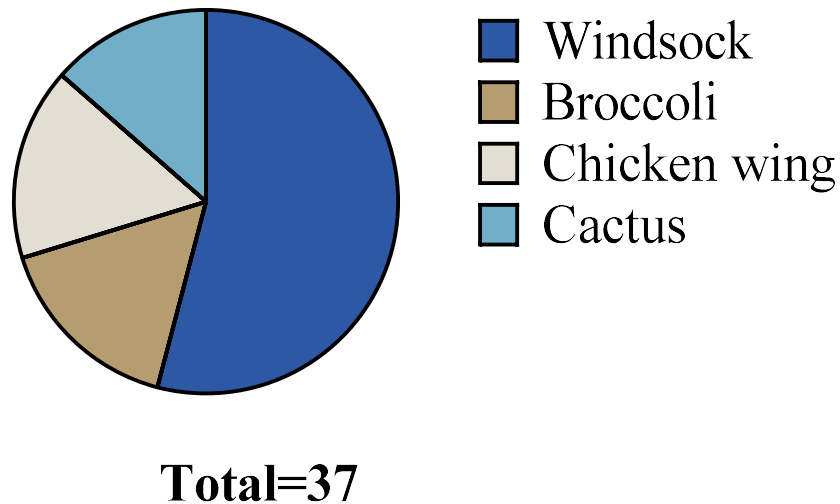
Table 2. Clinical features of the patients enrolled in the study

Clinical feature	
Age (years)	73.7 ± 7.6
M:F	2.46:1
CHA2DS2-VASc score	3.6 ± 1.4
HAS-BLED score	3.4 ± 1.0
Stroke	19 (51.4%)
Gastrointestinal bleeding	8 (21.6%)
Intracranial bleeding	21 (56.8%)
Other serious bleeding	1 (2.7%)
Coronary artery disease	9 (24.3%)
Percutaneous coronary intervention	6 (16.2%)
Previous cardiac surgery	0
Hypertension	27 (73.0%)
Diabetes mellitus	8 (21.6%)
Hyperlipidemia	19 (51.4%)
Smoke	4 (10.8%)
On anticoagulation before procedure	5 (13.5%)

#### *LAA characteristics:*

The most common shape of the LAA observed was windsock in 54% of the patients, followed by broccoli and chicken wing in 16% and cactus in 14% of patients.

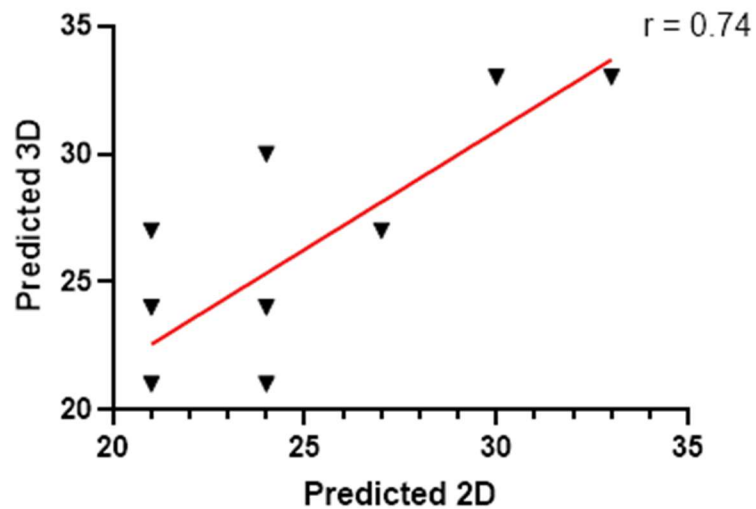
Figure 1. Distribution of the different shapes of the left atrial appendage among the enrolled patients



#### *Comparison of 2D vs 3D measurements*

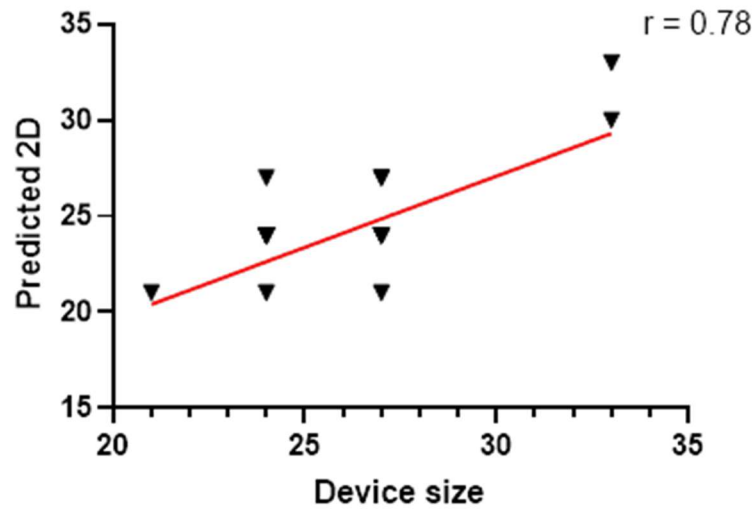
The device size was predicted using 2D and 3D Echo. There was a strong correlation between 2D and 3D predicted Watchman size (Pearson's Correlation coefficient  $r = 0.74$ ) and a moderate inter agreement between the 2 techniques (Weighted Cohen's Kappa = 0.49; 95% CI 0.27 to 0,71) (Figure 2).

Figure 2: Correlation between 2D and 3D predicted measurements.



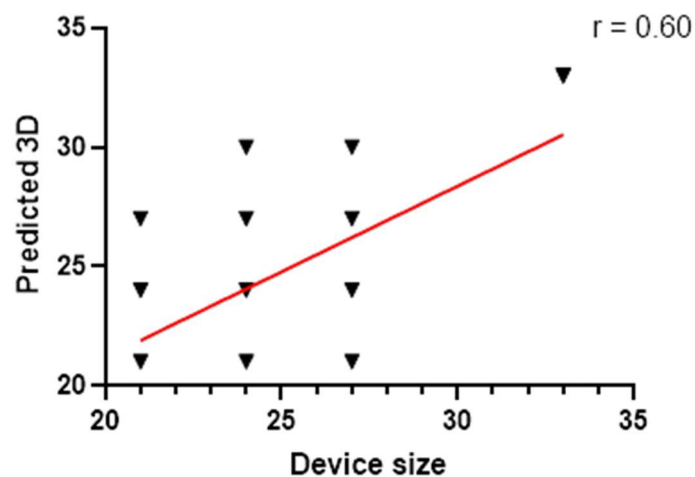
The predicted device size calculated from 2D and 3D echo was then compared with the final device size obtained after multiples evaluations. There was a strong correlation ( $r = 0.77$ ) and a moderate agreement (Weighted Cohen's Kappa = 0.48; 95% CI 0.27 to 0.70) between the 2D measurements and the final size of the device (Figure 3).

Figure 3: Correlation between 2D predicted measurements and final device size.



A moderate correlation ( $r = 0.59$ ) and a fair agreement (Weighted Cohen's Kappa = 0.40; 95% CI 0.14 to 0.65) between the 3D measurements and the final size of the device (Figure 4).

Figure 4: Correlation between 3D predicted measurements and final device size.

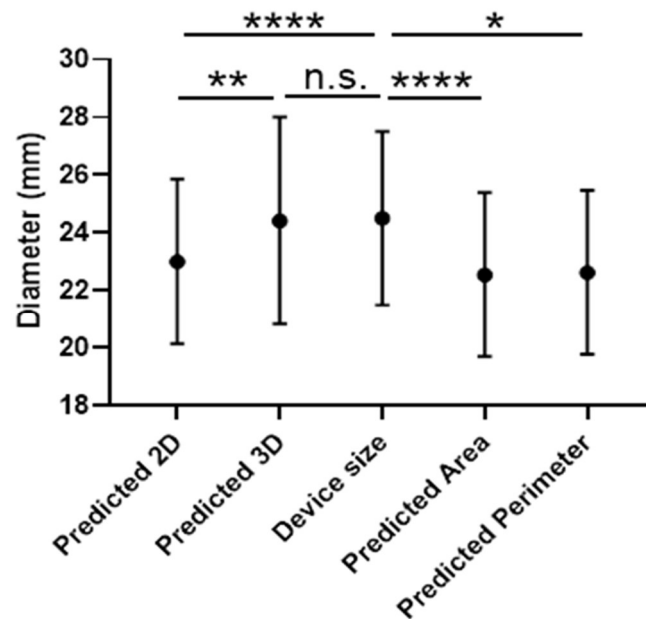


The mean of the 2D predicted device size was significantly lower than the final size of the device ( $23 \pm 2.87$  vs  $24.5 \pm 3.00$ ;  $p < 0.0001$ ) and of the mean of the 3D predicted size ( $23 \pm 2.87$  vs  $24.4 \pm 3.60$ ;  $p = 0.013$ ) (Figure 5). On the contrary, no statically significant difference was observed between the mean of the 3D predicted size and the final size of the device ( $24.4 \pm 3.60$  vs  $24.5 \pm 3.00$ ;  $p = 0.87$ ) (Figure 5). This evidence suggests that 2D Echocardiography systematically underestimates the real diameter of the LAA as confirmed by the fact that in 17 out of 37 cases it was necessary to choose a larger device for the definitive implant. On the contrary the size was underestimated in only 7 cases using 3D measurements, resulting in an higher accuracy in the prediction of the final size of the device for 3D vs 2D even though the difference was not statistically significant (70% vs 54%  $p = 0.23$ ). In 10 cases 3D Echocardiography overestimated the final size of the device.

An average diameter was calculated using 3D derived area and 3D derived perimeter of the LAA orifice. The area and perimeter derived diameters were significantly smaller than the final size with no statistically significant difference from the 2D measurements, leading to the same systematic underestimation of the final size of the device (Figure 5). This may be due to the fact that these measurements are based on the geometrical assumption that the orifice of the LAA is circular.



Figure 5: Mean diameter of the LAA measured with 2D maximum diameter, 3D maximum diameter, 3D area derived diameter and 3D perimeter derived diameter compared with final device size.



### *Outcome of the procedure*

Device compression, residual leak, and the development of complications at the time of the procedure and after 6 weeks, were evaluated to determine the outcome of the procedure. Final device compression was lower than 8% in 5/37 cases. In 2 of these 5 cases this was associated with a residual leak <5 mm. In 2 cases there was evidence of peri-device leak <5 mm post-implant. In 13 cases there a leak <5 mm was detected at the 6 weeks TOE follow-up. We then evaluated if the occurrence of a residual leak was associated with an underestimation of predicted size at the 2D Echocardiography compared with

the 3D Echocardiography. In 6 out of 13 of these patients, the 2D predicted size of the device was lower than the 3D predicted size. Moreover, we evaluated if the overestimation of 3D predicted device size was associated with the presence of a residual leak. In 4 out 10 patients (40%) in whom 3D predicted a larger device size, a <5 mm leak around the device was detected at the 6 weeks post implant TOE. Furthermore, in 1 of these 10 patients the final device compression was suboptimal despite the absence of a detectable leak.

One patient out of 37 had a stroke 69 days after the device implantation and a thrombus was found adjacent to the LAA occluder. In this patient a <5mm leak had been identified during the 6 weeks post-procedure TOE.

Table 3. Short term outcomes and rate of complications after Watchman implantation

Outcomes and complications	Peri-procedural	6 weeks after the procedure
Leak (< 5mm)	2 (5.4%)	13 (35%)
Leak (> 5mm)	0	0
Any complications	5 (13.5%)	-
Effusion	3 (8.1%)	-
Tamponade percutaneous drainage	0	-
Tamponade surgical drainage	1 (2.7%)	-
Embolization	0	1 (2.7%)
Clot	1 (2.7%)	1 (2.7%)
LAA rupture	0	0
Great vessel injury	2 (5.4%)	-
Death	1 (2.7%)	1 (2.7%)*
Hospitalization	1 (2.7%)	1 (2.7%)

\* Died of acute liver failure

We reported 2 death during the study. One patient died after surgical drainage of pericardial tamponade. 1 patient died during follow up for acute liver failure not related to the Watchman implantation.

## **Discussion**

The results of our study confirm our hypothesis that using 3D Echocardiography to assess the LAA characteristics has a better accuracy compared to the 2D measurements preventing the development of residual peri-device leak. This is due to the fact that as previously reported 2D Echocardiography measurements systematically tend to underestimate the final size of the device (30). One of the potential reasons for this, is this that the complex anatomy of the appendage cannot be completely analysed by single plane interrogations as also previously described for the sizing aortic annulus in Transcatheter Aortic Valve Implantation (11). This hypothesis was also confirmed by the fact that the sizing of the device was also underestimated when using a diameter of the LAA orifice calculated from perimeter and area measured from the 3D datasets. In fact, these calculations are based on the assumption that the shape of the LAA orifice is circular. However, this evidence is in contrast with a previous study showing that 3D area-derived diameter and perimeter-derived diameter may help with reducing intraprocedural recapture maneuvers, device size changes, and

peridevice leakage (31). Volumetric data obtained with 3D Echocardiography can overcome this limitation by allowing the measurement of the maximum and minimum diameter. Apart from the individualized anatomy, other factors can contribute to define the complexity of the anatomy of the LAA including different loading conditions and appendage contractile cycle (32-35).

The fact that the correlation and the agreement between the 2D measurement versus the final device size were higher than the one for 3D measurements versus the final device size can be explained by the fact that in case of discrepancies between 2D and 3D, the operators followed the manufacturer guidelines and used the 2D measurements.

The correct sizing is pivotal in order to improve the success rate of the procedure. In fact in this study where the choice of the device was based on the instruction for use of the manufacturer, the underestimation of the 2D compared to the 3D was associated with the development of a leak in 6 out of 13 cases. Moreover, the presence of a <5mm leak in 4 out of 10 cases where 3D overestimated the final device size suggests that in these cases patient could have benefitted from a larger device implantation.

Multi-planar assessment of the LAA could also be achieved by using other imaging techniques such as CT scan. However, the use of 3D Echocardiography offers the advantage of limiting the exposure of patients to ionizing radiations.

The use of a more accurate imaging modality for the sizing also offers other advantages including less need of resizing allowing to reduce the waste of devices and shortening of the procedure time, further reducing the exposure ionizing radiations.

In conclusion this study provides evidence that 3D transesophageal Echocardiography is more accurate than two-dimensional transesophageal Echocardiography in supporting LAA percutaneous closure procedure. Other multi-planar techniques have been shown to give an accurate assessment of LAA shape, however, 3D transesophageal Echocardiography should be preferred since it can provide accurate measurements without requiring exposure to ionizing radiation or contrast administration (26, 27).

## **LIMITATIONS**

Limitation of this study could be the small sample size, the lack of a second cohort where 3D was used as a preferred method to determine the size of the device and determine the outcome of the procedure in these cases. More data is necessary in order to compare all multi-planar modalities with a larger sample size.

## CHAPTER 4

**The impact of vendor-specific ultrasound beam-forming and processing techniques on the visualisation of in-vitro experimental “scar”: implications for myocardial scar imaging using 2D and 3D echocardiography. \***

Alexandros Papachristidis<sup>a</sup>, Sandro Queirós<sup>b</sup>, Konstantinos C. Theodoropoulos<sup>a</sup>, Jan D’hooge<sup>c</sup>, Patrick Rafter<sup>d</sup>, Giovanni Masoero<sup>a</sup>, Spyridon Zidros<sup>a</sup>, Gianpiero Pagnano<sup>a</sup>, Marilou Huang<sup>a</sup>, Luke Dancy<sup>a</sup>, Daniel Sado<sup>a</sup>, Ajay M. Shah<sup>a,e</sup>, Francis D. Murgatroyd<sup>a</sup>, and Mark J. Monaghan<sup>a</sup>.

a) Cardiology Department, King’s College Hospital, SE5 9RS, London, UK.

b) Life and Health Sciences Research Institute (ICVS), School of Medicine, University of Minho, Braga, Portugal; ICVS/3B’s—PT Government Associate Laboratory, Braga/Guimarães, Portugal; and Lab on Cardiovascular Imaging and Dynamics, Department of Cardiovascular Sciences, KU Leuven, Leuven, Belgium.

c) Lab on Cardiovascular Imaging and Dynamics, Department of Cardiovascular Sciences, KU Leuven, Leuven, Belgium.

d) Clinical Scientist, Philips Healthcare, Andover, MA, USA.

e) King’s College London, British Heart Foundation Centre, 125 Coldharbour Lane, London SE5 9NU, UK.

**Corresponding author:**

Dr Alexandros Papachristidis

King's College Hospital.

Denmark Hill, SE5 9RS, London, UK

Tel: +447550013006, Fax: +442032991745

E-mail: alexandros.papachristidis@nhs.net

**\* This article is also part of Dr Alexandros Papachristidis PhD Thesis.**

## **Abstract**

### **Objective**

Myocardial scar appears brighter compared to normal myocardium in echocardiography due to differences in tissue characteristics. We tested how different ultrasound pulse characteristics impact on the brightness contrast (i.e. contrast ratio, CR) between tissues of different acoustic properties, as well as the accuracy of assessing tissue volume.

### **Methods-Results**

An experimental in-vitro “scar” model was created using overheated and raw pieces of commercially available bovine muscle. 2D and 3D ultrasound scanning of the model was performed using combinations of ultrasound pulse characteristics: ultrasound frequency, harmonics, pulse amplitude, power modulation (PM), and pulse inversion modalities.

In both 2D and 3D imaging, the CR between the “scar” and its adjacent tissue was higher when PM was used. PM, as well as steady pulse ultrasound imaging, provided good “scar” volume quantification. When tested on 10 “scars” of different size and shape, PM resulted in lower bias ( $-9.7\text{mm}^3$  vs.  $54.2\text{mm}^3$ ) and narrower limits of agreement (LOA:  $-168.6\text{mm}^3$  -  $149.2\text{mm}^3$  vs.  $-296.0\text{mm}^3$  -  $404.4\text{mm}^3$ ;  $p=0.03$ ). The interobserver variability for



“scar” volume was better with PM (ICC:0.901 vs 0.815). 2D and 3D echocardiography in PM and SP emission modalities was performed on 15 individuals with a myocardial scar secondary to infarction. The CR was higher in PM imaging. Using cardiac magnetic resonance (CMR) as reference, quantification of myocardial scar volume showed better agreement when PM was used (bias:-645mm<sup>3</sup>, LOA:-3,158-1,868mm<sup>3</sup>) as opposed to steady pulse (bias:-1,138mm<sup>3</sup>, LOA:-5,510-3,233mm<sup>3</sup>).

## **Conclusion**

The PM modality increased the CR between tissues with different acoustic properties in an experimental in-vitro “scar” model, while allowing accurate quantification of “scar” volume. By applying the in-vitro findings to humans, PM resulted in higher CR between scarred and healthy myocardium, providing better scar volume quantification than SP compared to CMR.

## **Highlights**

1. Ultrasound imaging can provide accurate volume quantification of scar-like tissue.
2. Power modulation increases the contrast ratio between “scar” and normal tissue.
3. Power modulation provides more accurate scar volume quantification.
4. Power modulation increases the contrast ratio between infarct scar and normal myocardium in humans.
5. A higher contrast ratio improves agreement between modalities and operators.

## **Keywords**

ultrasound beam forming; power modulation; contrast ratio; myocardial scar

## **Abbreviations**

2D: two-dimensional

3D: three-dimensional

AE: Manufacturer specific pre-set (Philips Healthcare, Andover, MA) named “Adult Echo”. CR: Contrast ratio

CMR: Cardiovascular magnetic resonance

LOA: Limits of agreement

LVO: Manufacturer specific pre-set (Philips Healthcare, Andover, MA) named “Left Ventricle Opacification”.

ICC: Intraclass Correlation Coefficient

MI: Mechanical Index

PI: Pulse inversion

PM: Power modulation

SP: Steady pulse

VI: Volume Index

## **1. Introduction**

The presence of myocardial scar in the context of coronary artery disease or other inflammatory or infiltrative diseases is an important prognostic factor, as it has been associated with mortality, arrhythmic burden, and prognosis after myocardial infarction (36-39). The size of the infarcted area has been proven to be a stronger predictor of outcome (death, recurrent myocardial infarction and heart failure) after ST elevation myocardial infarction, compared to left ventricular ejection fraction (LVEF) (36). In addition, the presence and extent of the infarct surface and mass have been shown to better identify the patients who have a substrate for ventricular arrhythmias, when compared to LVEF (37).

Currently, cardiac magnetic resonance (CMR) imaging is the gold standard to diagnose and quantify myocardial scar (36-39). Nevertheless, the role of echocardiography has been investigated since 1978 (40), and more recently published data suggest that echo can be useful in identifying myocardial scar related to a previous myocardial infarction (41, 42). Clinical experience and previous studies have demonstrated that the infarcted myocardium appears brighter on echocardiography compared to adjacent healthy tissue (40-42). In addition, the fibrotic and disarrayed scarred myocardium has a non-linear ultrasound response as opposed to normal myocardium which responds in a more linear fashion (42). Nonlinearity is a

medium property by which the amplitude and shape of an ultrasound signal is not proportional to the input excitation (43). In recent years, there has been a lot of interest in ultrasound non-linear imaging methods which have been reported to provide improved contrast resolution (44-48), hence may have an impact on myocardial scar visualization in echocardiography.

We hypothesized that ultrasound pulse characteristics and beam forming techniques, as available in commercial ultrasound systems, may impact on the contrast ratio (CR) between scarred and normal tissue. Based on previous published data in humans (41, 42), we sought to identify if the power modulation (PM) modality and other pulse characteristics can increase the CR. Our hypothesis was tested on an experimental in-vitro model, using commercially available ultrasound equipment, and the results were extrapolated and selectively tested in humans.

## **2. Methods**

### *2. 1 Experimental in-vitro model*

#### *2.1.1 Scar Model*

An in-vitro experimental model was created to allow prolonged ultrasound scanning with several combinations of pulse characteristics and techniques. An in-vitro model was considered necessary for testing a very large number of variables that could be narrowed down for studies in

humans. For that purpose, a rectangular cuboid piece of commercially available bovine muscle was overheated in a conventional oven. This served as a tissue of high acoustic impedance and it is described as “scar” in the manuscript. A larger piece of commercially available raw bovine muscle was used to accommodate the “scar”. An incision was performed in the middle of the raw muscle, where the “scar” was embedded to form the model. The “scar” is expected to have different acoustic properties from the raw muscle due to moisture loss and histopathological changes in the tissue, such as unfolding and aggregation of proteins, associated with heating (49). These changes are expected to result in different interaction with the ultrasound waves compared to the normal architecture of the raw muscle fibers. Our model was designed to mimic human tissues of different acoustic impedance and in particular the disarrayed scarred tissue after myocardial infarction, where myo-fibers have been replaced by collagen (50).

The “scar” dimensions were measured with an accurate digital calliper, before being inserted in the raw muscle, and the volume was calculated as 6,500mm<sup>3</sup>. The dimensions of the raw muscle were 7 x 10 x 15 cm approximately. To allow ultrasound imaging, the model was immersed in a water tank, which was lined with a towel to reduce reverberation artefacts. The water was left in the tank for more than 16 hours, before scanning, to allow degassing. The tip of an ultrasound transducer was immersed a couple of millimetres into the water to allow good transmission of the ultrasound

waves. The distance between the transducer tip and the surface of the model was approximately 2 cm, whereas the distance between the transducer and the “scar” was 5 cm. No special consideration was taken to keep the ultrasound beam vertical (at 90 degrees) to the long axis of the “scar”, hence the intercept angle was roughly around 80 degrees.

### *2.1.2 Image acquisition*

Two and three-dimensional images were acquired using a Philips Epiq 7 ultrasound system with an X5-1 x-MATRIX array transducer (Philips Healthcare, Andover, MA). The depth of the image was adjusted to 9-10 cm to allow good visualization of the “scar” and the focus was placed at the level of the “scar”. The total gain was adjusted by the operator as necessary, ranging from 65% to 95%, with lower gain at high mechanical indices (MI) and higher gain at lower MI to compensate for signal attenuation. The pre-processing transmitting and receiving techniques that were tested were the following:

- Frequency of the emitted ultrasound pulse (fundamental mode)
- Harmonic frequencies
- Pulse inversion (PI) technique
- Power modulation modality

The frequency information that we deliver in this study represents the central frequency of the bandwidth and has been provided by the relevant vendor.

Two manufacturer-specific pre-sets were used. One is referred by the manufacturer as “Non-contrast” pre-set, implementing either “steady pulse sequence (SP)” or PI technique, and is named “Adult Echo” (AE). The other pre-set, referred as “Contrast” pre-set, is utilizing either PM modality or PI technique, and is named “Left Ventricular Opacification” (LVO). We have taken the liberty to use the term “steady pulse sequence” to describe the default ultrasound beam modality, where all pulses of the emitted ultrasound beam are identical to each other. This is the default and most-commonly used pre-set in all ultrasound machines. In PM a full-amplitude pulse is alternating with a half-amplitude pulse and in PI modality the pulses are of alternating polarity (i.e. every other pulse has inverted waveform). The dynamic range of the images and the compression was at the default setting for all image acquisitions. In total, 12 combinations of different ultrasound characteristics and techniques were used in 2D imaging (Table 1) and 8 in 3D imaging (Table 2). These combinations were tested over several MI’s (51), resulting in 138 2D images and 95 3D data sets.

### *2.1.3. Image Analysis*



The 2D images were converted to an appropriate externally readable 8-bit format (.srd format) and were processed with a custom non-commercial software, named “SPEQLE 3D” (Software Package for Echocardiographic Quantification LEuven), developed at the University of Leuven and customised (by S.Q.) for the needs of the study (52). The area of the “scar” was traced manually along with an adjacent area of normal tissue (Figure 1). The average videointensity of each area was provided by the application and the CR of the “scar” and normal tissue was calculated, based on the following formula (41):

$$CR = \frac{\text{Mean "Scar" Videointensity} - \text{Mean Muscle Videointensity}}{256} \times 100$$

where 256 is the dynamic range of the image, i.e. 256 grey scale levels, implying that CR values are ranging between -100 and 100%. All images were acquired above noise floor and not above saturation level, which allows the application of 256 as the dynamic range.

The 3D datasets were converted to an appropriate externally readable format (.srd format) and were processed with a non-commercial software, named MITK Workbench 2016.3.0 (ITK 4.7.1 VTK 6.2.0 Qt 5.4.2), developed by the Division of Medical and Biological Informatics of the German Cancer Research Center (DKFZ; Heidelberg, Germany) (53). Using multiplanar reconstruction (MPR), the “scar” area was traced in transverse (short axis)

slices and a three-dimensional model of the “scar” was then produced with 3D interpolation (Figure 1). An adjacent volume of normal tissue was also manually traced. The CR was calculated as above. The volume of the “scar” was calculated by the application and the “Volume Index” (VI) was then derived based on the following formula, to express the relationship between the measured ultrasound and the actual “scar” volume:

$$VI = \frac{\text{Ultrasound "scar" volume}}{\text{Actual "scar" volume}}$$

#### *2.1.4 Accuracy and reproducibility analysis*

To test the effect of the CR on “scar” volume quantification, 10 new “scars” of different shape and size were created using the same method (overheated commercially available bovine muscle embedded in the previous raw muscle). These model “scars” were smaller in size compared to the initial one and their volume was measured using a volumetric cylinder filled with water. The smallest “scar” volume was 2,000mm<sup>3</sup>, and the largest 4,500mm<sup>3</sup> (average: 3,300 ± 857 mm<sup>3</sup>) (Appendix, Figure A1). The 10 model “scars” were scanned using two different combinations (modalities) of the aforementioned pulse characteristics (AE pre-set for SP and LVO pre-set for PM), which had provided good volumetric quantification, but different CR of the initial “scar” (44.81% vs 52.82%). Again, no special consideration was

taken to keep the ultrasound beam vertical (at 90 degrees) to the long axis of the “scar”, hence the intercept angle was randomly ranging between 70-90 degrees. The volumes derived by the two modalities were compared to the actual “scar” volumes using the Bland-Altman method (54), and the bias and limits of agreement were calculated. The variability of differences was assessed with a two-tailed F-test. P value < 0.05 was considered statistically significant. To test the interobserver variability, the 10 “scars” were traced by a second operator, who was blinded to the initial tracings. The agreement between operators was compared with the intra-class correlation coefficient (ICC) for single measures in a two-way mixed model, using SPSS version 20.0.0 (IBM, Somers, NY).

## *2.2 Application of findings in humans*

Following the in-vitro experimental model, we prospectively recruited fifteen individuals with a history of a clinically documented myocardial infarction (55) more than 2 months old, who had undergone an invasive coronary angiography and CMR imaging, as clinically indicated. Following the CMR scan, a transthoracic echocardiogram was performed within 0 to 33 days (median 12 days) according to the protocol described below. The study was reviewed and approved by the West of Scotland Research Ethics Committee 4 (REC reference number: 15/WS/0186).

### *2.2.1 Cardiovascular Magnetic Resonance Imaging*

The CMR was performed with a 1.5-T magnet (Siemens® Aera with the “Body 18” coil, 18-channel design with 18 integrated preamplifiers and the Siemens® Avanto with the “Body Matrix Coil”, 6-element design with 6 integrated preamplifiers, Siemens Healthcare Limited, Surrey, UK). The full scanning protocol is described in detail in the Appendix.

The CMR images were post processed with the “cmr42” software (Figure 2) [v. 5.5.1 (559), Circle Cardiovascular Imaging Inc., Alberta, Canada]. Using the “Tissue Characterization” application and applying the “full width at half maximum” method (56), the enhanced myocardium was identified and traced automatically in all short axis slices. The contours were adjusted manually by the operator according to their discretion. The total scar volume was calculated by the application. The operator who performed the CMR image analyses had an experience of more than 200 CMR reports and was Level 2 CMR accredited physician (K.C.T.).

### *2.2.2. 2D and 3D Echocardiography*

Given that it was technically impossible to test on a single individual all ultrasound parameters that were studied in the in-vitro model, two different modalities which had provided high contrast ratio and good “scar” volume quantification were selectively tested: a) Steady Pulse (“Adult Echo” pre-set) at fundamental imaging (2.2MHz), and b) Power Modulation (“Contrast LVO” pre-set) at second harmonic (1.3/2.6MHz). All echocardiograms were

performed with a Philips Epiq 7 ultrasound machine and an X5-1 xMATRIX array transducer (Philips Healthcare, Andover, MA) as in the in-vitro study. 2D and 3D data sets were acquired at several MI's, ranging from 0.1 to 1.0 with increments of 0.1. Given that the PM modality has been developed in clinical ultrasound to enhance the signal of intravenous contrast agents and suppress the myocardial signal, we aimed to explore whether the non-linear signal from the scar would be affected by the presence of microbubbles. Hence, with power modulation the images were obtained with and without use of intravenous ultrasound contrast agent (SonoVue sulphur hexafluoride microbubbles, Bracco UK Ltd, Buckinghamshire, UK). The contrast agent was administered with a continuous infusion rate of 1ml/min. The acquisition protocol is described in the Appendix. Overall, 26 2D images and 26 3D data sets were acquired on each patient (10 images/data sets with SP technique, 8 with unenhanced and 8 with contrast-enhanced PM modality at incremental MI's).

The 2D and 3D datasets were converted to an appropriate format and processed with the same custom non-commercial software as the in-vitro data sets (section 2.1.3). The scarred area was manually traced (Figure 2) as was an adjacent area and the CR and the VI were calculated as described in section 2.1.3. The operator who performed the echocardiograms and the echocardiography analyses (A.P.) had an experience of more than 400 3D echo LV analyses.

A second operator (K.C.T.) traced fully manually the myocardial scar in 3D echocardiograms of 10 randomly selected patients in both SP and PM modalities. The operator was blind to first operator's tracings and to his own CMR tracings. The time window between the echocardiography and CMR image analysis was more than 2 months.

Descriptive statistics are presented as mean values plus-minus standard deviation. The agreement between echocardiography and CMR in scar volume quantification was tested with the Bland – Altman method (54) for each one of the 26 combinations of ultrasound pulse characteristics in 3D echocardiography. The interobserver variability between operators was tested with the ICC for absolute agreement in a two-way mixed model, using SPSS, version 20.0.0.1 (IBM Somers, NY).

### **3. Results**

#### *3.1. In-Vitro model*

##### *3.1.1. 2D Imaging*

Initially, we tested the SP technique (AE pre-set) in fundamental frequencies (Figure 3). Lower frequency (2.2MHz) provided consistently higher CR. The same trend was observed using harmonics with the lower-range frequency (1.3/2.6MHz) providing higher CR (Figure 3).

Subsequently, we examined whether PI (AE pre-set) impacts on the CR compared to SP. At low frequency (1.3/2.6MHz), PI results in lower CR for all power outputs (Figure 4). At mid- and high-range frequencies (1.6/3.2MHz and 1.9/3.8MHz), PI results in higher CR at higher power output ( $MI > 0.6$ ) (Figure 4).

The PM modality (LVO pre-set), operating at the low harmonic frequency 1.3/2.6MHz, resulted in the highest CR between all tested modalities (Figures 5 and 6), going well above 50% for  $MI > 0.6$ . The PI modality (in the LVO pre-set) is available by the manufacturer only at mid-range harmonic frequency (1.6/3.2MHz) and it was found to improve the CR compared to PM at the same frequency (Figure 5).

### *3.1.2. 3D Imaging*

We initially explored the SP mode. As in 2D imaging, a lower frequency resulted in higher CR, both in fundamentals and harmonics, apart from very low MI (0.1-0.2) in fundamentals (Figure 7).

The power modulation modality in 3D imaging provided the highest CR compared to all tested parameters, as in 2D images, with a significant drop in CR with decreasing MI (Figure 8 and Appendix Figure A2). Lower frequencies resulted in higher CR (Figure 8).

### 3.1.3. *In-vitro* “Scar” volume quantification

The VI was plotted versus MI for all tested combinations of ultrasound pulse characteristics. SP provides more constant “scar” volume quantification with VI’s close to 1.0 at a wide range of MI’s (Figure 9, left), whereas PM resulted in significant signal drop in lower MI’s, leading to volume underestimation (Figure 9, right; Appendix Figure A3). With SP, many combinations provided good volume quantification of the “scar”, but using PM, it was only the lower harmonic frequency (1.3/2.6MHz) that provided a VI close to 1.0 at mid-range MI (0.6 – 1.0).

Based on the above results, two combinations of ultrasound pulse characteristics, i.e. one with SP emission (AE pre-set, fundamental frequency 2.2MHz at intermediate MI – 0.6) and one with PM (LVO pre-set, harmonics 1.3/2.6MHz at high MI – 1.0), which had provided good “scar” volume quantification and high, but different CR, were selected to scan the 10 experimental in-vitro “scars”. Bias was lower ( $-9.7\text{mm}^3$  vs  $54.2\text{mm}^3$ ) and limits of agreement (LOA) were narrower with PM modality, which had a higher CR, compared to SP (LOA:  $-168.6\text{mm}^3$  to  $149.2\text{mm}^3$  vs.  $-296.0\text{mm}^3$  to  $404.4\text{mm}^3$ ,  $p=0.03$ ) (Appendix – Figure A4). The interobserver variability between two independent operators was also better with PM (ICC: 0.901; 95% CI: 0.651-0.975 vs 0.815, 95% CI: 0.408-0.951). The mean coefficient of variation was 0.04 for the PM data sets and 0.09 for the SP data sets.



### *3.2. Results in humans*

All fifteen patients' echocardiograms were included in the analysis. Baseline characteristics are shown in Table 3. The mean age of our population was  $67 \pm 16$  years and 80% were male. The median time from myocardial infarction to CMR scan was 2,278 days, ranging from 77 days to 29 years. All patients were in sinus rhythm, except one who was in atrial fibrillation at the time of both CMR and echocardiography scans.

#### *3.2.1. 2D echocardiography*

In 2D echocardiography, PM with no contrast enhancement provided the highest CR at mid and high range of MI's, followed by the contrast-enhanced Power Modulation (PM-CE) and the SP (Figure 10). As in the in-vitro model, there was a gradual drop in CR at lower MI's.

#### *3.2.2. 3D echocardiography*

In 3D data sets, the same pattern of CR was observed between modalities (Figure 11, left), with PM providing higher CR at mid-range MI, followed by the PM-CE and the SP. The SP provided higher CR compared to unenhanced and enhanced PM at MI's lower than 0.5. The CR in SP and PM versus MI follows the same pattern as in the in-vitro imaging.

SP provided good scar volume quantification in the whole range of MI's (VI ranging from 0.92 to 0.97) (Figure 11, right). PM provided VI between 0.92 and 0.98 at MI 0.5-0.8, but the calculated VI dropped significantly at lower MI's similarly to the in-vitro model. PM-CE provided consistently lower volumes compared to the other two modalities, with the highest VI observed at MI 0.7 and 0.8, and a significant drop in lower MI's. Comparing the absolute scar volumes between CMR and echocardiography with the Bland-Altman method, the PM modality showed best agreement with CMR at MI 0.8 (bias:  $-645\text{mm}^3$ , LOA:  $-3,158$  to  $1,868\text{ mm}^3$ ) (Appendix Figure A5). The SP had best agreement with CMR at MI 0.8 (bias:  $-1,138\text{mm}^3$ , LOA:  $-5,510$  to  $3,233\text{ mm}^3$ ) and the PM-CE at MI 0.8 (bias:  $-2,472\text{mm}^3$ , LOA:  $-7,786$  to  $2,842\text{mm}^3$ ) (Appendix Figure A5). The bias was higher and LOA wider in lower MI, for all modalities.

### 3.3.3. *Interobserver variability*

Both SP and PM provided good scar volume quantification compared to CMR. However, PM results in higher CR, which allows better delineation of scar borders (Figure 12). A second operator (K. C. T.), with an experience of more than 100 3D LV data set analyses, traced the SP and PM 3D data sets of ten randomly selected cases. The agreement between the two operators was tested with the ICC and was higher for the PM data sets (0.967, 95% CI: 0.882-0.992) compared to SP (0.832, 95% CI: 0.467-0.955).

## 4. Discussion

The main findings of our study are: a) in an in-vitro experimental model, three-dimensional ultrasound imaging can provide accurate volume quantification of a disarrayed tissue with acoustic properties different to that of the surrounding normal tissue; b) the power modulation modality resulted in higher contrast ratio between “scarred” and normal tissue in 2D and 3D ultrasound imaging, c) lower frequencies seem better to distinguish scarred from normal tissue, d) when tested in humans, power modulation modality provided higher contrast ratio between myocardial scar and healthy myocardium similarly to in-vitro testing, e) the addition of intravenous ultrasound contrast agent reduced the contrast ratio in power modulation echocardiography, f) 3D echocardiography provided volume quantification of myocardial infarct scar with good agreement to CMR, g) a higher contrast ratio facilitated delineation of myocardial scar and improved agreement between imaging modalities and between operators.

A constant observation in our study is that lower frequencies result in higher CR in both 2D and 3D echocardiography. This observation may be attributable to the fact that frequency dependency of the scattering process may be different between scar and non-scar tissue. That means that in lower frequencies, the difference in scattering process between the two tissues may

be larger, resulting in higher contrast ratio. However, this is just an assumption.

In both two-dimensional and three-dimensional ultrasound imaging, PM provided the highest CR. This is consistent in both in vitro and in vivo testing. PM has been developed for contrast echocardiography (57-60) and is based on the principle that the tissue and the contrast micro-bubbles have a different acoustic response to ultrasound waves. Tissue demonstrates a linear behaviour whereas the micro-bubbles a non-linear response at several energy levels (57). By using multiple transmitted pulses of different amplitude (e.g. the second pulse amplitude is half of first's, etc.), the reflected echo waves from the tissue are of full and half amplitude in alternate fashion (i.e. full, half, full, half, etc.). Every second pulse is scaled (multiplied by 2) and subtracted from the previous one resulting in zero signal. On the contrary, the non-linear reflection from bubbles is producing pulses which differ significantly in amplitude and shape, therefore by scaling and subtracting every other pulse the signal will not be cancelled out allowing micro-bubble detection.

The matured myocardial infarct tissue is consisted of disarranged type I and III collagen fibers, myofibroblasts and pigmented mononuclear cells (50, 61) and the scar's response to ultrasound is non-linear, similar to micro-bubbles. Therefore, with a pulse cancellation technique it is possible to

suppress the linear signal from the normal myocardium by scaling and subtracting the backscattered ultrasound waves as described above. On the other hand, the non-linear signal from the scarred tissue can be enhanced similarly to the microbubbles signal. In our study the PM provided higher CR and better VI in high MI, though this technique has been developed to produce higher CR at low MI when used with intravenous contrast agents. This discrepancy can be attributed to the physical differences between the solid scar tissue and the gas microbubbles as the latter implode at high MI's, whereas the tissue needs a higher amount of delivered energy to resonate as shown in our study where the backscattered signal was significantly attenuated at low MI.

Another multi-pulse technique that we tested was the PI modality, which consists of multiple pulses of alternating polarity and it is again used in contrast echocardiography (62-64). The principle is similar to power modulation, though in PI the pulses alternate in polarity, i.e normal, inverted, normal, inverted, etc. The returning pulses from tissues with linear response are alternating in the same fashion and by summing the pulses the signal is cancelled. On the other hand, the returning pulses from the non-linear microbubble oscillation are again of alternating polarity by they also differ in amplitude and shape. Therefore, by summation the signal is not cancelled out. Traditionally, the PI technique is used in very low MI modes ( $MI < 0.2$ ) to allow visualization of the wall thickening and contrast enhancement at the

same time, whilst ensuring the CR remains very high (65). In our study, the PI technique in 2D imaging improved the CR at mid- and high-range harmonic frequencies and high MI compared to SP. This is probably due to different behaviour of the “scarred” tissue and the microbubbles at very low output and, similarly to PM, the tissue signal is significantly attenuated at very low MI, whereas the microbubbles oscillate without being destroyed and they produce a high intensity signal and high CR. On the contrary at high MI the microbubbles are destroyed by the delivered energy, whereas the scar tissue is responding non-linearly and the high energy pulse ensures little signal attenuation.

Gaibazzi et al. (42) have used the principle of pulse-cancellation 2D echocardiography, to detect the myocardial scar in 20 patients post ST-elevation myocardial infarction. We tested the same hypothesis using both 2D and 3D echo, and we also compared the PM modality to SP emission and contrast enhanced PM. Montant et al. (41) tested the PM technique using 3D echocardiography only, and they found that it does not change significantly the CR compared to SP mode. However, they calculated CR using the average videointensity only in a region of interest positioned onto the scar, whereas in our study the average videointensity of the whole scar volume was calculated in a 3D fashion. When they added a contrast agent the CR dropped, which is consistent with the findings in our study in both 2D and 3D. Additionally, we noticed that the calculated scar volume was consistently

lower when contrast agent was used. The signal attenuation from the contrast-filled left ventricle may account for the lower scar volumes. It may also contribute to lower scar videointensity, which in combination with the high videointensity of the contrast-enhanced perfused myocardium, reduces the CR compared to unenhanced PM.

In our study the highest CR was achieved with PM modality in both in-vitro and in-vivo testing, but a VI close to 1 was achieved with other ultrasound pulse modalities as well. This is because a high CR does not necessarily correspond to more accurate volume quantification. A high CR is a result of enhanced signal from the deranged histologically tissue (scar) along with suppression of linear signal from normal tissue. This process may lead to loss or gain of scattered signals that may make 3D volume quantification inaccurate. Adjusting the ultrasound beam characteristics and processing parameters to make structures look “crisper”, does not necessarily depict them more accurate size-wise. Hence, in our study, we aimed to select as optimal ultrasound characteristics those which combine high CR and good volume quantification. High CR is desirable in imaging and as shown in our study, a higher CR can improve consistency in measurements and agreement between operators, when a tissue of different grey scale intensity from the surrounding medium is traced manually. A higher CR is also expected to be useful in semi-automated or automated detection and tracing algorithms.

### *Study Limitations:*

The in-vitro model allowed testing of hundreds of different combinations of ultrasound pulse characteristics, which would not be feasible in humans. However, this carries the limitation of applicability of the results in humans given the histological differences between the overheated “scar” model and the human myocardial scar along with the surrounding tissues. Besides, the scar in the myocardium is not always discrete as was the “scar” in our model. Imaging in a water tank allowed optimal imaging of the model, however it does not mimic the attenuation or the non-linear propagation that occurs when imaging humans. In clinical practice the scar is not necessarily at optimal depth and orientation, and this might influence some of the findings, and is a rationale for the second part of the study in humans. In addition, our model was still as opposed to the contracting myocardium. The 3D datasets were all fully manually traced. Hence, some differences observed in CR and VI may just reflect the systematic error of the method. The performed incision in the raw muscle to accommodate the “scar” caused a strong reflector, producing a high videointensity signal, and this does not mimic the characteristics of the human scars. Despite extra caution being taken to recognize this “artefact” (Appendix Figure A2), some differences in VI between the tested pulse characteristics may just reflect artefact’s misinterpretation.



By exploring in humans the usefulness of the in-vitro study findings we diminished many of the above-mentioned limitations. However, this remains a single center study with the inherent limitations and bias. The acquisition and interpretation of 3D echo data sets were performed in a center with high expertise in 3D echocardiography, hence the results may not apply to a wider range of Cardiology centers. The operators who traced the 3D echo data sets were not fully blinded, given that the recruited population was known to have a myocardial infarction as per inclusion criteria. Whether echocardiography can perform as well when the operators are fully blinded in respect to the presence or absence of myocardial scar needs to be tested. No patients were excluded from the study because of poor acoustic windows. However, in a larger population, echocardiography is expected to not be interpretable in some patients with poor imaging. All our patients had a myocardial infarction older than 2 months, hence the results may not apply in the early phase of myocardial infarction.

In addition, all the imaging was performed on a vendor specific ultrasound system and therefore the results cannot be automatically translated to other systems. However, all vendors have similar contrast specific imaging modalities (PM and PI) designed to improve CR of contrast studies, therefore it is likely, but not proven, that the results may be similar. Non-commercial software tools were used to analyse the echo data sets and permit video intensity and volume measurements. However, these software

tools were simply used to provide objective validation of the impact of system settings on scar visualisation. They would not be necessary for scar imaging in conventional echocardiography.

## **5. Conclusions**

Ultrasound imaging can provide accurate volume quantification of a tissue with different acoustic properties compared to the surrounding tissue, and power modulation echocardiography increases the contrast ratio between an experimental in-vitro “scar” model and normal muscle providing more accurate “scar” volume quantification. The same applies to myocardial infarction scar in human hearts, where unenhanced power modulation modality provides higher contrast ratio. Power modulation on unenhanced echocardiographic images improves agreement in scar volume assessment between echocardiography and CMR and between independent operators.

## Disclosures:

Prof. Mark Monaghan has received research support from Philips and Speakers' Bureau for Philips.

Patrick Rafter is an employee of Philips Healthcare.

## Figures

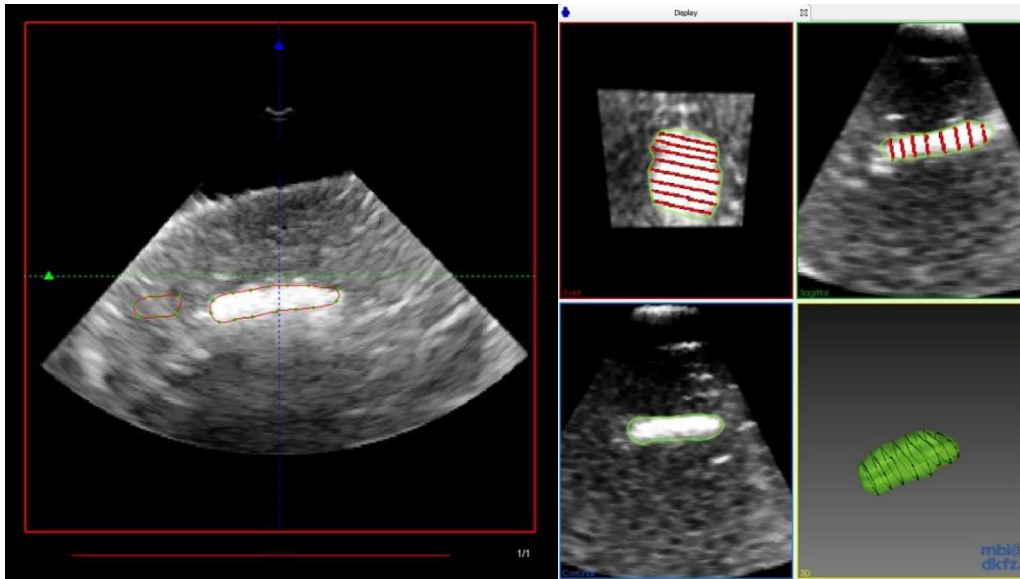


**Figure 1.** Left: Processing a 2D image of the in-vitro experimental “scar”, using the SPEQLE 3D application. Manual tracing of the “scar” and an adjacent muscle segment. Right: Processing a 3D dataset of the same “scar” with the Research-MITK Workbench software. Manual tracing of the “scar” and 3D interpolation to create the 3D mesh of the “scar”.

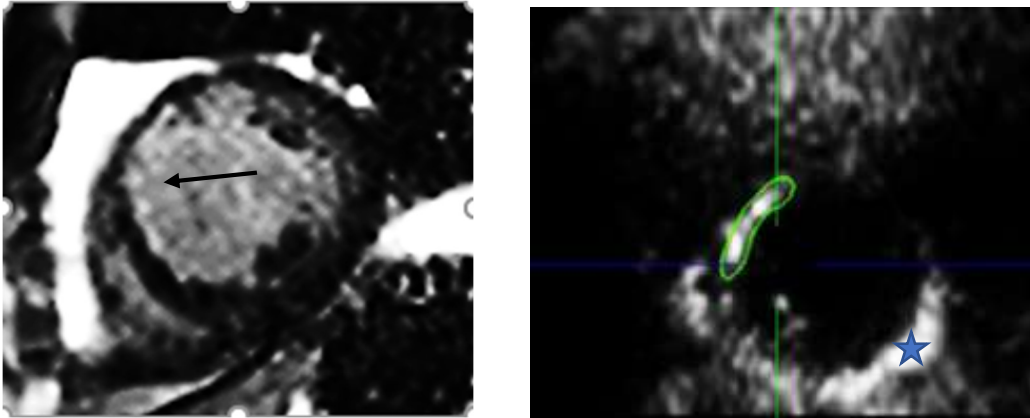


**Figure 2.** Cardiac magnetic resonance (CMR) image (short axis) with late gadolinium enhancement (LGE) (arrow) of a patient with previous myocardial infarction. Left: Short axis view of 3D echocardiography in power modulation technique of the same patient with manual tracing (green contour) of the bright area (scar). Asterisk denotes the enhanced backscattered signal from the pericardium.

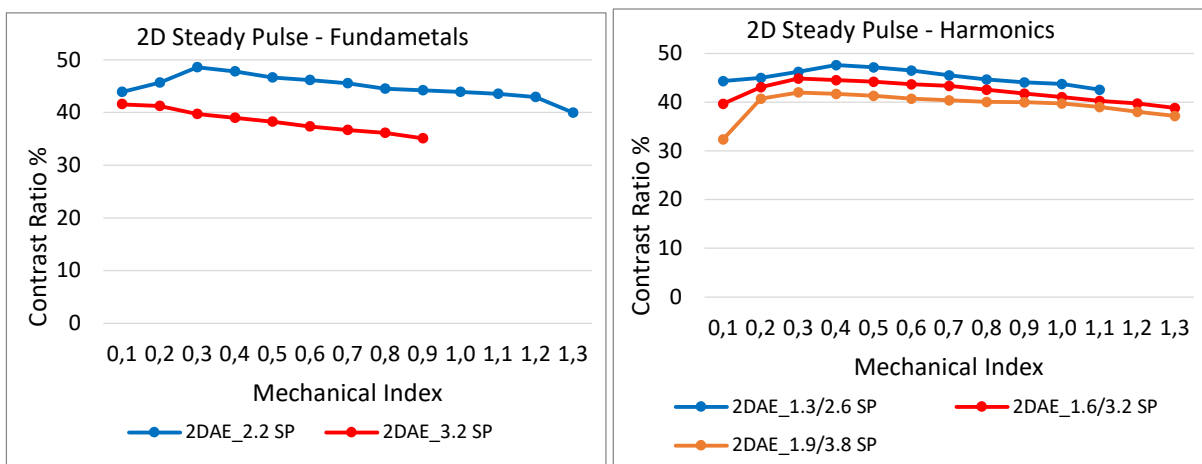


**Figure 3.** In-vitro experimental “scar”. Contrast ratio (CR) vs mechanical index for Adult Echo (AE) pre-set using 2D steady pulse technique in both fundamental (left) and harmonic (right) frequencies. 2D: two-dimensional, numbers indicate frequency; single numbers indicate fundamental frequency (i.e. sending and receiving frequency – in MHz) and dual numbers indicate harmonic frequency (i.e. sending/receiving frequency – in MHz), SP: steady pulse mode.

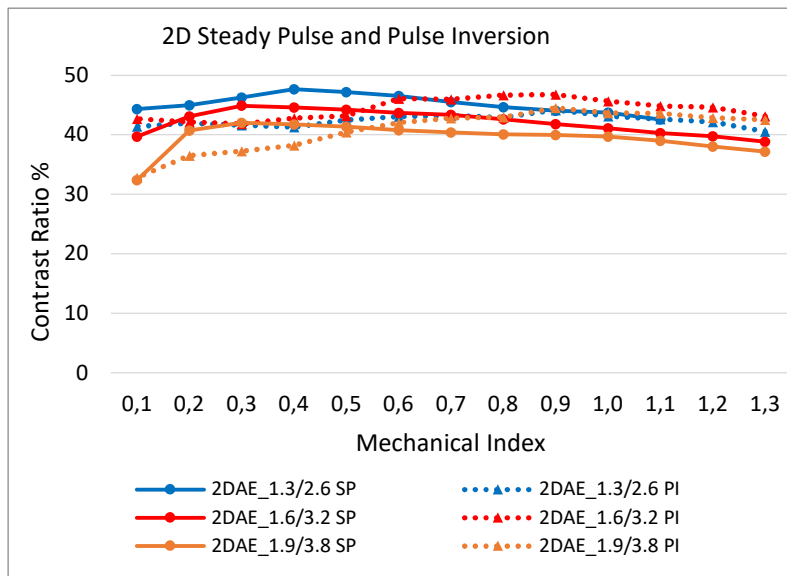


**Figure 4.** In-vitro experimental “scar”. Contrast ratio (CR) vs mechanical index for Adult Echo (AE) pre-set using 2D harmonic imaging, with steady pulse (continuous lines) and pulse inversion (dotted lines) techniques. Abbreviations as in Figure 3, PI: Pulse inversion.

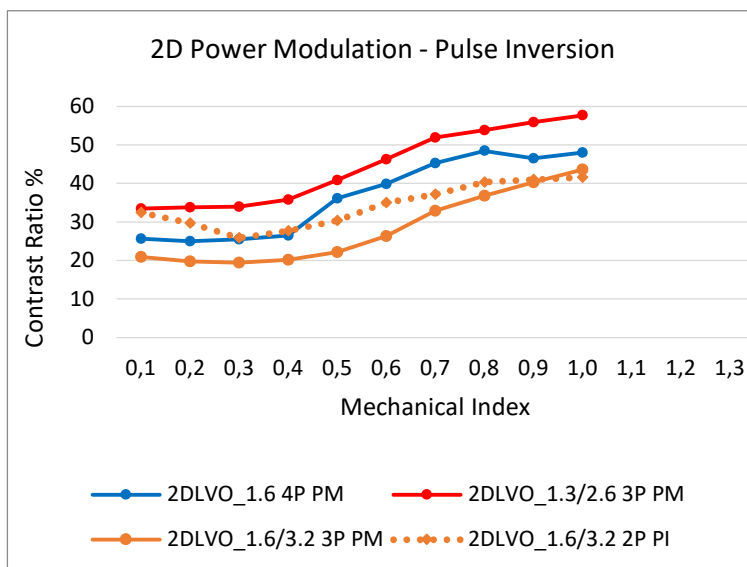


**Figure 5.** In-vitro experimental “scar”. Contrast ratio (CR) vs mechanical index for LVO pre-set. 2D fundamental and harmonic imaging using power modulation (continuous lines) and pulse inversion (dotted line) techniques. Abbreviations as in Figure 3, LVO: LVO pre-set, 3P and 4P: three and four pulses in power modulation modality respectively, PI: pulse inversion.

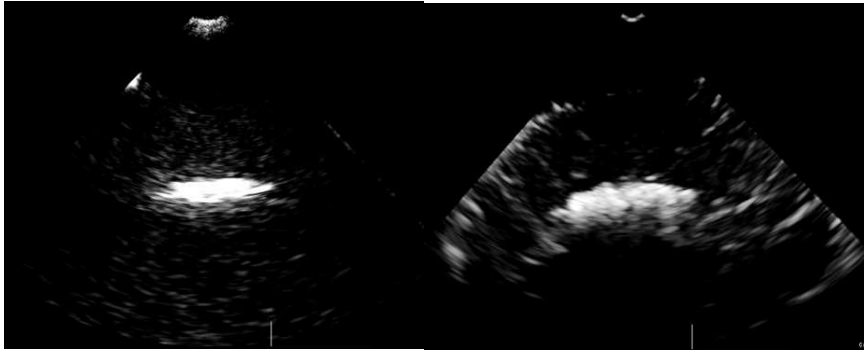


**Figure 6.** In-vitro experimental “scar”. Left: Power modulation modality with enhancement of the “scar” tissue and complete suppression of the surrounding tissue, resulting in high contrast ratio. Right: Steady pulse emission with less bright “scar” area but also detectable signals from the surrounding tissue.

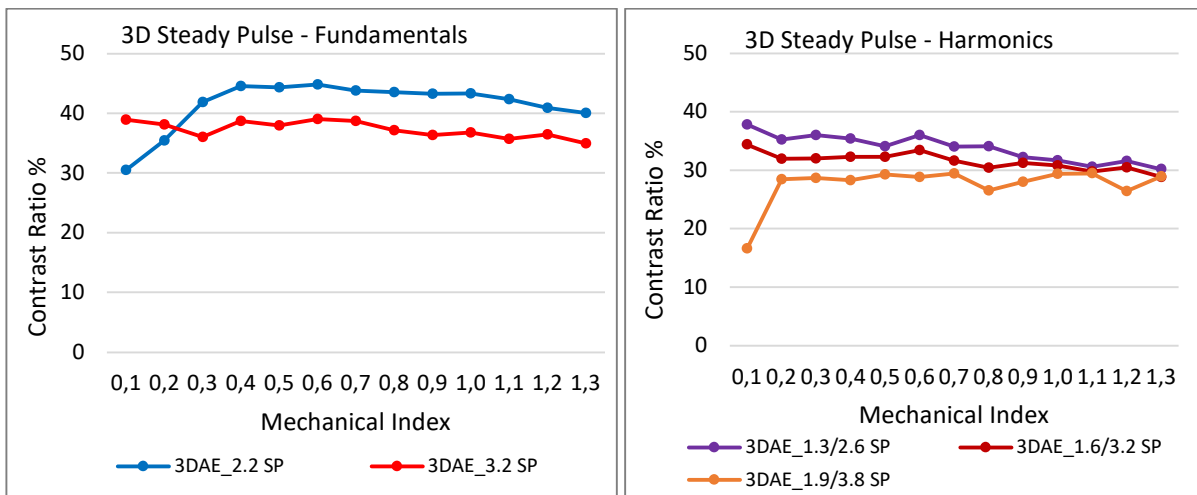


**Figure 7.** In-vitro experimental “scar”. Contrast ratio (CR) vs mechanical index for Adult Echo (AE) pre-set using 3D steady pulse technique in both fundamental (left) and harmonic (right) frequencies. Abbreviations as in Figure 3.

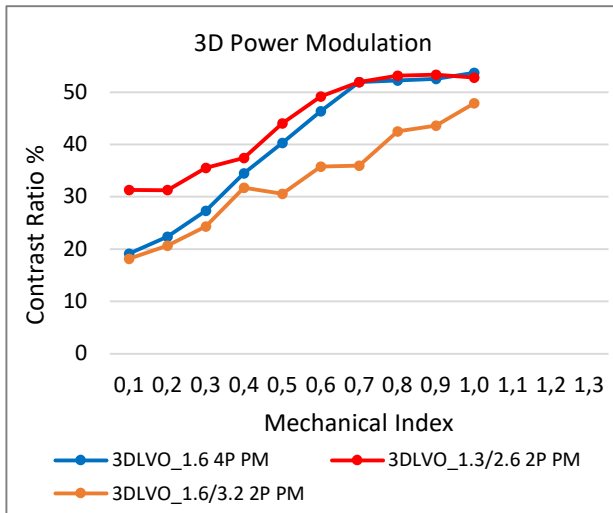


**Figure 8.** In-vitro experimental “scar”. Contrast ratio (CR) vs mechanical index for LVO pre-set. 3D fundamental and harmonic imaging using power modulation (PM) modality. Abbreviations as in Figure 3, 2P and 4P: two and four pulses in power modulation modality respectively.

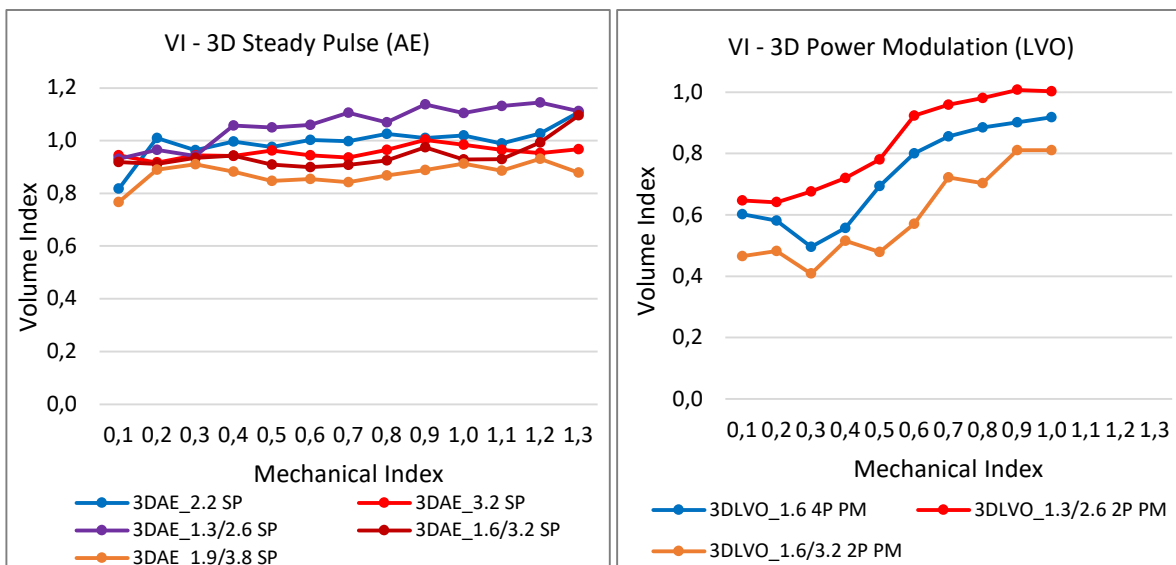


**Figure 9.** In-vitro experimental “scar”. Volume Index (VI) vs mechanical index (MI) for 3D “Adult Echo” (AE) pre-set with steady pulse (left), and “LVO” (LVO) pre-set with power modulation. Abbreviations as in Figure 3, 2P and 4P: two pulses and four pulses respectively in power modulation (PM) modality.

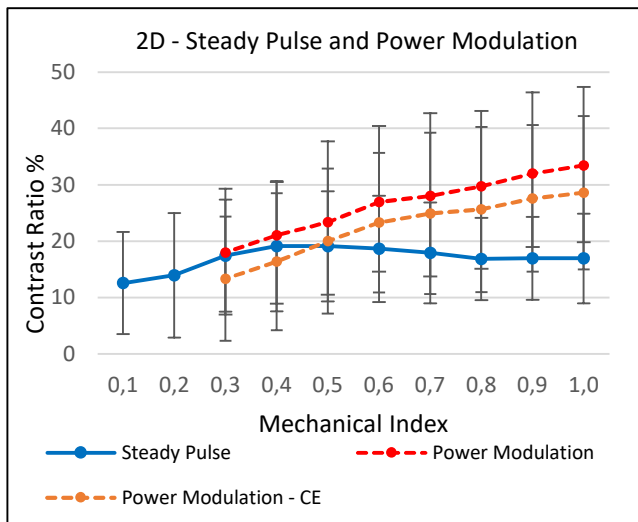


**Figure 10.** Contrast ratio vs mechanical index in human 2D echocardiograms. Blue line: steady pulse emission at 2.2MHz. Red dotted line: unenhanced power modulation modality at 1.3/2.6MHz. Orange dotted line: contrast-enhanced (CE) power modulation modality at 1.3/2.6MHz.

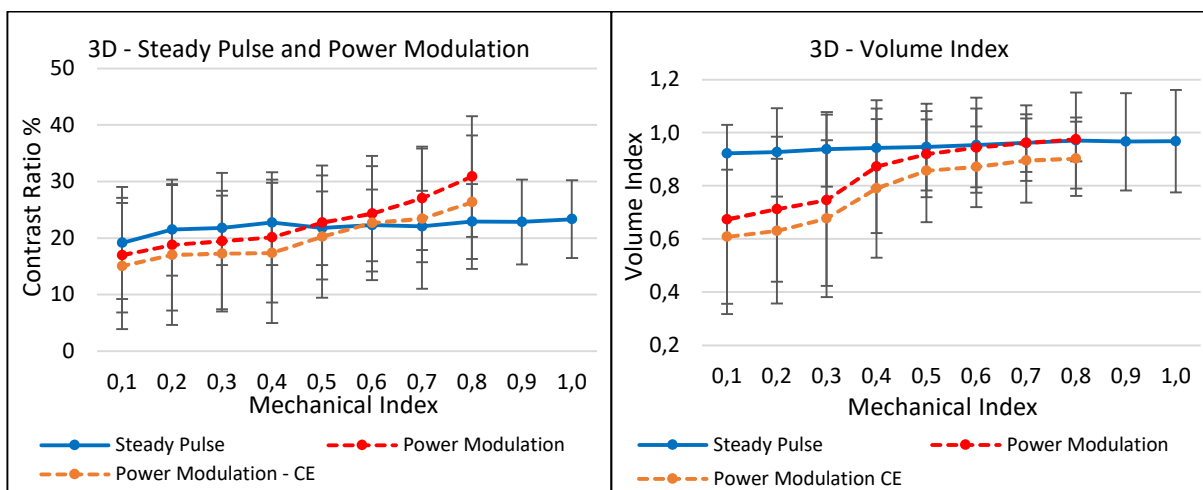


**Figure 11.** Contrast ratio vs mechanical index (left) and volume index vs mechanical index (right) in human 3D echocardiograms. Blue line: steady pulse emission at 2.2MHz. Red dotted line: unenhanced power modulation modality at 1.3/2.6MHz. Orange dotted line: contrast-enhanced (CE) power modulation modality at 1.3/2.6MHz.



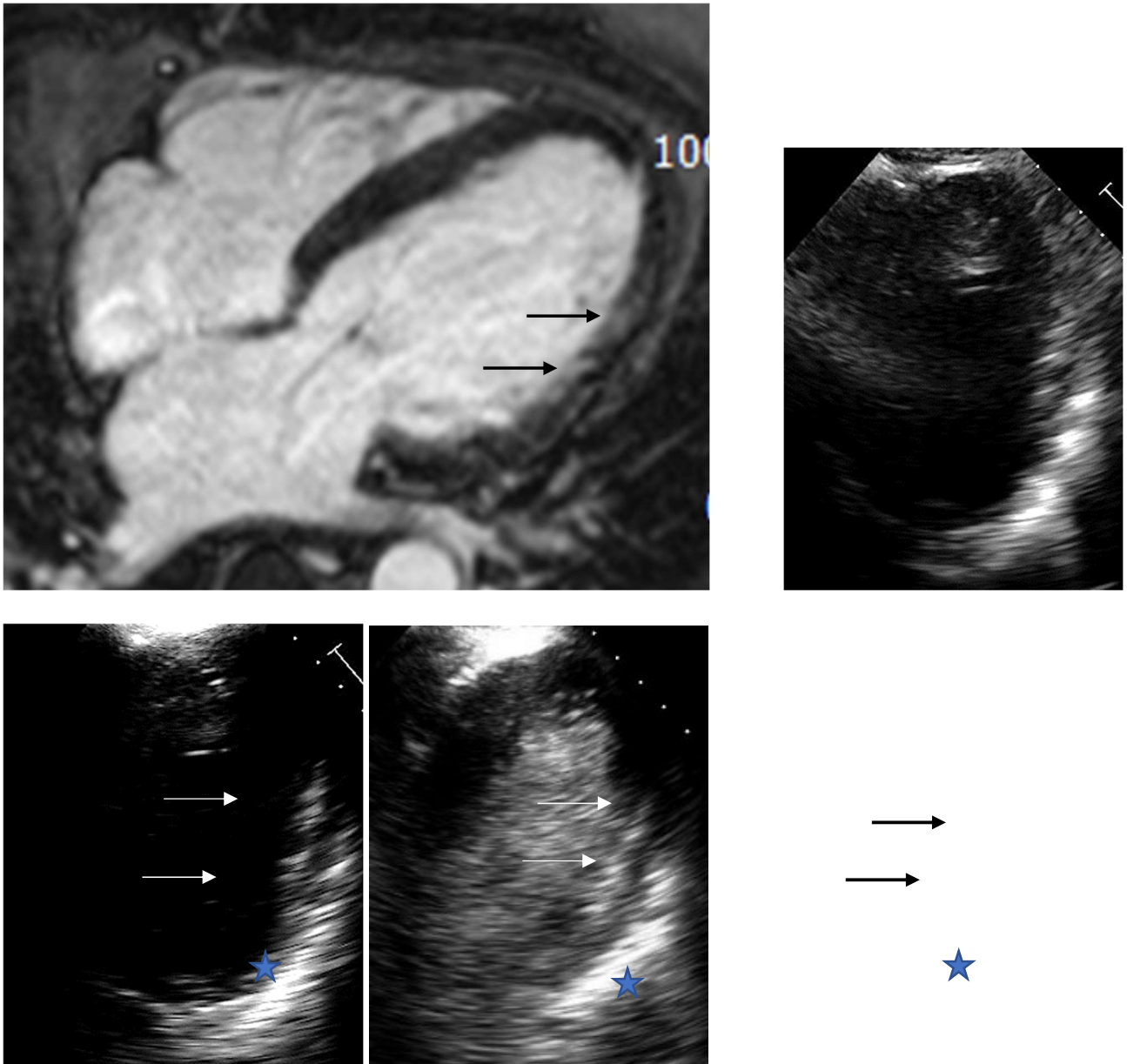


**Figure 12.** Upper panel: LGE CMR of a patient with lateral myocardial infarction. Four-chamber view with subendocardial scar seen in the lateral wall (arrows). Lower panel: 2D echocardiography four-chamber view of the same patient using steady pulse emission technique (left), power modulation (middle) and power modulation with contrast enhancement (right) with a scar seen in the lateral wall (arrows). Asterisk denotes the enhanced backscattered signal from the pericardium.

## Tables

**Table 1.** Manufacturer specific pre-sets and beam forming techniques in two-dimensional (2D) echocardiography for the Philips Epiq7 ultrasound system.

2D – Philips Epiq7 manufacturer specific pre-sets								
Code	Pre-set	Frequency (MHz)	DRS Function		Steady Pulse	Pulse Inversion	Power Modulation	Dynamic Range
2DAE_2.2 SP	Adult Echo	2.2	RS	High Pulse Repetition Frequency. (High Frame Rate)	Yes	-	-	45
2DAE_3.2 SP	Adult Echo	3.2	RS	High Pulse Repetition Frequency. (High Frame Rate)	Yes	-	-	43
2DAE_1.3/2.6 PI	Adult Echo	1.3/2.6	RS	Pulse Inversion	-	Yes	-	45
2DAE_1.3/2.6 SP	Adult Echo	1.3/2.6	S1	Non-Pulse Inversion	Yes	-	-	45
2DAE_1.6/3.2 PI	Adult Echo	1.6/3.2	RS	Pulse Inversion	-	Yes	-	46
2DAE_1.6/3.2 SP	Adult Echo	1.6/3.2	S1	Non-Pulse Inversion	Yes	-	-	46
2DAE_1.9/3.8 PI	Adult Echo	1.9/3.8	RS	Pulse Inversion	-	Yes	-	41
2DAE_1.9/3.8 SP	Adult Echo	1.9/3.8	S1	Non-Pulse Inversion	Yes	-	-	41
2DLVO_1.6 4P PM	LVO	1.6	R2	4 Pulses. Multi-transmit plane elevation compound	-	-	Yes	32
2DLVO_1.3/2.6 3P PM	LVO	1.3/2.6	R2	3 Pulses. Multi-transmit plane elevation compound	-	-	Yes	38
2DLVO_1.6/3.2 3P PM	LVO	1.6/3.2	R2	3 Pulses. Multi-transmit plane elevation compound	-	-	Yes	38
2DLVO_1.6/3.2 2P PI	LVO	1.6/3.2	S2	2 Pulses. Pulse Inversion. Single-Transmit Plane Elevation	-	Yes	-	40

Adult Echo (AE) and Left Ventricle Opacification (LVO) are manufacturer specific pre-sets for the Philips Epiq 7 ultrasound system. DRS: Manufacturer specific selector with five options/positions (R2, R1, RS, S1 and S2), with different allocated ultrasound beam characteristics for each pre-set and frequency. SP: Steady Pulse, PI: Pulse Inversion, PM: Power Modulation, 4P: four pulses, 3P: three pulses, 2P: two pulses.

**Table 2.** Manufacturer specific pre-sets and beam forming techniques in three-dimensional (3D) echocardiography for the Philips Epiq7 ultrasound system.

3D – Philips Epiq7 manufacturer specific pre-sets								
Code	Pre-set	Frequency (MHz)	DRS Function		Steady Pulse	Pulse Inversion	Power Modulation	Dynamic Range
3DAE_2.2 SP	Adult Echo	2.2	RS	High line density	Yes	-	-	45
3DAE_3.2 SP	Adult Echo	3.2	RS	High line density	Yes	-	-	43
3DAE_1.3/2.6 SP	Adult Echo	1.3/2.6	RS	High line density	Yes	-	-	45
3DAE_1.6/3.2 SP	Adult Echo	1.6/3.2	RS	High line density	Yes	-	-	46
3DAE_1.9/3.8 SP	Adult Echo	1.9/3.8	RS	High line density	Yes	-	-	41
3DLVO_1.6 4P PM	LVO	1.6	R2	4 pulses. High line density	-	-	Yes	32
3DLVO_1.3/2.6 2P PM	LVO	1.3/2.6	R1	2 pulses. High line density	-	-	Yes	38
3DLVO_1.6/3.2 2P PM	LVO	1.6/3.2	RS	2 pulses. Medium line density	-	-	Yes	38

Abbreviations as in Table 1.

**Table 3.** Baseline characteristics of the 15 patients with myocardial infarction.

Baseline Characteristics	
Age (years)	67 ± 16
Sex (male)	12 (80%)
Height (cm)	174 ± 9
Weight (kg)	85 ± 16
Body Surface Area	2.0 ± 0.2
LV EDV (ml)	205 ± 61
LV ESV (ml)	116 ± 53
Scar volume (mm3)	19,535 ± 11,406
Scar transmuralities	
<50%	1 (6.7%)
50-75%	3 (20%)
>75%	11 (73.3%)
Scar territory	
LAD only	4 (26.7%)
LCx only	3 (20%)
RCA only	4 (26.7%)
Multi-vessel	4 (26.7%)
EF (%)	46 ± 14
Hypertension	7 (47%)
Diabetes	5 (33%)
Hyperlipidaemia	5 (33%)
Smoking	1 (7%)
Lung Disease	3 (20%)
Atrial Fibrillation	2 (13%)

Continuous variables are presented as mean ± standard deviation and categorical variables as number and percentages

## Part II

### Echocardiographic and other cardiac findings in COVID-19

## CHAPTER 5

### **Right Ventricular-Arterial Uncoupling Independently Predicts Survival in COVID-19 ARDS**

Michele D'Alto, Alberto Marra, Sergio Severino, Andrea Salzano, Emanuele Romeo, Rosanna C De Rosa, Francesca Stagnaro, **Gianpiero Pagnano**, Raffaele Verde, Patrizia Murino, Andrea Farro, Giovanni Ciccarelli, Maria Vargas, Giuseppe Fiorentino, Giuseppe Servillo, Ivan Gentile, Antonio Corcione, Antonio Cittadini, Robert Naeije, Paolo Golino

#### **Background**

Severe Acute Respiratory Syndrome-CoronaVirus-2 (SARS-CoV-2) infection, or Corona Virus Infectious Disease 2019 (COVID-19), may be complicated by the acute respiratory distress syndrome (ARDS) with reported high mortality rates between 26% and 61% (66, 67). There are data suggesting that COVID-19 ARDS differs from "typical" ARDS by several aspects, including preserved respiratory system compliance (68), good tolerance to hypoxemia ("happy hypoxemia") (69), and prominent micro and macrovascular thrombotic changes in relation with extensive endothelial injury (70, 71). On the cardiac side, COVID-19 has also been associated with myocardial injury (72) and altered right ventricle (RV) strain as an independent predictor of poor prognosis (73). There is data suggesting that COVID-19 may predominantly

affect the RV and that is clinically relevant (74). Right heart failure ("acute cor pulmonale") is a long-recognized complication of ARDS, in relation to severity of the disease and ventilatory strategies associated with hyper-inflated lungs and permissive hypercapnia (75). We hypothesized that myocardial injury and inflammatory changes in COVID-19 could be an additional cause of ARDS-related acute right heart failure. We therefore assessed the coupling of RV function to the pulmonary circulation in COVID-19 ARDS patients. To this purpose, we used bedside trans-thoracic Echocardiography with focus on the tricuspid annular plane systolic excursion (TAPSE)/pulmonary artery systolic pressure (PASP) ratio, previously shown to be a valid surrogate of the gold standard ratio of end-systolic to arterial elastance ( $E_{es}/E_a$ ) for the assessment of RV-arterial coupling (76) and an independent predictor of outcome in heart failure and pulmonary arterial hypertension (77).

## **Methods**

### *Study design*

This was a prospective study from two Italian centres, Ospedale dei Colli (Monaldi-Cotugno) and Federico II Hospital, Naples, Italy, which are teaching hospitals authorized for COVID-19 patients. All patients were enrolled from 8 March to 8 May 2020. The diagnosis of COVID-19 was confirmed according

to the interim guidance of World Health Organization (78). The study was approved by local Ethics Committees (#AOC/0015171/2020).

### *Data collection*

Patients' demographics, clinical status, disease duration from the symptoms onset, medical history, comorbidities, laboratory examinations, concomitant treatment, type of ventilation, eventual complications, treatment, and outcomes were recorded. The diagnosis of ARDS rested on the Berlin consensus criteria and PaO<sub>2</sub>/FIO<sub>2</sub> ratios discriminating mild, moderate, and severe forms of the disease (79). Treatment was in keeping with current expert recommendations, with high-flow nasal O<sub>2</sub> as needed to restore arterial oxygenation, and ventilation with positive end-expiratory pressure by facial mask or tracheal intubation following current expert recommendations (80). Thus, tidal volume was kept as low as possible, on average to 6 ml/kg, positive end-expiratory pressure titrated by 2 to 3 cmH<sub>2</sub>O increments to a maximum of 10–15 cmH<sub>2</sub>O and a plateau pressure < 30 cmH<sub>2</sub>O. Non-invasive ventilation was applied when endotracheal intubation was not considered necessary.

### *Transthoracic Echocardiography*

Bedside transthoracic echocardiographic examinations were performed with the Vivid E9 ultrasound system (General Electrics Medical Systems, Andover,



MA, USA), according to the American Society of Echocardiography guidelines (8). Images were stored and analysed offline by three independent trained observers (MD, SS and AM).

### *Statistical analysis*

Kolmogorov-Smirnov test was applied to test the variable distribution. Normally distributed continuous variables were expressed as mean  $\pm$  standard deviation (SD); skewed distributed continuous data were expressed as median and interquartile range [IQR]; categorical variables were expressed as counts and percentages. Two-tailed t test for paired and unpaired data was used to assess changes between groups. Linear regression analyses and partial correlation test by Pearson's method were used to assess univariate relations. The association between analyzed variables and outcome (i.e. mortality) was established by using Cox proportional hazard regression analyses. Univariate and multivariable linear models were used to assess potential predictors of outcome. The following variables, selected according to their potential clinical relevance, were included in the analysis: age, sex, disease duration, previous lung disease, previous coronary artery disease, cardiovascular risk factors (hypertension, diabetes, obesity, smoke), therapy for COVID, type of ventilation, PaO<sub>2</sub>/FiO<sub>2</sub> ratio, creatinine, cardiac troponin I, C-reactive protein, activated partial thromboplastin time, N-terminal pro brain natriuretic peptide, Interleukine-6, left ventricle (LV) end-diastolic diameter, LV end-systolic diameter, left atrium

diameter, LV ejection fraction, mitral and aortic valve diseases, tricuspid regurgitation, TAPSE, PASP, TAPSE/PASP ratio, inferior vena cava dimension and ratio of RV to LV surface areas on an apical 4-chamber view. Results were expressed as hazard ratios with 95% confidence intervals. Outcome prediction accuracies were tested by calculating the area under the curve (AUC) for the receiver operator characteristics (ROC) curve analysis for TAPSE/PASP and PaO<sub>2</sub>/FiO<sub>2</sub> across the endpoint. Kaplan-Meier curves for cumulative survival were constructed for the endpoint to assess the impact of TAPSE/PASP and PaO<sub>2</sub>/FiO<sub>2</sub> on survival, categorizing patients using optimal cut-off points for TAPSE/PASP and PaO<sub>2</sub>/FiO<sub>2</sub> derived from Youden's Index from the ROC curve. Further, ROC curve analyses using the same multivariable model, with and without TAPSE/PASP and PaO<sub>2</sub>/FiO<sub>2</sub>, were used to investigate the gain in C-statistic for associations with outcome when compared to the same model without these parameters. Statistical analyses were performed using SPSS version 25.0 (SPSS Inc, Chicago, Illinois, USA). A value of  $p < 0.05$  was considered statistically significant.

## **Results**

Ninety-four patients were included in the study; they presented with fever (94/94, 100%), dyspnea (87/94, 93%), fatigue (94/94, 100%), and cough (58/94, 62%). All patients had a computed tomography scan diagnostic for

diffuse or localized pneumonia. The echocardiographic assessment was performed on average 3 days after hospital admission (range 1–7 days) after the patients had been stabilized with either high flow supplemental O<sub>2</sub> or invasive/noninvasive ventilation. The clinical data of the survivor and non-survivor patients are shown in Table 1.

Table 1  
Comparison Between Alive and Dead Patients affected by COVID-19

	Alive (n = 69)	Dead (n = 25)	p
Age (year)	62 ± 13	68 ± 12	0.033
Sex M (%)	53 (77)	17 (68)	0.549
Disease duration (day)	7.7 ± 3.3	7.7 ± 3.1	0.942
Lung disease (%)	17 (25)	11 (44)	0.079
Coronary artery disease (%)	14 (20)	3 (12)	0.545
Cardiovascular comorbidities			
Hypertension (%)	44 (64)	19 (76)	0.362
Diabetes (%)	11 (16)	5 (20)	0.99
Smoke (%)	7 (10)	8 (32)	0.021
Obesity (%)	18 (26)	13 (52)	0.025
Treatment			
Anticoagulants (%)	69 (100)	24 (96)	0.097
Hydroxychloroquine (%)	51 (74)	19 (76)	0.840
Antivirals (%)	43 (62)	23 (92)	0.005
Monoclonal antibodies (%)	8 (12)	10 (40)	0.005
Corticosteroids (%)	14 (20)	6 (24)	0.98
Type of ventilation			
Nasal oxygen (%)	35 (51)	0 (0)	< 0.001
Non-invasive ventilation (%)	22 (32)	0 (0)	< 0.001
Intubation (%)	12 (17)	25 (100)	< 0.032
Biochemistry			
Creatinine (mg/dl)	1.3 ± 1.3	2.8 ± 1.4	< 0.001
Cardiac Troponin I (pg/l)	365 ± 644	1245 ± 2049	< 0.002
D-dimer (ng/ml)	317 ± 557	919 ± 974	< 0.001
Value are represented as mean ± standard deviation or absolute value and (%).			
APTT: partial thromboplastin time. NT-proBNP: N-terminal prohormone of brain natriuretic peptide. PaO <sub>2</sub> : arterial partial pressure of oxygen. FiO <sub>2</sub> : fraction of inspired O <sub>2</sub> .			

	Alive (n = 69)	Dead (n = 25)	p
C-reactive protein (mg/dl)	10.6 ± 19.9	22.8 ± 27.3	< 0.023
Procalcitonin (ng/ml)	0.6 ± 1.5	1.8 ± 2.0	< 0.005
APTT (sec)	36.8 ± 6.7	40.6 ± 4.3	0.037
NT-proBNP (pg/ml)	686 ± 1224	3375 ± 3891	< 0.001
Interleukine-6 (ng/ml)	33.6 ± 33.4	246.4 ± 87.4	< 0.001
PaO <sub>2</sub> /FiO <sub>2</sub> ratio (mmHg)	270 ± 104	117 ± 56	< 0.001
Value are represented as mean ± standard deviation or absolute value and (%).			
APTT: partial thromboplastin time. NT-proBNP: N-terminal prohormone of brain natriuretic peptide. PaO <sub>2</sub> : arterial partial pressure of oxygen. FiO <sub>2</sub> : fraction of inspired O <sub>2</sub> .			

The patient population was globally relatively old, predominantly male, and presented with pulmonary comorbidities and cardiovascular risk factors. Non-survivors were older by an average of 6 years and were more frequently smokers and overweight. The majority of the patients were anti-coagulated and treated with hydroxychloroquine. A proportion of the patients also received anti-viral drugs, monoclonal antibodies, and corticosteroids. Non-survivors received more frequently anti-viral drugs and invasive mechanical ventilation. Serum creatinine, Cardiac troponin I, C-reactive protein, Interleukine-6, N-terminal pro brain natriuretic peptide, activated partial thromboplastin time, and pro-calcitonin were higher and

PaO<sub>2</sub>/FIO<sub>2</sub> lower in non-survivors. Echocardiographic findings shown in Table 2 disclosed a significant increase in PASP, inferior vena cava dimensions and a decrease in TAPSE/PASP in non-survivors, as compared to survivors.

Table 2  
Echocardiographic features

	Alive (n = 69)	Dead (n = 25)	p
LVEDD (mm)	48 ± 5	49 ± 4	0.388
LVESD (mm)	29 ± 7	31 ± 5	0.059
LAD (mm)	38 ± 6	40 ± 5	0.082
LVEF (%)	60 ± 7	58 ± 8	0.209
MVD	5 (7)	1 (4)	0.574
AVD	1 (1)	0 (0)	0.550
TR	2 (3)	3 (12)	0.084
TAPSE (mm)	25 ± 4	19 ± 4	< 0.001
PASP (mmHg)	30 ± 7	42 ± 12	< 0.001
TAPSE/PASP	0.89 ± 0.29	0.51 ± 0.22	< 0.001
IVC (mm)	15 ± 4	20 ± 3	< 0.001
Pericardial effusion	6 (9)	4 (16)	0.375
Echocardiographic phenotypes			
Normal	50 (73)	10 (40)	0.007
Hyperkinetic	9 (13)	3 (12)	0.99
Right	3 (4)	12 (48)	< 0.001
LV depression	3 (4)	0 (0)	0.57
Severe pericardial effusion	4 (6)	0 (0)	0.57
<p>LVEDD: left ventricle end-diastolic diameter; LVESD: left ventricle end-systolic diameter; LAD: left atrium diameter; LVEF: left ventricle ejection fraction; MVD: mitral valve disease moderate-to-severe; AoVD: aortic valve disease moderate-to-severe; TR: tricuspid regurgitation; TAPSE: tricuspid annulus plane systolic excursion; PASP: pulmonary artery systolic pressure; IVC: inferior vena cava.</p> <p>Value are represented as mean ± standard deviation or absolute value and (%). <i>p</i>&lt;0.05 statistically significant.</p>			

A typical right heart phenotype echocardiographic examination is shown in Fig. 1 (Panel A and B). The results of univariate and multivariable analyses are shown respectively in Table 3 and Table 4.

Table 3  
Single predictor models of Cox proportional Hazard Analysis

Variables	HR	95% (CI)	p
Age (year)	1.04	1.003–1.078	0.035
Sex (Female)	0.006	0.000-0.216	0.006
Fever (days)	1.001	0.912–1.098	0.98
Pulmonary disease	1.998	0.906–4.408	0.086
Coronary artery disease	0.556	0,166-1.858	0.340
Hypertension	1,767	0.706–4.429	0.224
Diabetes	1.525	0.571–4.072	0.40
Smokers	3.050	1.313–7.086	0.10
Obesity	2.252	1.027–4.936	0.044
Risk factors	-	-	0.025
0	Ref	-	-
1	6.608	0.853-51	0.07
2	5.126	0.617–42.6	0.13
3	15.518	1.861-129	0.011
4	46.105	2.772-766	0.008
Nasal Oxygen	0.019	0.001–0.512	0.018
Non-Invasive Ventilation	0.031	0.001–1.386	0.073
Intubation	223,89	4.81–10415	0.006
PaO <sub>2</sub> /FiO <sub>2</sub> ratio (mmHg)	0.986	0.981–0.992	0.001
Heparin	0.274	0.037–2.039	0.206
Antivirals	5.935	1.398–25.186	0.016
Hydroxicloroquine	1.195	0.477–2.995	0.704
Monoclonal antibody	3.301	1.481–7.356	0.003
Corticosteroids	1.308	0.521–3.279	0.568

APTT: partial thromboplastin time. NT-proBNP: N-terminal prohormone of brain natriuretic peptide. LVEDD: left ventricle end-diastolic diameter; LVESD: left ventricle end-systolic diameter; LAD: left atrium diameter; LVEF: left ventricle ejection fraction; MVD: mitral valve disease moderate-to-severe; AoVD: aortic valve disease moderate-to-severe; TR: tricuspid regurgitation; TAPSE: tricuspid annulus plane systolic excursion; PASP: pulmonary artery systolic pressure; IVC: inferior vena cava.

Variables	HR	95% (CI)	p
Creatinine (mg/mL)	1.236	1.067–1.432	0.005
Troponine (pg/l)	1.000	1.000–1.000	0.003
D-dimer (ng/ml)	1.000	1.000–1.001	< 0.001
C-Reactive Protein (mg/dl)	1.014	1.004–1.024	0.006
Procalcitonin (ng/ml)	1.108	0.975–1.259	0.115
NT-proBNP (pg/ml)	1.000	1.000–1.000	< 0.001
APTT (sec)	0.997	0.982–1.012	0.687
Interleukine-6 (ng/ml)	1.010	1.007–1.013	< 0.001
Heart rate (bpm)	1.031	1.006–1.058	0.016
Systolic blood pressure (mmHg)	0.976	0.949–1.003	0.076
Diastolic blood pressure (mmHg)	0.912	0.868–0.958	< 0.001
LVEDd (mm)	1.031	0.948–1.121	0.473
LVESd (mm)	1.039	0.99–1.091	0.123
LAD (mm)	1.066	0.995–1.143	0.068
LVEF (%)	0.972	0.934–1.011	0.151
Severe MR	0.526	0.071–3.887	0.529
Severe AR	0.049	0–201330	0.697
Severe TR	2.671	0.798–8.95	0.111
TAPSE (mm)	0.796	0.727–0.871	< 0.001
PASP (mmHg)	1.085	1.054–1.118	< 0.001
TAPSE/PASP (mm/mmHg)	0.013	0.002–0.069	< 0.001
IVC (mm)	1.335	1.201–1.483	< 0.001
IVC Respiratory changes	1.591	0.702–3.606	0.226
Pericardial effusion	1.693	0.580–4.940	0.335
Pleural effusion	0.868	0.204–3.689	0.848

APTT: partial thromboplastin time. NT-proBNP: N-terminal prohormone of brain natriuretic peptide. LVEDD: left ventricle end-diastolic diameter; LVESD: left ventricle end-systolic diameter; LAD: left atrium diameter; LVEF: left ventricle ejection fraction; MVD: mitral valve disease moderate-to-severe; AoVD: aortic valve disease moderate-to-severe; TR: tricuspid regurgitation; TAPSE: tricuspid annulus plane systolic excursion; PASP: pulmonary artery systolic pressure; IVC: inferior vena cava.



Variables	HR	95% (CI)	p
Right Phenotype	4.232	1.505–11.902	0.006
APTT: partial thromboplastin time. NT-proBNP: N-terminal prohormone of brain natriuretic peptide. LVEDD: left ventricle end-diastolic diameter; LVESD: left ventricle end-systolic diameter; LAD: left atrium diameter; LVEF: left ventricle ejection fraction; MVD: mitral valve disease moderate-to-severe; AoVD: aortic valve disease moderate-to-severe; TR: tricuspid regurgitation; TAPSE: tricuspid annulus plane systolic excursion; PASP: pulmonary artery systolic pressure; IVC: inferior vena cava.			

Table 4  
Multivariable Models of Cox Proportional Hazard Analysis

Variables	HR	95% (CI)	p
Age (year)	1.002	0.944–1.063	0.953
Obesity	0.626	0.171–2.295	0.480
Creatinine (mg/mL)	1.033	0.746–1.429	0.847
Troponine (pg/L)	1.00	0.999–1.001	0.774
D-dimer (ng/mL)	1.00	0.999–1.001	0.442
C-Reactiv protein (mg/mL)	1.01	0.996–1.024	0.171
Heart rate (bpm)	0.996	0.961–1.032	0.817
Systolic blood pressure (mmHg)	1.038	0.988–1.09	0.137
Diastolic blood pressure (mmHg)	0.915	0.837–1.002	0.054
LVEDd (mm)	1.064	0.991–1.550	0.508
LVESd (mm)	0.899	0.707–1.143	0.385
LVEF (%)	1.022	0.900–1.161	0.739
LAD (mm)	0.947	0.858–1.046	0.947
TAPSE/PASP (mm/mmHg)	0.026	0.01–0.579	0.019
PaO <sub>2</sub> /FiO <sub>2</sub> ratio (mmHg)	0.988	0.977–0.998	0.018
LVEDD: left ventricle end-diastolic diameter; LVESD: left ventricle end-systolic diameter; LVEF: left ventricle ejection fraction; LAD: left atrium diameter; TAPSE: tricuspid annulus plane systolic excursion; PASP: pulmonary artery systolic pressure. PaO <sub>2</sub> : arterial partial pressure of oxygen. FiO <sub>2</sub> : fraction of inspired O <sub>2</sub> .			

While at univariate analysis most of the biological and echocardiographic differences between survivors and non-survivors were significantly associated with survival (Table 3), only PaO<sub>2</sub>/FIO<sub>2</sub> and TAPSE/PASP emerged as independent predictors after adjustment at multivariable analysis [hazard ratio

(95% confidence interval); p value: 0.988 (0.977–0.998); p = 0.018 and 0.026 (0.01–0.579); p = 0.019, respectively] (Table 4).

Individual values for TAPSE/PASP and PaO<sub>2</sub>/FIO<sub>2</sub> in survivors and non-survivors are presented in Fig. 2.

ROC curves to predict outcome of these two variables are shown in the Fig.

3. When patients were dichotomised according to the Youden's Index for optimal cut-off point from the ROC curve (159 mmHg and 0.635 mm/mmHg, PaO<sub>2</sub>/FIO<sub>2</sub> and TAPSE/PASP respectively), Kaplan-Meier curves of % survival as a function of time in patients showed that patients with TAPSE/PASP or PaO<sub>2</sub>/FIO<sub>2</sub> below ROC-derived cut-off values have reduced survival (chi square; log rank test p: 26.43;<0.001 and 42.83;<0.001 respectively) (Fig. 4). Furthermore, when patients were categorized according to value of both parameters, patients with reduction of both parameters showed the lowest survival (chi square: 45.87; log rank test p: <0.001), significantly different to those with normal levels (chi square: 50.32, p < 0.001) or only one

parameter impaired (chi square: 9.56, p = 0.001). A combination of high TAPSE/PASP or PaO<sub>2</sub>/FIO<sub>2</sub> allowed for a very high likelihood of survival.

## Discussion

The present results show that COVID 19-induced ARDS is associated with early and pronounced uncoupling of right ventricular function from the pulmonary circulation, and that its non-invasive echocardiographic assessment by the TAPSE/PASP ratio adds significantly and independently to the prognostic relevance of the PaO<sub>2</sub>/FIO<sub>2</sub> ratio in these patients.

The reported COVID-19 patients were diagnosed with pneumonia complicated by ARDS based on clinical presentation of severe dyspnea, cough and fatigue, compatible chest computed tomography findings, and the PaO<sub>2</sub>/FIO<sub>2</sub> ratio. At the moment of echocardiographic evaluation, the PaO<sub>2</sub>/FIO<sub>2</sub> ratio had been corrected in a proportion of the survivors (Fig. 2). The patients were treated empirically with drugs expected to be of benefit, such as hydroxychloroquine and were anticoagulated. Their ventilatory management included proning, application of positive end-expiratory pressure and so-called "protective ventilation" with a low as possible tidal volumes (80). This resulted in a 26% mortality at the lower range of currently reported (81).

Pulmonary hypertension in the present study was mild to moderate as based on echocardiographic estimates of PASP. A PASP of 40 mmHg in the non-survivors would indeed be at the upper limit of normal taken into account age, sex, and body weight (82). On the other hand, the TAPSE was decreased but

still above the lower limit of normal in the non-survivors (83). Accordingly, the TAPSE/PASP at  $0.89 \pm 0.29$  in survivors was mildly decreased compared to the value of  $1.11 \pm 0.03$  previously reported in 209 subjects older than 60 years (83). However, it was markedly decreased to  $0.51 \pm 0.22$  mm/mmHg in non-survivors, approaching values below 0.50 mm/mmHg previously shown to be of poor prognosis in heart failure and severe pulmonary hypertension (77).

In a recent report of 200 hospitalized with COVID-19 in non-ICU departments, PASP was  $> 35$  mmHg in 12% and the TAPSE  $< 17$  mm in 14.5%, but increased PASP and not decreased TAPSE was found to predict a poor outcome (84). Mild pulmonary hypertensions along with moderate decrease in TAPSE in that study are in keeping with the present findings in more severely ill patients with respiratory insufficiency.

The TAPSE/PASP ratio was initially proposed as an estimate of RV myocardial length-tension relationship, and as such showed to be of prognostic relevance in heart failure (84). Subsequent studies confirmed its prognostic capability, not only in heart failure (85) but also in pulmonary arterial hypertension (86) and in patients with chronic lung diseases (87). In these studies, the TAPSE/PASP was assumed to inform about RV-PA coupling, with TAPSE considered as a load-dependent surrogate of Ees and PASP as an indirect estimate of Ea (85-87). The TAPSE/PASP has been shown to be superior to other composite echocardiographic indices in the

assessment of RV-PA and correlated to gold standard invasive (76) or indirectly assessed Ees/Ea ratios (85). As in the present study the TAPSE/PASP ratio was mostly decreased in invasively ventilated patients, one could wonder if the application of positive end-expiratory pressure could have contributed to increased PAP and RV-PA uncoupling (88). COVID-19 ARDS patients could have presented with increased transmission of alveolar pressures to pulmonary resistive vessels because of preserved lung compliance (68). Mechanics of the respiratory system were not assessed in the present study. However, the notion of preserved compliance in COVID-19 ARDS may not be confirmed in most of these patients (89), and the "protective ventilation" approach in the present study would be expected to avoid to high volumes and alveolar pressures as a cause of excessive RV afterload (75). This was confirmed by only mild increases in PASP disclosed by the echocardiographic examinations. The reason for RV-PA uncoupling in the presence of only mildly increased PAP is not immediately apparent. The basic response of RV function to increased afterload is homeometric, with increased Ees (contractility) to match Ea (afterload), and uncoupling expected but only in severe or rapidly evolving pulmonary hypertension (90). However, early RV-PA uncoupling may be observed in severe inflammatory conditions such as sepsis (91) or also in left heart failure because of negative ventricular interactions (92). Both may occur in COVID-19 patients (72). Therefore, the

right heart in COVID-19 patients may fail even in the presence of only modest increase in afterload.

The present results are in keeping with a recent echocardiographic study in patients with COVID-19 ARDS, in which non-survivors had a PASP at the upper limit of normal, decreased indices of RV systolic function and longitudinal strain identified as an independent predictor of outcome (73). The TAPSE/PASP is easier to assess, can be part of standard bedside echocardiographic assessments as it does not require off-line analysis of images and specific software, and may be a more sensitive assessment of RV-PA coupling.

The high prevalence of RV dilatation and dysfunction in the range of 40–50% recently reported in patients with COVID-19 (74, 93) underscore the exquisite sensitivity of the RV to this newly appeared viral infection.

The most potent predictor of outcome in ARDS is the PaO<sub>2</sub>/FIO<sub>2</sub> ratio, which as such is part of the definition of the syndrome (78). In the present study, the TAPSE/PASP emerged with equally potent prognostic capability, suggesting a major component of acute cor pulmonale in COVID-19 ARDS pathophysiology. Whether this is entirely particular to COVID-19 ARDS is uncertain as there have been no systematic evaluations of RV-PA coupling in more "typical" ARDS or other viral pneumonia ARDS controls.

Approximately 4 decades ago, Zapol and Snider called attention to the pulmonary circulation and the right heart in severe ARDS (94). Pulmonary hypertension in these patients is nowadays uncommon along with progress in management, but "acute cor pulmonale" continues to be reported, albeit generally in the context of ventilatory settings associated with excessive increase in alveolar pressure and permissive hypercapnia (75). The present investigation shows that acute uncoupling of the right heart from the quasi-normotensive pulmonary circulation may also occur in the context of severe systemic inflammation and vasculitis.

## **Conclusions**

COVID 19-induced ARDS is associated with early and pronounced right ventricular-arterial uncoupling, and its non-invasive echocardiographic assessment by the TAPSE/PASP ratio adds significantly and independently to the prognostic relevance of the PaO<sub>2</sub>/FIO<sub>2</sub> ratio in these patients.

## **Limitations**

The present study is limited by relatively small sample size, absence of respiratory system compliance measurements, absence of non-COVID-19 viral pneumonia controls, and exclusively non-invasive evaluations of the right heart and the pulmonary circulation. However, the results call attention to cor

pulmonale as an important component of COVID-19 ARDS and plea for systematic bedside echocardiographic assessments added to blood gases and lung mechanics in the management of these patients.





## Clinical characteristics and prognosis of hospitalized COVID-19 patients with incident sustained tachyarrhythmias: A multicenter observational study

Vincenzo Russo<sup>1</sup> | Marco Di Maio<sup>2</sup> | Filiberto Fausto Mottola<sup>1</sup> |  
Gianpiero Pagnano<sup>3</sup> | Emilio Attena<sup>4</sup> | Nicoletta Verde<sup>1</sup> | Pierpaolo Di Micco<sup>5</sup> |  
Angelo Silverio<sup>6</sup> | Fernando Scudiero<sup>7</sup> | Luigi Nunziata<sup>8</sup> | Nunzia Fele<sup>3</sup> |  
Antonello D'Andrea<sup>9</sup> | Guido Parodi<sup>10</sup> | Stefano Albani<sup>11</sup> | Paolo Scacciatella<sup>11</sup> |  
Gerardo Nigro<sup>1</sup> | Sergio Severino<sup>3</sup>

<sup>1</sup>Department of Translational Medical Sciences, University of Campania 'Luigi Vanvitelli'—Monaldi Hospital, Naples, Italy

<sup>2</sup>Cardiology Division, "Maria S.S. Addolorata" Hospital, ASL Salerno, Salerno, Italy

<sup>3</sup>Cardiology Unit, Cotugno Hospital, Naples, Italy

<sup>4</sup>Medicine Unit, Division of Cardiology, San Giuliano Hospital, Naples, Italy

<sup>5</sup>Fatebenefratelli Hospital of Naples, Naples, Italy

<sup>6</sup>Cardiology Division, Cardiovascular and Thoracic Department, University Hospital "San Giovanni di Dio e Ruggi d' Aragona", Salerno, Italy

<sup>7</sup>Cardiology Unit, Health Authority Bergamo East, Italy

<sup>8</sup>Cardiology Unit, Boscorecase Hospital, Naples, Italy

<sup>9</sup>Division of Cardiology and Intensive Care Unit, Umberto I Hospital, Nocera Inferiore, Italy

<sup>10</sup>Clinical and Interventional Cardiology, Sassari University Hospital, Sassari, Italy

<sup>11</sup>Cardiology Department, Aosta Valley Health Authority, Aosta, Italy

### Correspondence

Vincenzo Russo, Department of Translational Medical Sciences, University of Campania 'Luigi Vanvitelli'—Monaldi Hospital, Via Leonardo Bianchi, 80131 Naples, Italy.  
Email: vincenzo.russo@unicampania.it

### Abstract

**Introduction:** Little is still known about the prognostic impact of incident arrhythmias in hospitalized patients with COVID-19. The aim of this study was to evaluate the incidence and predictors of sustained tachyarrhythmias in hospitalized patients with COVID-19, and their potential association with disease severity and in-hospital mortality.

**Materials and methods:** This was a retrospective multicenter observation study including consecutive patients with laboratory confirmed COVID-19 admitted to emergency department of ten Italian Hospitals from 15 February to 15 March 2020. The prevalence and the type of incident sustained arrhythmias have been collected. The correlation between the most prevalent arrhythmias and both baseline characteristics and the development of ARDS and in-hospital mortality has been evaluated.

**Results:** 414 hospitalized patients with COVID-19 ( $66.9 \pm 15.0$  years, 61.1% male) were included in the present study. During a median follow-up of 28 days (IQR: 12–45), the most frequent incident sustained arrhythmia was AF (N: 71; 17.1%), of which 50 (12.1%) were new-onset and 21 (5.1%) were recurrent, followed by VT (N: 14, 3.4%) and supraventricular arrhythmias (N: 5, 1.2%). Incident AF, both new-onset and recurrent, did not affect the risk of severe adverse events including ARDS and death during hospitalization; in contrast, incident VT significantly increased the risk of in-hospital mortality (RR: 2.55;  $P$ : .003).

**Conclusions:** AF is the more frequent incident tachyarrhythmia; however, it not seems associated to ARDS development and death. On the other hand, incident VT is a not frequent but independent predictor of in-hospital mortality among hospitalized COVID-19 patients.

**KEYWORDS**

Atrial Fibrillation, Covid-19, Covid-19 and arrhythmia, Covid-19 and cardiovascular complications, Covid-19 and cardiovascular System, SARS-CoV-2, SARSCoV-2 and ventricular arrhythmias

**1 | INTRODUCTION**

Severe acute respiratory syndrome coronavirus 2 (SARS-CoV-2) is a highly pathogenic human coronavirus recently recognized as the cause of the coronavirus disease 2019 (COVID-19). The outbreak sparked in China and spread rapidly to other countries, reaching devastating pandemic proportion.<sup>1</sup> Italy is the one of the hardest hit countries by COVID-19, with more than 236 000 laboratory-confirmed cases by 14 June 2020.<sup>2</sup> The clinical course of COVID-19 may be frequently complicated by cardiac arrhythmias, both atrial and ventricular.<sup>3</sup> Actually, little is still known about the clinical characteristics of COVID-19 patients who developed arrhythmias during hospitalization<sup>4</sup>; the type and burden of incident sustained tachyarrhythmias; the clinical impact of atrial fibrillation (AF) or ventricular tachycardia (VT) on disease severity and in-hospital mortality.

The aim of this multicenter study was to evaluate the incidence and the predictors of sustained tachyarrhythmias in hospitalized patients with COVID-19, and their potential association with disease severity and in-hospital mortality.

**2 | MATERIALS AND METHODS**

All consecutive patients with laboratory confirmed COVID-19 admitted to emergency department of ten Italian Hospitals from 15th February to 15th March were included in this retrospective observational study. All patients underwent medical history, physical examination, electrocardiographic and laboratory evaluation. Chest X-Ray and/or computed tomography (CT) scan were also performed to rule out pneumonia in one or multiple sites. The primary aim of our study was to explore the incidence

**TABLE 1** Distribution of patients' characteristics and their association with incident AF among COVID-19 study population

	Incident AF free group	Incident AF group	Univariable RR (CI), <i>P</i> value	Multivariable RR (CI), <i>P</i> value
<i>n</i>	343	71		
Male gender, <i>n</i> (%)	207 (60.3)	46 (64.8)	1.17 (0.75, 1.76), <i>P</i> : .485	-
Age (mean (SD))	65.54 (15.48)	73.69 (9.90)	1.04 (1.02, 1.05), <i>P</i> < .001	1.03 (1.01, 1.05), <i>P</i> : .002
Smoker, <i>n</i> (%)	63 (18.4)	21 (29.6)	1.62 (1.02, 2.36), <i>P</i> : .035	NS
Hypertension, <i>n</i> (%)	206 (60.2)	57 (80.3)	2.08 (1.37, 3.02), <i>P</i> : .002	NS
Diabetes, <i>n</i> (%)	84 (24.6)	22 (31.0)	1.29 (0.81, 1.93), <i>P</i> : .261	-
Dyslipidaemia, <i>n</i> (%)	94 (27.5)	24 (33.8)	1.27 (0.80, 1.88), <i>P</i> : .285	-
Obesity, <i>n</i> (%)	24 (13.3)	5 (10.6)	0.82 (0.30, 1.67), <i>P</i> : .632	-
History of AF, <i>n</i> (%)	51 (15.0)	21 (29.6)	1.93 (1.24, 2.73), <i>P</i> : .004	NS
Heart Failure, <i>n</i> (%)	29 (8.5)	17 (23.9)	2.41 (1.53, 3.35), <i>P</i> < .001	1.88 (1.09, 2.86), <i>P</i> : .023
Previous Stroke, <i>n</i> (%)	25 (7.3)	10 (14.1)	1.75 (0.92, 2.78), <i>P</i> : .068	NS
CKD, <i>n</i> (%)	47 (13.8)	17 (23.9)	1.69 (0.61, 5.80), <i>P</i> : .034	NS
CAD, <i>n</i> (%)	45 (13.2)	21 (29.6)	2.12 (1.38, 2.96), <i>P</i> < .001	1.75 (1.07, 2.59), <i>P</i> : .024
COPD, <i>n</i> (%)	65 (19.0)	23 (32.4)	1.73 (1.12, 2.48), <i>P</i> : .134	-
ACEI/ARBs, <i>n</i> (%)	132 (41.4)	38 (55.9)	1.57 (1.05, 2.25), <i>P</i> : .030	NS
Ca-Antagonists, <i>n</i> (%)	79 (23.0)	21 (29.6)	1.32 (0.83, 2.08), <i>P</i> : .236	-
Beta-Blockers, <i>n</i> (%)	46 (13.4)	12 (16.9)	0.95 (0.83, 1.09), <i>P</i> : .477	-
Incident VT, <i>n</i> (%)	7 (2.0)	7 (9.9)	3.04 (1.55, 4.47), <i>P</i> : .003	2.94 (1.37, 4.49), <i>P</i> : .008

Abbreviations: ACEI, angiotensin-converting enzyme inhibitor; AF, atrial fibrillation; ARBs, angiotensin II receptor blockers; CAD, coronary artery disease; CKD, chronic kidney disease; COPD, chronic obstructive pulmonary disease; DCM, dilated cardiomyopathy; VT, ventricular tachycardia.

and predictors of most common incident tachyarrhythmias (ie atrial fibrillation and ventricular tachycardias) in hospitalized COVID-19 patients. The secondary aim was to verify whether atrial fibrillation and/or ventricular tachycardias were independently associated with ARDS and/or in-hospital mortality. The correlation between the most prevalent arrhythmias and both baseline characteristics and the development of ARDS and in-hospital mortality has been evaluated. ARDS diagnosis was defined according to the Berlin definition.<sup>5</sup>

## 2.1 | Statistical analysis

Distribution of continuous data was tested with the Kolmogorov-Smirnov and the Shapiro-Wilk test. Normally distributed variables were expressed as mean  $\pm$  standard deviation (SD), whereas non-normal distributed ones as median and interquartile range (IQR). Categorical variables were reported as numbers and percentages. The unadjusted (univariable) and adjusted (multivariable) risk ratios (RR) both for incident tachyarrhythmias and the outcomes of interest

were calculated using logistic regression models and presented as RR with their 95% confidence intervals (CI). All independent variables showing a *P* value  $<.1$  for the association with the response variable at univariable analysis were tested in the multivariable model. For all tests, a *P* value  $<.05$  was considered statistically significant. Analyses were performed by using R version 3.5.1 (R Foundation for Statistical Computing, Vienna, Austria).

## 3 | RESULTS

414 hospitalized patients with COVID-19 were included in the present study. The mean age was  $66.9 \pm 15.0$  years; 253 (61.1%) were males. The median follow-up was 28 days (IQR: 12-45). Incident tachyarrhythmias were reported in 90 cases (21.7%). The most frequent incident sustained arrhythmia was AF (N: 71; 17.1%), of which 50 (12.1%) were new-onset and 21 (5.1%) were recurrent, followed by VT (N: 14; 3.4%) and supraventricular arrhythmias (N: 5; 1.2%).

COVID-19 patients who experienced incident AF during the hospitalization were older compared to those without

**TABLE 2** Distribution of patients' characteristics and their association with VT occurrence among COVID-19 study population

	Incident VT free group	Incident VT group	Univariable RR (CI), <i>P</i> value	Multivariable RR (CI), <i>P</i> value
n	400	14		
Male gender, n (%)	245 (61.3)	8 (57.1)	0.85 (0.30, 2.47), <i>P</i> : .757	-
Age (mean (SD))	66.86 (15.06)	69.07 (12.95)	1.01 (0.98, 1.05), <i>P</i> : .588	-
Smoker, n (%)	80 (20.1)	4 (28.6)	1.56 (0.44, 4.33), <i>P</i> : .440	-
Hypertension, n (%)	253 (63.4)	10 (71.4)	1.42 (0.48, 4.65), <i>P</i> : .542	-
Diabetes, n (%)	101 (25.3)	5 (35.7)	1.60 (0.50, 4.30), <i>P</i> : .386	-
Dyslipidaemia, n (%)	111 (27.8)	7 (50.0)	2.46 (0.87, 6.30), <i>P</i> : .081	NS
Obesity, n (%)	27 (12.2)	2 (33.3)	3.38 (0.49, 13.09), <i>P</i> : .149	-
History of AF, n (%)	68 (17.1)	4 (28.6)	1.88 (0.53, 5.12), <i>P</i> : .274	-
Heart Failure, n (%)	44 (11.0)	2 (14.3)	1.33 (0.21, 4.51), <i>P</i> : .704	-
Previous Stroke, n (%)	31 (7.8)	4 (28.6)	4.20 (1.23, 10.20), <i>P</i> : .012	NS
CKD, n (%)	60 (15.1)	4 (28.6)	2.16 (0.61, 5.80), <i>P</i> : .181	-
CAD, n (%)	61 (15.3)	5 (35.7)	2.88 (0.92, 7.22), <i>P</i> : .505	-
COPD, n (%)	85 (21.3)	3 (21.4)	1.01 (0.23, 3.07), <i>P</i> : .991	-
ACEI/ARBs, n (%)	163 (43.7)	7 (50.0)	1.28 (0.44, 3.48), <i>P</i> : .642	-
Ca-Antagonists, n (%)	96 (24.0)	4 (28.6)	1.26 (0.40, 3.92), <i>P</i> : .695	-
Beta-Blockers, n (%)	56 (14.0)	2 (14.3)	1.02 (0.23, 4.45), <i>P</i> : .976	-
Incident AF, n (%)	64 (16.0)	7 (50.0)	1.70 (1.05, 2.74), <i>P</i> : .033	-
New-onset AF, n (%)	47 (11.8)	3 (21.4)	1.98 (0.46, 5.72), <i>P</i> : .284	-
AF recurrence, n (%)	17 (4.2)	4 (28.6)	7.09 (2.20, 15.18), <i>P</i> $<.001$	7.09 (2.20, 15.18), <i>P</i> $<.001$

Abbreviations: ACEI, angiotensin-converting enzyme inhibitor; AF, atrial fibrillation; ARBs, angiotensin II receptor blockers; CAD, coronary artery disease; CKD, chronic kidney disease; COPD, chronic obstructive pulmonary disease; DCM, dilated cardiomyopathy; VT, ventricular tachycardia.



incident AF ( $P < .001$ ) and showed higher prevalence of smoking habit ( $P = .035$ ), hypertension ( $P = .002$ ), history of AF ( $P = .004$ ), heart failure ( $P < .001$ ), chronic kidney disease (CKD,  $P = .034$ ), coronary artery disease (CAD,  $P < .001$ ), angiotensin-converting enzyme inhibitors (ACE-I) and/or angiotensin II receptor blockers (ARBs) use ( $P = .030$ ) and incident VT ( $P = .003$ ); however at multivariate regression model only older age (RR: 1.03;  $P = .002$ ), heart failure (RR: 1.88;  $P = .023$ ), CAD (RR: 1.75;  $P = .024$ ) and incident VT (RR: 2.94,  $P = .008$ ) were associated with increased risk of incident AF (Tables 1-3).

COVID-19 patients who experienced incident VT during the hospitalization showed more frequently history of previous stroke ( $P = .024$ ) and AF recurrence during hospitalization ( $P < .001$ ); however, at multivariate regression model only AF recurrence (RR: 7.09;  $P < .001$ ) was associated with increased risk of incident VT.

During the hospitalization, 132 patients (31.9%) developed ARDS and 104 patients (25.8%) died. COVID-19 patients with ARDS were older ( $70.52 \pm 11.89$  vs  $65.26 \pm 15.97$  years;  $P = .001$ ), more frequently male (70.5% vs 56.7%;  $P = .01$ ) more likely affected by diabetes mellitus (32.6% vs 22.4%;  $P = .037$ ) and CKD (22.0% vs 12.5%;  $P = .02$ ) than those without ARDS. No statistically significant difference in both incident AF (22.7% vs 16.3%;  $P = .15$ ) and VT (3.8% vs 3.2%;  $P = .98$ ) has been found between the two groups (Figure 1). At multivariate regression model, only older age (RR: 1.02;  $P = .001$ ) and male gender (RR: 1.47;  $P = .0006$ ) were significantly associated with increased risk of ARDS.

Not survived COVID-19 patients were older ( $P = .001$ ) and more frequently male ( $P = .02$ ) than those who survived and showed higher prevalence of hypertension ( $P = .001$ ), CKD ( $P = .002$ ), CAD ( $P = .023$ ) and incident

**TABLE 3** Distribution of patients' characteristics and their association with death occurrence among COVID-19 study population

	Survival COVID-19 Group	Deceased COVID-19 Group	Univariable RR (CI), <i>P</i> value	Multivariable RR (CI), <i>P</i> value
n	307	107		
Male gender, n (%)	177 (57.7)	76 (71.0)	1.49 (1.09, 1.96), <i>P</i> : .015	1.63 (1.19, 2.13), <i>P</i> : .004
Age (mean (SD))	65.26 (15.67)	71.75 (11.60)	1.02 (1.01, 1.04), <i>P</i> < .001	1.02 (1.01, 1.04), <i>P</i> : .001
Smoker, n (%)	62 (20.3)	22 (20.6)	1.01 (0.65, 1.46), <i>P</i> : .947	-
Hypertension, n (%)	184 (60.1)	79 (73.8)	1.53 (1.11, 2.00), <i>P</i> : .012	NS
Diabetes, n (%)	74 (24.2)	32 (29.9)	1.23 (0.85, 1.67), <i>P</i> : .244	-
Dyslipidaemia, n (%)	84 (27.5)	34 (31.8)	1.16 (0.81, 1.58), <i>P</i> : .394	-
Obesity, n (%)	20 (11.1)	9 (18.8)	1.57 (0.79, 2.53), <i>P</i> : .163	-
History of AF, n (%)	51 (16.7)	21 (19.6)	1.15 (0.74, 1.64), <i>P</i> : .496	-
Heart Failure, n (%)	29 (9.5)	17 (15.9)	1.49 (0.95, 2.10), <i>P</i> : .073	NS
Previous Stroke, n (%)	26 (8.5)	9 (8.4)	0.99 (0.50, 1.64), <i>P</i> : .970	-
CKD, n (%)	37 (12.1)	27 (25.2)	1.78 (1.27, 2.30), <i>P</i> : .002	1.58 (1.06, 2.15), <i>P</i> : .026
CAD, n (%)	41 (13.4)	25 (23.4)	1.57 (1.09, 2.10), <i>P</i> : .017	NS
COPD, n (%)	63 (20.6)	25 (23.4)	1.12 (0.75, 1.58), <i>P</i> : .546	-
ACEI/ARBs, n (%)	120 (42.6)	50 (47.6)	1.16 (0.83, 1.54), <i>P</i> : .372	-
Ca-Antagonists, n (%)	76 (24.8)	24 (22.4)	0.91 (0.61, 1.35), <i>P</i> : .631	-
Beta-Blockers, n (%)	45 (14.7)	13 (12.1)	0.85 (0.51, 1.41), <i>P</i> : .528	-
VT, n (%)	5 (1.6)	9 (8.4)	2.55 (1.53, 3.35), <i>P</i> : .003	2.55 (1.50, 3.35), <i>P</i> : .003
Incident AF, n (%)	50 (16.3)	21 (19.6)	1.18 (0.76, 1.67), <i>P</i> : .431	-
New-onset AF, n (%)	34 (11.1)	16 (15.0)	1.28 (0.79, 1.85), <i>P</i> : .291	-
AF recurrence, n (%)	16 (5.2)	5 (4.7)	0.92 (0.35, 1.74), <i>P</i> : .827	-

Abbreviations: ACEI, angiotensin-converting enzyme inhibitor; AF, atrial fibrillation; ARBs, angiotensin II receptor blockers; CAD, coronary artery disease; CKD, chronic kidney disease; COPD, chronic obstructive pulmonary disease; DCM, dilated cardiomyopathy; VT, ventricular tachycardia.

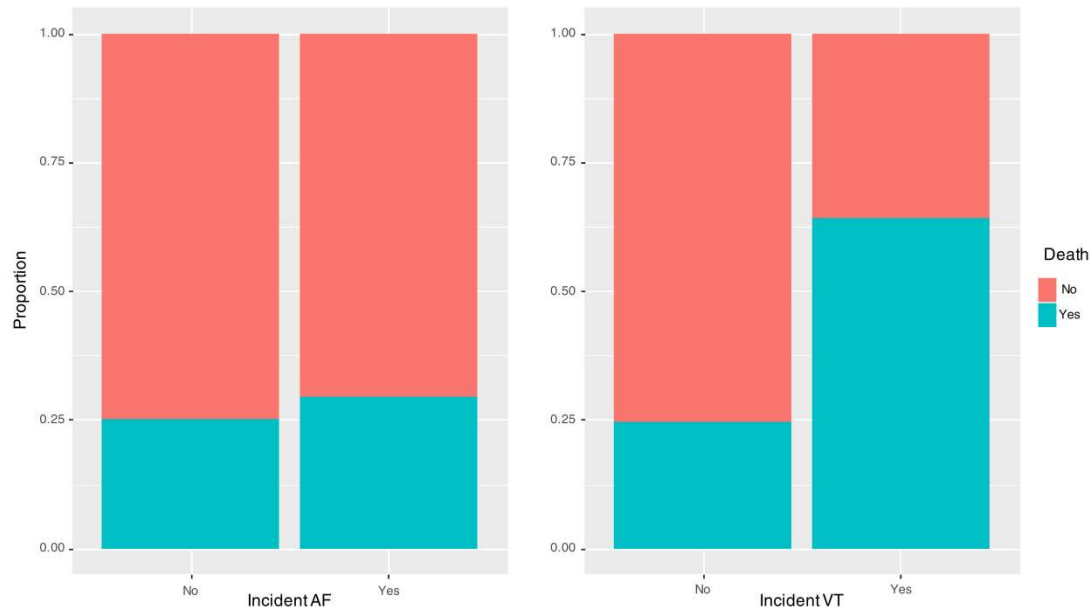


**FIGURE 1** Proportion of incident tachyarrhythmias among survived or not COVID-19 patients

VT ( $P = .002$ ). No statistically significant differences in incident AF (22.7% vs 16.3%;  $P = .15$ ) have been found between the two groups. Age (RR: 1.63;  $P = .004$ ), male gender (RR: 1.02;  $P = .001$ ), CKD (RR: 1.58;  $P = .026$ ) and incident VT (RR: 2.55;  $P = .003$ ) have been found to be strong independent predictors of in-hospital mortality. Figure 2 shows a forest plot visual summary of the results of logistic regression models.

#### 4 | DISCUSSION

The main findings of the present study can be summarized as follows: the incident sustained tachyarrhythmias occur in 21% of our study population including COVID-19 hospitalized patients. AF was the most prevalent arrhythmia accounting for the 18.45% of cases, and its independent predictors were older age, male gender, HF and CAD; moreover,

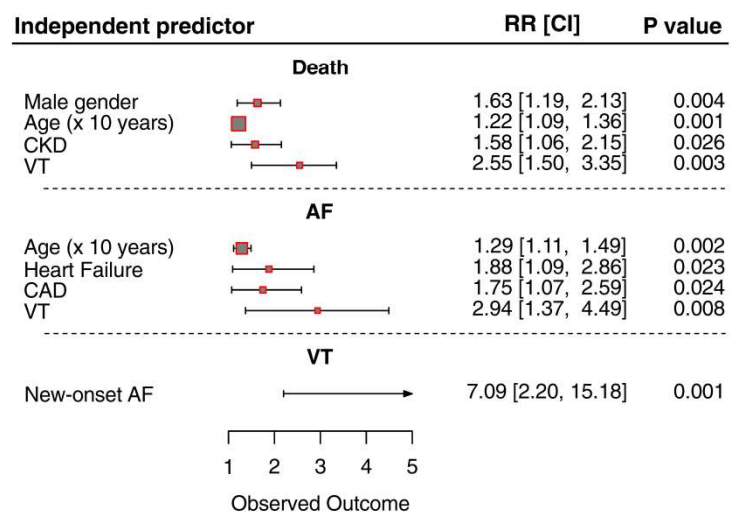


**FIGURE 2** Forest plot visual summary of the results of logistic regression models. AF, atrial fibrillation; CAD, coronary artery disease; CKD, chronic kidney disease; VT, ventricular tachycardia

incident AF was a significantly associated with incident VT. VT occurred in a small percentage of COVID-19 patients (3.4%) and was independently associated with recurrent AF.

Incident AF, both new-onset and recurrent, did not affect the risk of severe adverse events including ARDS and death during hospitalization; in contrast incident sustained VT significantly increased the risk of in-hospital mortality.

There are few and conflicting data about the occurrence of arrhythmias in the context of COVID-19; however, the clinical presentation seems not different from that described in general population.<sup>6</sup> In the cohort study by Wang et al,<sup>7</sup> an arrhythmia has complicated the clinical course of the disease during hospitalization in 16.7% of COVID-19 patients; moreover, arrhythmias were significantly higher in patients receiving intensive care unit (ICU) care than in those not receiving ICU care (44.4% vs 6.9%;  $P < .001$ ); however, specifics about the types and duration of arrhythmias have not been provided. Two recent cohort studies by Bhatla et al<sup>8</sup> and Colon et al<sup>9</sup> showed that the incidence of arrhythmias, such as AF and nonsustained VT, among patients with COVID-19 corresponds to the severity of illness and was not the sole consequence of the viral infection. These results support the hypothesis of the multifactorial pathogenesis of arrhythmias in the clinical context of COVID-19. If on one hand, the direct effect of SARS-CoV-2 on myocardiocytes may lead to myocardial inflammation<sup>10</sup> predisposing per se to cells electrical instability, ischaemia from coronary microvascular disease, gap junction dysfunction and abnormal calcium handling<sup>11</sup>; on the other, the risk of arrhythmia may increase as the severity of the systemic inflammatory response,<sup>12</sup> which determines an imbalance in autonomic tone,<sup>13</sup> hypoxia, metabolic disarray and significant electrolyte disturbances, leading to the instability of underlying chronic cardiovascular diseases. Moreover, some experimental pharmacological treatments currently administered in COVID-19 patients may impact on ventricular repolarization, enhancing the susceptibility to QT-related life-threatening ventricular arrhythmias.<sup>14</sup>

In the present analysis, the incident AF, both new-onset and recurrent, did not influence the clinical outcome of patients with COVID-19 in terms of ARDS developing and survival, differently from what happens in critically ill patients with sepsis among general population.<sup>15</sup> In contrast, the incident VT seems to be a strong independent predictor of in-hospital mortality among COVID-19 patients; to date, VT has not ever been described as mortality predictor in the clinical context of sepsis or viral infection.<sup>16,17</sup> Based on our results, tachyarrhythmias, in particular AF, could complicate the clinical course of COVID-19 during hospitalization and, in case of VT, could worsen the prognosis of infected patients. Thereafter, a careful electrocardiographic monitoring would be advisable in COVID-19 patients to early detect incident tachyarrhythmias that, even though not matching

the apparent disease status, might be a red flag of worsening disease. The present study has several limitations: the retrospective nature of the analysis; our limited ability to detect subclinical arrhythmias; the heterogeneity in the characteristics of the different wards where the study patients were hospitalized; and the relatively high number of covariates tested in the regression models in relation of the number of patients. Furthermore, some potential confounders could have been not considered in our analysis that was restricted on available data. Larger multicenter prospective studies are required to confirm our preliminary findings.

## 5 | CONCLUSION

Incident sustained tachyarrhythmias represent a not rare complication of COVID-19. Among them, AF is the more frequent; however, it not seems associated with ARDS development and death. On the other hand, incident VT is a not frequent but independent predictor of in-hospital mortality among hospitalized COVID-19 patients. The careful electrocardiographic monitoring would be advisable in COVID-19 patients to optimize the clinical management of the disease.

## CONFLICT OF INTEREST

No Conflict of Interest.

## ORCID

Vincenzo Russo  <https://orcid.org/0000-0002-9227-0360>

Marco Di Maio  <https://orcid.org/0000-0001-8665-9890>

Filiberto Fausto Mottola  <https://orcid.org/0000-0002-6066-5384>

## REFERENCES

1. Hui DS, I Azhar E, Madani TA, et al. novel coronavirus outbreak in Wuhan, China. *Int J Infect Dis*. 2019;2020(91):264-266.
2. World Health Organization Coronavirus disease (COVID-19). Situation Report—146. [https://www.who.int/docs/default-source/coronaviruse/situation-reports/20200614-covid-19-sitrep-146.pdf?sfvrsn=5b89bdad\\_4](https://www.who.int/docs/default-source/coronaviruse/situation-reports/20200614-covid-19-sitrep-146.pdf?sfvrsn=5b89bdad_4). Accessed June 14, 2020.
3. Richardson S, Hirsch JS, Narasimhan M, et al. Presenting characteristics, comorbidities, and outcomes among 5700 patients hospitalized with COVID-19 in the New York City area. *JAMA*. 2020;323(20):2052-2059.
4. Russo V, Bottino R, Carbone A, et al. COVID-19 and heart: from clinical features to pharmacological implications. *J Clin Med*. 2020;9(6):1944.
5. Ranieri VM, Rubenfeld GD, Thompson BT, et al. ARDS Definition Task Force. Acute respiratory distress syndrome: the Berlin Definition. *JAMA*. 2012;307(23):2526-2533.
6. Chen C, Chen C, Yan JT, Zhou N, Zhao JP, Wang DW. Analysis of myocardial injury in patients with COVID-19 and association between concomitant cardiovascular diseases and severity of COVID-19. *Zhonghua Xin Xue Guan Bing Za Zhi*. 2020;48(0):E008.



7. Wang D, Hu B, Hu C, et al. Clinical characteristics of 138 hospitalized patients with 2019 novel coronavirus-infected pneumonia in Wuhan, China. *JAMA*. 2020;323(11):1061-1069.
8. Bhatla A, Mayer MM, Adusumalli S, et al. COVID-19 and Cardiac Arrhythmias [published online ahead of print, 2020 Jun 20]. *Heart Rhythm*. 2020;17(9):1439-1444.
9. Colon Chad M, Barrios James G, Chiles Joe W, et al. Atrial Arrhythmias in COVID-19 Patients. *JACC: Clinical Electrophysiology*. 2020; <http://dx.doi.org/10.1016/j.jacep.2020.05.015>
10. Inciardi RM, Lupi L, Zaccone G, et al. Cardiac involvement in a patient with coronavirus disease 2019 (COVID-19). *JAMA Cardiol*. 2020;5(7):819.
11. Peretto G, Sala S, Rizzo S, et al. Arrhythmias in myocarditis: state of the art. *Heart Rhythm*. 2019;16:793-801.
12. Shahreyar M, Fahhoum R, Akinseye O, Bhandari S, Dang G, Khouzam RN. Severe sepsis and cardiac arrhythmias. *Ann Transl Med*. 2018;6:6.
13. Werdan K, Schmidt H, Ebelt H, et al. Impaired regulation of cardiac function in sepsis, SIRS, and MODS. *Can J Physiol Pharmacol*. 2009;87:266-274.
14. Lazzarini PE, Boutjdir M, Capecchi PL. COVID-19, arrhythmic risk and inflammation: mind the gap!. *Circulation*. 2020;142(1):7-9.
15. Salman S, Bajwa A, Gajic O, Afessa B. Paroxysmal atrial fibrillation in critically ill patients with sepsis. *J Intensive Care Med*. 2008;23(3):178-183.
16. Yang J, Zheng Y, Gou X, et al. Prevalence of comorbidities and its effects in patients infected with SARS-CoV-2: a systematic review and meta-analysis. *Int J Infect Dis*. 2020;94:91-95. <http://dx.doi.org/10.1016/j.ijid.2020.03.017>
17. Ruan Q, Yang K, Wang W, Jiang L, Song J. Clinical predictors of mortality due to COVID-19 based on an analysis of data of 150 patients from Wuhan, China. *Intensive Care Med*. 2020;3:1-3.

**How to cite this article:** Russo V, Di Maio M, Mottola F, et al. Clinical characteristics and prognosis of hospitalized COVID-19 patients with incident sustained tachyarrhythmias: A multicenter observational study. *Eur J Clin Invest*. 2020;00:e13387. <https://doi.org/10.1111/eci.13387>

## Part III

### Unusual echocardiographic findings



# CHAPTER 7

Journal of Geriatric Cardiology (2018) 15: 244–245  
©2018 JGC All rights reserved; www.jgc301.com



Letter to the Editor

• Open Access •

## Mitral pseudostenosis due to a large left atrial myxoma

Konstantinos C Theodoropoulos\*, Giovanni Masoero, Gianpiero Pagnano, Nicola Walker, Alexandros Papachristidis, Mark J Monaghan

Department of Cardiology, King's College Hospital NHS Foundation Trust, King's College London, London, UK

J Geriatr Cardiol 2018; 15: 244–245. doi:10.11909/j.issn.1671-5411.2018.03.009

**Keywords:** Mitral stenosis; Myxoma; Transesophageal echocardiography

Myxomas are benign cardiac tumours that are mostly (75%) located in the left atrium, but they also can be found in the right atrium (15%–20%), in the right ventricle (4%) and in the left ventricle (3%).<sup>[1]</sup>

A 71-year-old male presented to a district hospital with

exertional dyspnea, orthopnea, postural dizziness and significant weight loss over the last year. He had no known previous cardiac history and from his medical history he had only hypertension and diabetes. A transthoracic echocardiogram showed a large mass in the left atrium (Figure 1A),

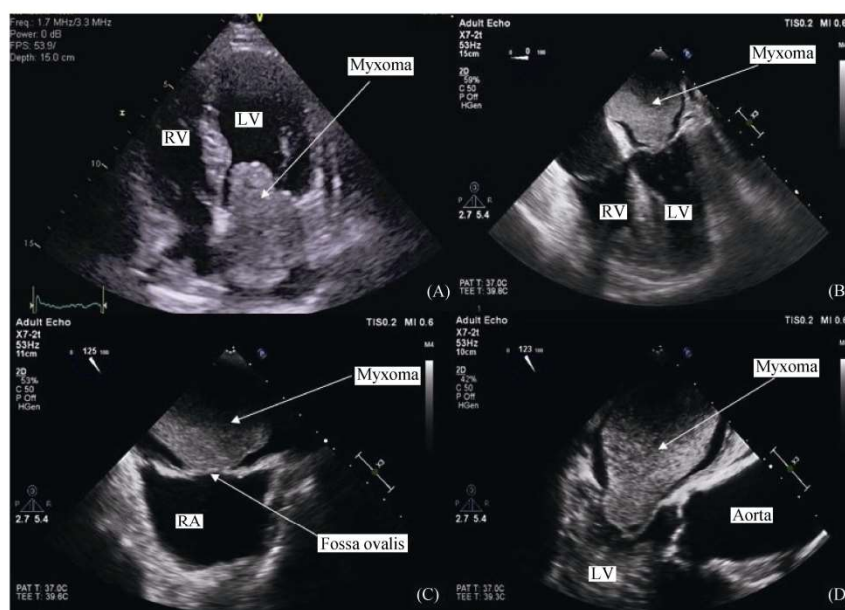


**Figure 1.** Echocardiographic assessment of atrial myxoma. (A): Transthoracic echocardiogram, apical four chambers view in diastole, showing the myxoma in the left atrium, protruding in the left ventricle through the mitral valve; (B): TEE, mid-esophageal four chambers view in systole, showing the myxoma in the left atrium; (C): TEE, mid-esophageal bicaval view showing the myxoma in the left atrium attached to the fossa ovalis; (D): TEE, mid-esophageal long axis view in early diastole, showing the myxoma in the left atrium whilst starting to protrude in the left ventricle through the mitral valve. LV: left ventricle; RA: right atrium; RV: right ventricle; TEE: transesophageal echocardiogram.

\*Correspondence to: ktheod2005@hotmail.com

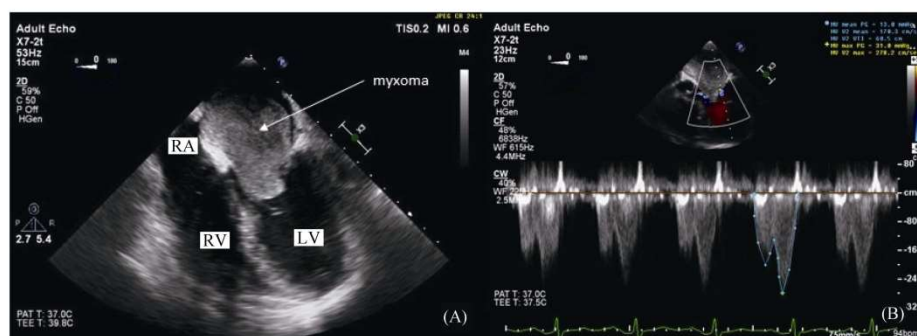


**Figure 2.** Doppler and 2D assessment of mitral pseudostenosis. (A): TEE, mid-esophageal four chambers view in diastole, showing the myxoma in the left atrium, which protrudes in the left ventricle through the mitral valve; (B): continuous wave Doppler through the mitral valve in the mid-esophageal four chambers view showing a mean pressure gradient of 13 mmHg. LV: left ventricle; RA: right atrium; RV: right ventricle; TEE: transesophageal echocardiogram.

otherwise the rest of the study was unremarkable. The patient was transferred to our tertiary centre for prompt resection of a possible left atrial myxoma. The pre-operative transesophageal echocardiogram demonstrated the large mass filling the whole left atrium with measured dimensions of 7.2 cm and 4.5 cm (Figure 1B). It was attached on the left side of the fossa ovalis (Figure 1C) and was protruding during the diastole through the mitral valve into the left ventricle (Figures 1D, 2A). This was causing mitral pseudostenosis with a mean pressure gradient of 13 mmHg, suggesting severe mitral stenosis (Figure 2B). The mitral valve leaflets were intact and only trace mitral regurgitation was detected. The mass and part of the interatrial septum were surgically removed and sent to histopathology. The interatrial septum was repaired with an oval bovine pericardial patch. The post-operative transesophageal echocardiogram showed no interatrial communication or significant mitral regurgitation. The histopathology report confirmed the diagnosis of a myxoma and the patient had an uneventful recovery.

Myxomas, as already been mentioned are benign cardiac tumours, and their size varies. They can have a diameter that ranges between 1–15 cm. Their clinical features are determined by their size, location and mobility.<sup>[1,2]</sup> Most symptomatic patients will have findings from the classic triad of intracardiac obstruction, embolism and constitutional symptoms.<sup>[1]</sup> The obstructive findings (dizziness, dyspnea, cough, pulmonary edema and heart failure) can occur due to atrio-ventricular valve obstruction. Our patient's symptoms were caused by the obstruction of the mitral valve from the

myxoma during the diastolic phase of the cardiac cycle. This can result the 'pseudostenosis' of a structurally normal mitral valve. Embolic phenomena can affect the pulmonary or the systemic circulation, depending on the tumour location and the existence of interatrial communication. The constitutional symptoms (weight loss, fever, myalgia, arthralgia, Raynaud syndrome) are mainly attributed to the secretion of interleukin-6 by the myxoma tumour cells.<sup>[3]</sup> Small myxomas can be asymptomatic and are incidentally found with echocardiography or other imaging modalities. The only acceptable therapy for cardiac myxomas is the prompt surgical resection in order to eliminate the risk of embolization. The overall risk for recurrence of a myxoma after resection is 2%–13%, thus it is recommended semi-annual follow-up with echocardiography for at least a period of four years after resection.<sup>[1,4]</sup>

## References

- 1 Bruce CJ. Cardiac tumours: diagnosis and management. *Heart* 2011; 97: 151–160.
- 2 El Sabbagh A, Al-Hijji MA, Thaden JJ, *et al.* Cardiac myxoma: the great mimicker. *JACC Cardiovasc Imaging* 2017; 10: 203–206.
- 3 Endo A, Ohtahara A, Kinugawa T, *et al.* Characteristics of cardiac myxoma with constitutional signs: a multicenter study in Japan. *Clin Cardiol* 2002; 25: 367–370.
- 4 Elbardissi AW, Dearani JA, Daly RC, *et al.* Survival after resection of primary cardiac tumors: a 48-year experience. *Circulation* 2008; 118: S7–S15.

## CHAPTER 8

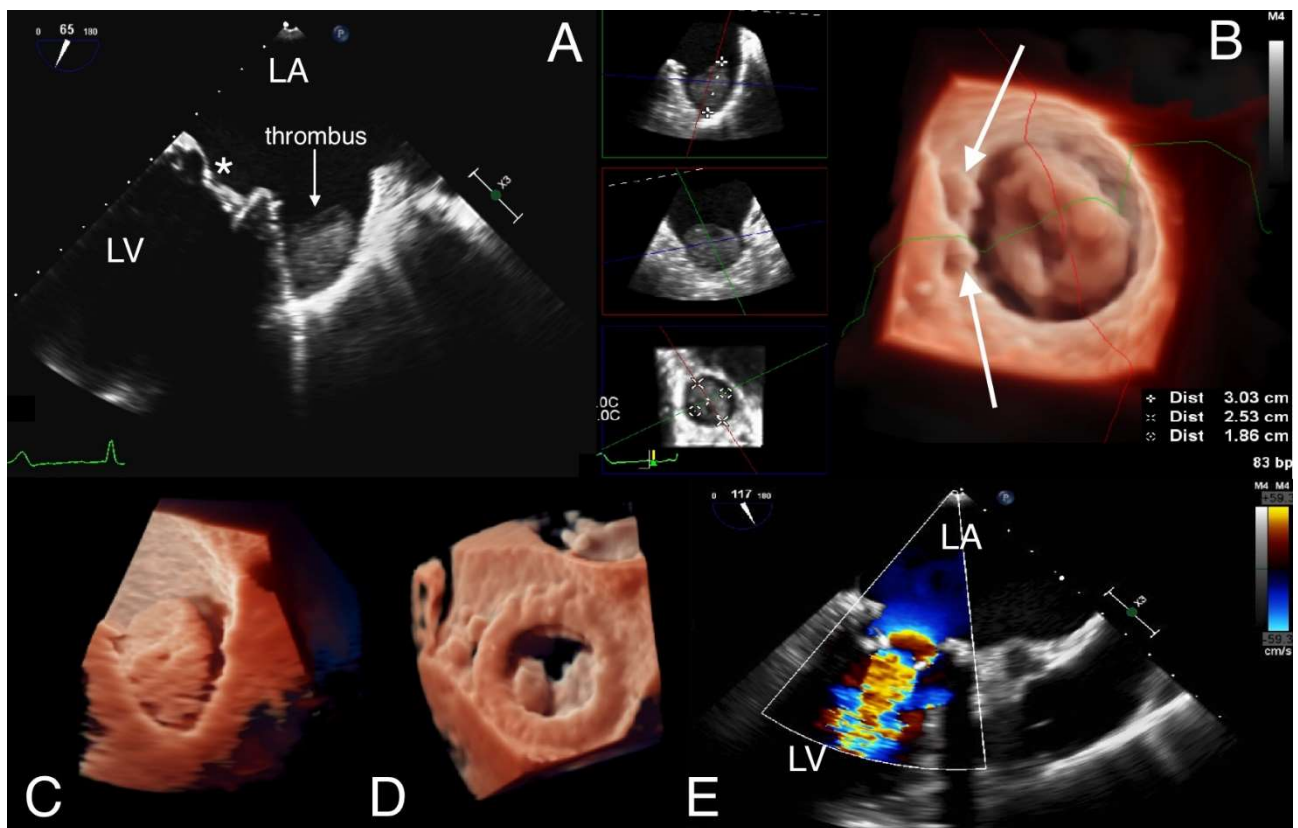
### **Unexpected Thrombus in a previously closed left atrial appendage**

Michael Papitsas, **Gianpiero Pagnano**, Mark J Monaghan

A 64-year-old female was referred to cardiology for progressive dyspnea on exertion. Her previous medical history included a tissue mitral valve replacement (tMVR) for rheumatic mitral stenosis 8 years ago. At the same time left atrial appendage (LAA) ligation was performed, due to permanent atrial fibrillation (AF) and intolerance to vitamin K antagonists and low molecular weight heparin. Recently, she was diagnosed with an acute left leg arterial thrombosis with spontaneous resolution of thrombus. On physical examination a low frequency diastolic murmur was identified, and transthoracic Echocardiography (TTE) demonstrated increased pressure gradient across the mitral bioprosthesis (mean gradient 13mmHg). A transoesophageal echocardiogram (TOE) was performed to further assess the prosthetic valve. It showed a degenerated bioprosthesis with thickened and restricted valve leaflets (Panel E, 2D TOE Colour Doppler & D, 3D TOE† valve in open position) (see also Supplementary data online, Movies S1), and surprisingly a large thrombus in the LAA, which had free communication with the left atrium (LA) despite previous ligation. (Panel A, 2D TOE, arrow & C, 3D TOE†, asterisk shows tMVR) The thrombus was measured 30mm x 25mm x 19mm in 3D multi-planar reconstruction. (Panel

B, 3D TOE† multi-planar reconstruction, arrows showing ruptured sutures)  
 (see also Supplementary data online, Movies S2, S3) Anticoagulation was commenced and three months later, a repeat TOE demonstrated complete resolution of the LAA clot. The degenerated valve was treated with transapical valve-in-valve implantation, resulting in dramatic improvement of patient's breathlessness. A follow-up echocardiogram confirmed normal functioning prosthetic valve.

(†) All 3D processed with TrueVue visualization technique, Philips®, Andover, MA



## CHAPTER 9

### **Differential diagnosis of a mass attached to mechanical mitral valve.**

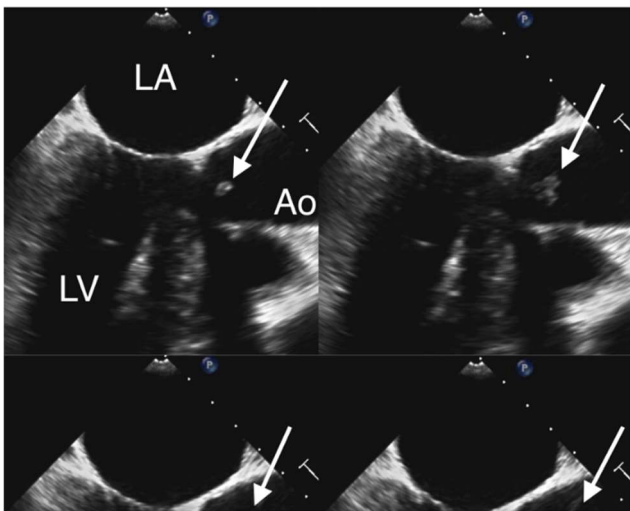
Michael Papitsas, **Gianpiero Pagnano**, Mark J Monaghan, Alexandros Papachristidis

A 47-year-old male transferred to our hospital for assessment by the cardiothoracic surgeons due to a mobile mass on his mechanical aortic valve that was found to be increasing in size. The patient was admitted in his local hospital after a routine transthoracic echocardiogram (TTE) that revealed a mobile structure on the aortic side of a well-functioning aortic prosthesis. There was no clinical or biochemical evidence of infective endocarditis, so on the grounds of low INR level it was considered to be likely a thrombus. The oral anticoagulation dose was increased, and intravenous heparin was added till the target INR level was achieved. Despite that, in repeated transoesophageal echocardiograms (TOE) the mass appeared to grow in size from 7 to 9mm within ten days. During a multidisciplinary team meeting in our hospital, decision was made to continue anticoagulation and repeat a TOE for further assessment of the mass. A very focused and meticulous study unveiled that what appeared as a mass was actually a cluster of microbubbles that subsequently disperse away from the valve to smaller particles (Panel A, 2D-TOE, arrows). It appears after the closing of the valve (Panel B, 3D-TOE, arrow) (see also Supplementary data online, Videos S1),

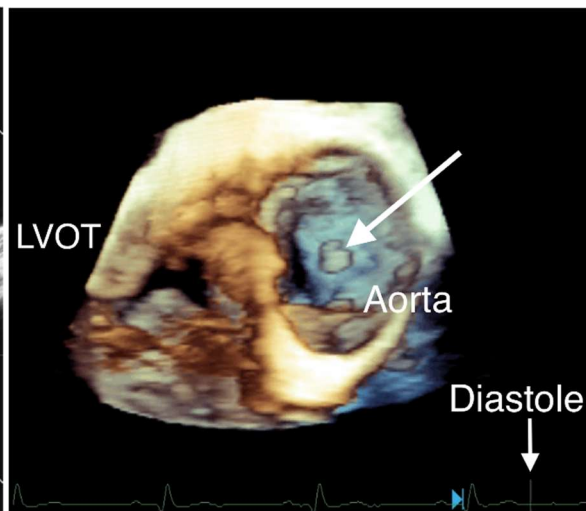


it is not attached anywhere and the aortic prosthesis function is not affected. Microbubble formation has been associated with mechanical prosthetic valves but usually appear as multiple small, less than 1mm, highly mobile echoes. This is a rare case where they imitate a much bigger mass and can easily deceive even experienced operators and lead to misdiagnosis. The patient was discharged with the recommendation for better control of his anticoagulation treatment.

Panel A



Panel B



## Part IV

### Discussion and Conclusions

## **Discussion and Conclusions:**

In addition to the known advantages offered by 3D Echocardiography on the assessment of the cardiac structures, our data support the hypothesis that 3D Echocardiography allows a better evaluation of the ascending aorta compared to the 2D Echocardiography (Chapter 2). In fact, 3D Echocardiography also allows the evaluation of other diameters apart from the anteroposterior. Moreover, it allows to avoid the underestimation of the diameter due to a non-correct alignment of a 2D plane on an oblique section of the aorta. A few studies in the recent past have tried to study the application of 3D Echocardiography to the aorta mainly in paediatric populations that are easier to assess (19). However, it should be noted that differently from other multiplanar techniques, 3D Echocardiography does not allow the visualization of the entire ascending aorta due to acoustic impedance of the chest wall. Akdogan et al. have tried to overcome the difficulties in the assessment of the whole ascending aorta by using the right parasternal approach which has given better results but was possible only in 67% of their study population (95). A limitation of our study is that we did not compare Echocardiography to “gold standard” techniques, such as angio-CT scan. This limitation does not allow to draw conclusions about the diagnostic accuracy of the 3D measurements. For this reason, it would be useful in the future to compare 3D Echocardiography with the other multiplanar techniques (CT and MR) in the assessment of aortic dilatation.



3D Echocardiography has had an important impact in the development of transcatheter structural heart intervention. 3D Echocardiography is fundamental during Percutaneous Transcatheter Edge-to-Edge MitraClip implantation and it is used also to assess TAVI implantation and follow-up (12). Another application for 3D Echo can be the LAA closure in patients with chronic atrial fibrillation and contraindication to oral anticoagulation. In the most recent guidelines for management of atrial fibrillation is suggested that due to the large introduction in clinical practise of the Direct Oral Anticoagulants, it may be necessary to compare the outcome of low dose anticoagulation in these patients with the implant of a LAA closure device. Shah et al. have published an initial study in 2008 demonstrating the accuracy of 3D echocardiography in the assessment of the LAA anatomy (96). A few studies since then have explored the accuracy of 3D echo measurements for LAA anatomy and after that for the guidance of the first LAA closure devices.

This study (Chapter 3) provides evidence that 3D transesophageal Echocardiography is more accurate than two-dimensional transesophageal Echocardiography in supporting LAA percutaneous closure procedure. Other multi-planar techniques have been shown to give an accurate assessment of LAA shape, however, 3D transesophageal Echocardiography should be preferred since it can provide accurate measurements without requiring exposure to ionizing radiation or contrast administration (26, 27).

Limitation of this study could be the small sample size, the lack of a second cohort where 3D was used as a preferred method to determine the size of the device and determine the outcome of the procedure in these cases. More data is necessary in order to compare all multi-planar modalities with a larger sample size.

The rapid technological advancement of the ultrasound machines and the software for analysis of the datasets will improve the quality of the analysis and acquisition of the images, increasing the diagnostic accuracy of the 3D measurements further increasing the already wide applications of 3D Echocardiography.

The study of the ascending aorta is an example of how 3D Echocardiography technological progress can lead to reduction of the costs and amount of ionizing radiations necessary to follow-up patients with cardiac pathologies. This progress is also opening new prospective on the transcatheter structural heart intervention alongside making the current ones more accurate and reducing the intraoperative complications.

In the study in chapter 4 we showed how the use of 3D echocardiography can also be applied to myocardial scars allowing an assessment of the volume of the scar using an optimal image setting for a high contrast ratio. Even if this study was mainly performed with in vitro models, an initial evaluation on a selected small population shows how this can also be applied to patients with optimal acoustic windows. More studies and larger populations are required

to further investigate the accuracy of 3D echocardiography in the evaluation of myocardial scar when compared to the “gold standard” cardiac magnetic resonance.

The second part of this thesis was focused on the definition of the cardiac involvement in Covid-19 patients. None of the patients, including those with increased troponin, showed signs of left systolic impairment. It should be noted that myocardial involvement cannot be completely ruled out with echocardiogram. Other techniques, including magnetic resonance, could help better defining myocardial involvement in SARS-CoV-2. Covid 19-induced ARDS was associated with early and pronounced right ventricular-arterial uncoupling (Chapter 4), and its non-invasive echocardiographic assessment by the TAPSE/PASP ratio added significantly and independently to the prognostic relevance of the PaO<sub>2</sub>/FIO<sub>2</sub> ratio in enrolled patients. In a multicenter study (Chapter 5) the analysis of cardiac involvement of Covid-19 patients was focused on the tachyarrhythmias. The most represented arrhythmias in these patients were atrial fibrillation and ventricular tachycardia. Only ventricular tachycardia showed statistically significant relationship with mortality.

These studies show that cardiac involvement in Covid-19 patients is present but still under definition with myocardial injury suggested by increased Troponin I levels without clear left ventricular involvement. Right side involvement is present with TAPSE/PASP ratio being a potential prognostic

factor for the follow-up of these patients. Despite being frequent atrial fibrillation has not a negative prognostic value while ventricular tachycardia in a minority of patients predict a worse outcome.

The last part of the thesis shows how 3D Echocardiography can be applied to single interesting cases allowing a better definition of the cardiac structures and thus improving the diagnostic process in those patients where standard cardiac imaging does not give enough information. Even though case reports are of limited scientific value, these articles confirm the importance of 3D Echocardiography in different clinical settings.

## **Bibliography**

1. Alfakih K, Reid S, Jones T, Sivananthan M. Assessment of ventricular function and mass by cardiac magnetic resonance imaging. *Eur Radiol.* 2004;14(10):1813-22.
2. Ioannidis JP, Trikalinos TA, Dantas PG. Electrocardiogram-gated single-photon emission computed tomography versus cardiac magnetic resonance imaging for the assessment of left ventricular volumes and ejection fraction: a meta-analysis. *J Am Coll Cardiol.* 2002;39(12):2059-68.
3. Mesquita CT, Pessoa MC, Vasconcelos PP, Oliveira Júnior AC, Dohmann HF, Reis AG, et al. Ventricular function following coronary artery bypass grafting: comparison between gated SPECT and cardiac magnetic resonance imaging. *Arq Bras Cardiol.* 2009;92(5):327-33, 44-50, 57-63.
4. Pennell DJ. Ventricular volume and mass by CMR. *J Cardiovasc Magn Reson.* 2002;4(4):507-13.
5. Jenkins C, Bricknell K, Chan J, Hanekom L, Marwick TH. Comparison of two- and three-dimensional echocardiography with sequential magnetic resonance imaging for evaluating left ventricular volume and ejection fraction over time in patients with healed myocardial infarction. *Am J Cardiol.* 2007;99(3):300-6.

6. Mannaerts HF, Van Der Heide JA, Kamp O, Papavassiliu T, Marcus JT, Beek A, et al. Quantification of left ventricular volumes and ejection fraction using freehand transthoracic three-dimensional echocardiography: comparison with magnetic resonance imaging. *J Am Soc Echocardiogr*. 2003;16(2):101-9.
7. Jenkins C, Moir S, Chan J, Rakhit D, Haluska B, Marwick TH. Left ventricular volume measurement with echocardiography: a comparison of left ventricular opacification, three-dimensional echocardiography, or both with magnetic resonance imaging. *Eur Heart J*. 2009;30(1):98-106.
8. Lang RM, Badano LP, Mor-Avi V, Afilalo J, Armstrong A, Ernande L, et al. Recommendations for cardiac chamber quantification by echocardiography in adults: an update from the American Society of Echocardiography and the European Association of Cardiovascular Imaging. *J Am Soc Echocardiogr*. 2015;28(1):1-39.e14.
9. Moustafa SE, Chandrasekaran K, Khandheria B, Tajik J, Mookadam F. Real-time three-dimensional transesophageal echocardiography assessment of the mitral valve: perioperative advantages and game-changing findings. *J Heart Valve Dis*. 2011;20(2):114-22.
10. Papachristidis A, Galli E, Geleijnse ML, Heyde B, Alessandrini M, Barbosa D, et al. Standardized Delineation of Endocardial Boundaries in Three-Dimensional Left Ventricular Echocardiograms. *J Am Soc Echocardiogr*. 2017;30(11):1059-69.

11. Papachristidis A, Papitsas M, Roper D, Wang Y, Dworakowski R, Byrne J, et al. Three-Dimensional Measurement of Aortic Annulus Dimensions Using Area or Circumference for Transcatheter Aortic Valve Replacement Valve Sizing: Does It Make a Difference? *J Am Soc Echocardiogr*. 2017;30(9):871-8.
12. Katz WE, Conrad Smith AJ, Crock FW, Cavalcante JL. Echocardiographic evaluation and guidance for MitraClip procedure. *Cardiovasc Diagn Ther*. 2017;7(6):616-32.
13. Asmarats L, Puri R, Latib A, Navia JL, Rodés-Cabau J. Transcatheter Tricuspid Valve Interventions: Landscape, Challenges, and Future Directions. *J Am Coll Cardiol*. 2018;71(25):2935-56.
14. Faza NN, Little SH. Role of 3-dimensional transesophageal echocardiography in guiding transcatheter mitral valve replacement. *Echocardiography*. 2020;37(6):945-53.
15. Chowdhury R, Boorla VS, Maranas CD. Computational biophysical characterization of the SARS-CoV-2 spike protein binding with the ACE2 receptor and implications for infectivity. *Comput Struct Biotechnol J*. 2020;18:2573-82.
16. Zhou F, Yu T, Du R, Fan G, Liu Y, Liu Z, et al. Clinical course and risk factors for mortality of adult inpatients with COVID-19 in Wuhan, China: a retrospective cohort study. *Lancet*. 2020;395(10229):1054-62.

17. Goldstein SA, Evangelista A, Abbara S, Arai A, Asch FM, Badano LP, et al. Multimodality imaging of diseases of the thoracic aorta in adults: from the American Society of Echocardiography and the European Association of Cardiovascular Imaging: endorsed by the Society of Cardiovascular Computed Tomography and Society for Cardiovascular Magnetic Resonance. *J Am Soc Echocardiogr*. 2015;28(2):119-82.
18. Evangelista A, Aguilar R, Cuellar H, Thomas M, Laynez A, Rodríguez-Palomares J, et al. Usefulness of real-time three-dimensional transoesophageal echocardiography in the assessment of chronic aortic dissection. *Eur J Echocardiogr*. 2011;12(4):272-7.
19. Noel CV, Choy RM, Lester JR, Soriano BD. Accuracy of matrix-array three-dimensional echocardiographic measurements of aortic root dilation and comparison with two-dimensional echocardiography in pediatric patients. *J Am Soc Echocardiogr*. 2012;25(3):287-93.
20. Bleakley C, Eskandari M, Monaghan M. 3D transoesophageal echocardiography in the TAVI sizing arena: should we do it and how do we do it? *Echo Res Pract*. 2017;4(1):R21-r32.
21. Meijboom LJ, Groenink M, van der Wall EE, Romkes H, Stoker J, Mulder BJ. Aortic root asymmetry in marfan patients; evaluation by magnetic resonance imaging and comparison with standard echocardiography. *Int J Card Imaging*. 2000;16(3):161-8.



22. Lansac E, Lim HS, Shomura Y, Lim KH, Rice NT, Goetz WA, et al. Aortic root dynamics are asymmetric. *J Heart Valve Dis.* 2005;14(3):400-7.
23. Bauer M, Glicch V, Siniawski H, Hetzer R. Configuration of the ascending aorta in patients with bicuspid and tricuspid aortic valve disease undergoing aortic valve replacement with or without reduction aortoplasty. *J Heart Valve Dis.* 2006;15(5):594-600.
24. Hindricks G, Potpara T, Dagres N, Arbelo E, Bax JJ, Blomström-Lundqvist C, et al. 2020 ESC Guidelines for the diagnosis and management of atrial fibrillation developed in collaboration with the European Association of Cardio-Thoracic Surgery (EACTS). *Eur Heart J.* 2020.
25. Blackshear JL, Odell JA. Appendage obliteration to reduce stroke in cardiac surgical patients with atrial fibrillation. *Ann Thorac Surg.* 1996;61(2):755-9.
26. Yosefy C, Laish-Farkash A, Azhibekov Y, Khalameizer V, Brodtkin B, Katz A. A New Method for Direct Three-Dimensional Measurement of Left Atrial Appendage Dimensions during Transesophageal Echocardiography. *Echocardiography.* 2016;33(1):69-76.
27. Nucifora G, Faletra FF, Regoli F, Pasotti E, Pedrazzini G, Moccetti T, et al. Evaluation of the left atrial appendage with real-time 3-dimensional

- transesophageal echocardiography: implications for catheter-based left atrial appendage closure. *Circ Cardiovasc Imaging*. 2011;4(5):514-23.
28. Zhou Q, Song H, Zhang L, Deng Q, Chen J, Hu B, et al. Roles of real-time three-dimensional transesophageal echocardiography in peri-operation of transcatheter left atrial appendage closure. *Medicine (Baltimore)*. 2017;96(4):e5637.
  29. Meier B, Blaauw Y, Khattab AA, Lewalter T, Sievert H, Tondo C, et al. EHRA/EAPCI expert consensus statement on catheter-based left atrial appendage occlusion. *Europace*. 2014;16(10):1397-416.
  30. Eng MH, Wang DD, Greenbaum AB, Gheewala N, Kupsky D, Aka T, et al. Prospective, randomized comparison of 3-dimensional computed tomography guidance versus TEE data for left atrial appendage occlusion (PRO3DLAAO). *Catheter Cardiovasc Interv*. 2018;92(2):401-7.
  31. Schmidt-Salzmann M, Meincke F, Kreidel F, Spangenberg T, Ghanem A, Kuck KH, et al. Improved Algorithm for Ostium Size Assessment in Watchman Left Atrial Appendage Occlusion Using Three-Dimensional Echocardiography. *J Invasive Cardiol*. 2017;29(7):232-8.
  32. Saw J, Fahmy P, Spencer R, Prakash R, McLaughlin P, Nicolaou S, et al. Comparing Measurements of CT Angiography, TEE, and Fluoroscopy of the Left Atrial Appendage for Percutaneous Closure. *J Cardiovasc Electrophysiol*. 2016;27(4):414-22.

33. Budge LP, Shaffer KM, Moorman JR, Lake DE, Ferguson JD, Mangrum JM. Analysis of in vivo left atrial appendage morphology in patients with atrial fibrillation: a direct comparison of transesophageal echocardiography, planar cardiac CT, and segmented three-dimensional cardiac CT. *J Interv Card Electrophysiol*. 2008;23(2):87-93.
34. Patel AR, Fatemi O, Norton PT, West JJ, Helms AS, Kramer CM, et al. Cardiac cycle-dependent left atrial dynamics: implications for catheter ablation of atrial fibrillation. *Heart Rhythm*. 2008;5(6):787-93.
35. Spencer RJ, DeJong P, Fahmy P, Lempereur M, Tsang MYC, Gin KG, et al. Changes in Left Atrial Appendage Dimensions Following Volume Loading During Percutaneous Left Atrial Appendage Closure. *JACC Cardiovasc Interv*. 2015;8(15):1935-41.
36. Wu E, Ortiz JT, Tejedor P, Lee DC, Bucciarelli-Ducci C, Kansal P, et al. Infarct size by contrast enhanced cardiac magnetic resonance is a stronger predictor of outcomes than left ventricular ejection fraction or end-systolic volume index: prospective cohort study. *Heart*. 2008;94(6):730-6.
37. Bello D, Fieno DS, Kim RJ, Pereles FS, Passman R, Song G, et al. Infarct morphology identifies patients with substrate for sustained ventricular tachycardia. *J Am Coll Cardiol*. 2005;45(7):1104-8.
38. Cheong BY, Muthupillai R, Wilson JM, Sung A, Huber S, Amin S, et al. Prognostic significance of delayed-enhancement magnetic resonance

imaging: survival of 857 patients with and without left ventricular dysfunction. *Circulation*. 2009;120(21):2069-76.

39. Dawson DK, Hawlisch K, Prescott G, Roussin I, Di Pietro E, Deac M, et al. Prognostic role of CMR in patients presenting with ventricular arrhythmias. *JACC Cardiovasc Imaging*. 2013;6(3):335-44.
40. Rasmussen S, Corya BC, Feigenbaum H, Knoebel SB. Detection of myocardial scar tissue by M-mode echocardiography. *Circulation*. 1978;57(2):230-7.
41. Montant P, Chenot F, Goffinet C, Poncelet A, Vancraeynest D, Pasquet A, et al. Detection and quantification of myocardial scars by contrast-enhanced 3D echocardiography. *Circ Cardiovasc Imaging*. 2010;3(4):415-23.
42. Gaibazzi N, Bianconcini M, Marziliano N, Parrini I, Conte MR, Siniscalchi C, et al. Scar Detection by Pulse-Cancellation Echocardiography: Validation by CMR in Patients With Recent STEMI. *JACC Cardiovasc Imaging*. 2016;9(11):1239-51.
43. Szabo TL. 12 - NONLINEAR ACOUSTICS AND IMAGING. In: Szabo TL, editor. *Diagnostic Ultrasound Imaging*. Burlington: Academic Press; 2004. p. 381-427.
44. Chen W, Wang P, Zhang Z, Deng X, Zhang C, Ju S. Nonlinear ultrasonic imaging in pulse-echo mode using Westervelt equation: a

preliminary research. *Comput Assist Surg* (Abingdon). 2019;24(sup2):54-61.

45. Prieur F, Johansen TF, Holm S, Torp H. Fast simulation of second harmonic ultrasound field using a quasi-linear method. *J Acoust Soc Am*. 2012;131(6):4365-75.
46. Varray F, Basset O, Tortoli P, Cachard C. Extensions of nonlinear B/A parameter imaging methods for echo mode. *IEEE Trans Ultrason Ferroelectr Freq Control*. 2011;58(6):1232-44.
47. Toulemonde M, Varray F, Basset O, Tortoli P, Cachard C, editors. High frame rate compounding for nonlinear B/A parameter ultrasound imaging in echo mode — simulation results. 2014 IEEE International Conference on Acoustics, Speech and Signal Processing (ICASSP); 2014 4-9 May 2014.
48. van Sloun R, Demi L, Shan C, Misch M. Ultrasound coefficient of nonlinearity imaging. *IEEE Trans Ultrason Ferroelectr Freq Control*. 2015;62(7):1331-41.
49. Yu TY, Morton JD, Clerens S, Dyer JM. Cooking-Induced Protein Modifications in Meat. *Compr Rev Food Sci Food Saf*. 2017;16(1):141-59.
50. Sun Y, Weber KT. Infarct scar: a dynamic tissue. *Cardiovasc Res*. 2000;46(2):250-6.

51. Christopher T, Carstensen EL. Finite amplitude distortion and its relationship to linear derating formulae for diagnostic ultrasound systems. *Ultrasound Med Biol*. 1996;22(8):1103-16.
52. Heyde B, Barbosa D, Claus P, Maes F, D'hooge J. Three-Dimensional cardiac motion estimation based on non-rigid image registration using a novel transformation model adapted to the heart. *Proceedings of the third international conference on Statistical Atlases and Computational Models of the Heart: imaging and modelling challenges; Nice, France: Springer-Verlag; 2012. p. 142–50.*
53. Nolden M, Zelzer S, Seitel A, Wald D, Müller M, Franz AM, et al. The Medical Imaging Interaction Toolkit: challenges and advances : 10 years of open-source development. *Int J Comput Assist Radiol Surg*. 2013;8(4):607-20.
54. Bland JM, Altman DG. Statistical methods for assessing agreement between two methods of clinical measurement. *Lancet*. 1986;1(8476):307-10.
55. Thygesen K, Alpert JS, Jaffe AS, Simoons ML, Chaitman BR, White HD, et al. Third universal definition of myocardial infarction. *J Am Coll Cardiol*. 2012;60(16):1581-98.
56. Flett AS, Hasleton J, Cook C, Hausenloy D, Quarta G, Ariti C, et al. Evaluation of techniques for the quantification of myocardial scar of

differing etiology using cardiac magnetic resonance. JACC Cardiovasc Imaging. 2011;4(2):150-6.

57. Dijkmans PA, Senior R, Becher H, Porter TR, Wei K, Visser CA, et al. Myocardial contrast echocardiography evolving as a clinically feasible technique for accurate, rapid, and safe assessment of myocardial perfusion: the evidence so far. J Am Coll Cardiol. 2006;48(11):2168-77.
58. Moreno R, Zamorano J, Serra V, Almería C, Rodrigo J, Alvarez L, et al. Weak concordance between wall motion and microvasculature status after acute myocardial infarction: study with myocardial contrast echocardiography in real time with power modulation. Eur J Echocardiogr. 2002;3(2):89-94.
59. Burns PN, Becher H. Contrast agents for echocardiography: principles and instrumentation. Handbook of Contrast Echocardiography: Springer; 2000. p. 1-44.
60. Stewart MJ. Contrast echocardiography. Heart. 2003;89(3):342-8.
61. Fishbein MC, Maclean D, Maroko PR. The histopathologic evolution of myocardial infarction. Chest. 1978;73(6):843-9.
62. Simpson DH, Chin CT, Burns PN. Pulse inversion Doppler: a new method for detecting nonlinear echoes from microbubble contrast agents. IEEE Trans Ultrason Ferroelectr Freq Control. 1999;46(2):372-82.

63. Shen C-C, Chou Y-H, Li P-C. Pulse Inversion Techniques in Ultrasonic Nonlinear Imaging. *Journal of Medical Ultrasound*. 2005;13(1):3-17.
64. Porter TR, Xie F, Silver M, Kricsfeld D, Oleary E. Real-time perfusion imaging with low mechanical index pulse inversion Doppler imaging. *J Am Coll Cardiol*. 2001;37(3):748-53.
65. Porter TR, Xie F. Contrast echocardiography: latest developments and clinical utility. *Curr Cardiol Rep*. 2015;17(3):569.
66. Grasselli G, Zangrillo A, Zanella A, Antonelli M, Cabrini L, Castelli A, et al. Baseline Characteristics and Outcomes of 1591 Patients Infected With SARS-CoV-2 Admitted to ICUs of the Lombardy Region, Italy. *Jama*. 2020;323(16):1574-81.
67. Bhatraju PK, Ghassemieh BJ, Nichols M, Kim R, Jerome KR, Nalla AK, et al. Covid-19 in Critically Ill Patients in the Seattle Region - Case Series. *N Engl J Med*. 2020;382(21):2012-22.
68. Gattinoni L, Coppola S, Cressoni M, Busana M, Rossi S, Chiumello D. COVID-19 Does Not Lead to a "Typical" Acute Respiratory Distress Syndrome. *Am J Respir Crit Care Med*. 2020;201(10):1299-300.
69. Ottestad W, Søvik S. COVID-19 patients with respiratory failure: what can we learn from aviation medicine? *Br J Anaesth*. 2020;125(3):e280-e1.



70. Klok FA, Kruip M, van der Meer NJM, Arbous MS, Gommers D, Kant KM, et al. Incidence of thrombotic complications in critically ill ICU patients with COVID-19. *Thromb Res.* 2020;191:145-7.
71. Huertas A, Montani D, Savale L, Pichon J, Tu L, Parent F, et al. Endothelial cell dysfunction: a major player in SARS-CoV-2 infection (COVID-19)? *Eur Respir J.* 2020;56(1).
72. Santoso A, Pranata R, Wibowo A, Al-Farabi MJ, Huang I, Antariksa B. Cardiac injury is associated with mortality and critically ill pneumonia in COVID-19: A meta-analysis. *Am J Emerg Med.* 2020.
73. Li Y, Li H, Zhu S, Xie Y, Wang B, He L, et al. Prognostic Value of Right Ventricular Longitudinal Strain in Patients With COVID-19. *JACC Cardiovasc Imaging.* 2020.
74. Szekely Y, Lichter Y, Taieb P, Banai A, Hochstadt A, Merdler I, et al. Spectrum of Cardiac Manifestations in COVID-19: A Systematic Echocardiographic Study. *Circulation.* 2020;142(4):342-53.
75. Vieillard-Baron A, Price LC, Matthay MA. Acute cor pulmonale in ARDS. *Intensive Care Med.* 2013;39(10):1836-8.
76. Tello K, Wan J, Dalmer A, Vanderpool R, Ghofrani HA, Naeije R, et al. Validation of the Tricuspid Annular Plane Systolic Excursion/Systolic Pulmonary Artery Pressure Ratio for the Assessment of Right Ventricular-Arterial Coupling in Severe Pulmonary Hypertension. *Circ Cardiovasc Imaging.* 2019;12(9):e009047.

77. Guazzi M. Use of TAPSE/PASP ratio in pulmonary arterial hypertension: An easy shortcut in a congested road. *Int J Cardiol.* 2018;266:242-4.
78. Organization WH. Clinical management of severe acute respiratory infection when novelcoronavirus (nCoV) infection is suspected. Published March 13, 2020.
79. Ranieri VM, Rubenfeld GD, Thompson BT, Ferguson ND, Caldwell E, Fan E, et al. Acute respiratory distress syndrome: the Berlin Definition. *Jama.* 2012;307(23):2526-33.
80. Matthay MA, Aldrich JM, Gotts JE. Treatment for severe acute respiratory distress syndrome from COVID-19. *Lancet Respir Med.* 2020;8(5):433-4.
81. Wunsch H. Mechanical Ventilation in COVID-19: Interpreting the Current Epidemiology. *Am J Respir Crit Care Med.* 2020;202(1):1-4.
82. McQuillan BM, Picard MH, Leavitt M, Weyman AE. Clinical correlates and reference intervals for pulmonary artery systolic pressure among echocardiographically normal subjects. *Circulation.* 2001;104(23):2797-802.
83. Ferrara F, Rudski LG, Vriza O, Gargani L, Afilalo J, D'Andrea A, et al. Physiologic correlates of tricuspid annular plane systolic excursion in 1168 healthy subjects. *Int J Cardiol.* 2016;223:736-43.

84. Guazzi M, Bandera F, Pelissero G, Castelveccchio S, Menicanti L, Ghio S, et al. Tricuspid annular plane systolic excursion and pulmonary arterial systolic pressure relationship in heart failure: an index of right ventricular contractile function and prognosis. *Am J Physiol Heart Circ Physiol*. 2013;305(9):H1373-81.
85. Guazzi M, Dixon D, Labate V, Beussink-Nelson L, Bandera F, Cuttica MJ, et al. RV Contractile Function and its Coupling to Pulmonary Circulation in Heart Failure With Preserved Ejection Fraction: Stratification of Clinical Phenotypes and Outcomes. *JACC Cardiovasc Imaging*. 2017;10(10 Pt B):1211-21.
86. Tello K, Axmann J, Ghofrani HA, Naeije R, Narcin N, Rieth A, et al. Relevance of the TAPSE/PASP ratio in pulmonary arterial hypertension. *Int J Cardiol*. 2018;266:229-35.
87. Tello K, Ghofrani HA, Heinze C, Krueger K, Naeije R, Raubach C, et al. A simple echocardiographic estimate of right ventricular-arterial coupling to assess severity and outcome in pulmonary hypertension on chronic lung disease. *Eur Respir J*. 2019;54(3).
88. Vieillard-Baron A, Prin S, Chergui K, Dubourg O, Jardin F. Echo-Doppler demonstration of acute cor pulmonale at the bedside in the medical intensive care unit. *Am J Respir Crit Care Med*. 2002;166(10):1310-9.

89. Ziehr DR, Alladina J, Petri CR, Maley JH, Moskowitz A, Medoff BD, et al. Respiratory Pathophysiology of Mechanically Ventilated Patients with COVID-19: A Cohort Study. *Am J Respir Crit Care Med*. 2020;201(12):1560-4.
90. Sanz J, Sánchez-Quintana D, Bossone E, Bogaard HJ, Naeije R. Anatomy, Function, and Dysfunction of the Right Ventricle: JACC State-of-the-Art Review. *J Am Coll Cardiol*. 2019;73(12):1463-82.
91. Lambermont B, Ghuysen A, Kolh P, Tchana-Sato V, Segers P, Gérard P, et al. Effects of endotoxic shock on right ventricular systolic function and mechanical efficiency. *Cardiovasc Res*. 2003;59(2):412-8.
92. Pagnamenta A, Dewachter C, McEntee K, Fesler P, Brimiouille S, Naeije R. Early right ventriculo-arterial uncoupling in borderline pulmonary hypertension on experimental heart failure. *J Appl Physiol* (1985). 2010;109(4):1080-5.
93. Mahmoud-Elsayed HM, Moody WE, Bradlow WM, Khan-Kheil AM, Senior J, Hudsmith LE, et al. Echocardiographic Findings in Patients With COVID-19 Pneumonia. *Can J Cardiol*. 2020;36(8):1203-7.
94. Zapol WM, Snider MT. Pulmonary hypertension in severe acute respiratory failure. *N Engl J Med*. 1977;296(9):476-80.
95. Akdogan RE, Srialluri S, Abdelsalam MGA, Hsiung MC, Nanda NC, Fadala H, et al. Incremental value of right parasternal transthoracic echocardiographic examination over the left parasternal approach in

assessing ascending aorta size: Additional benefit of three-dimensional echocardiography. *Echocardiography*. 2019;36(7):1306-14.

96. Shah SJ, Bardo DM, Sugeng L, Weinert L, Lodato JA, Knight BP, et al. Real-time three-dimensional transesophageal echocardiography of the left atrial appendage: initial experience in the clinical setting. *J Am Soc Echocardiogr*. 2008;21(12):1362-8.

## PERSONAL INFORMATION Gianpiero Pagnano

✉ [gianpieropagnano@gmail.com](mailto:gianpieropagnano@gmail.com)

Sex Male | Date of birth 02/09/1986 | Nationality Italian

**PREFERRED JOB** Medical Doctor – Division of Cardiology; Major interests: non-invasive Cardiology; Echocardiography; Vascular Ultrasound; Heart Failure;

## WORK EXPERIENCE

- |                        |  |
|------------------------|--|
| March 2020– Ongoing    | <ul style="list-style-type: none"><li>• Cardiology Consultant at “Ospedale Monaldi”, Napoli, Italy</li></ul>   |
| May 2016– January 2020 | <ul style="list-style-type: none"><li>• Echocardiography Fellow. Department of non invasive Cardiology of King’s College Hospital. London, United Kingdom under the supervision of Prof Mark J Monaghan.</li></ul> |

## EDUCATION AND TRAINING

- |                       |  |
|-----------------------|--|
| July 2012 – July 2017 | Residency in Cardiology.<br>School of Medicine, Federico II University of Naples, Italy. Principal subjects covered: Echocardiography, Vascular Ultrasound, Ergometry, Electrophysiology, Stress Echocardiography.   |
| 16-17 September 2014  | Training Course in "New US Technologies: 3d Echocardiography e Speckle Tracking in Hypertension, Heart Failure and Coronary Heart Disease" Federico II University of Naples, Italy.  |
| 20-22 March 2013      | Training Course in transthoracic Echocardiography, Federico II University of Naples, Italy.  |
| March 2012            | Medical Board, Medical Association of Naples.  |
| October 2011          | Medical Doctor Degree in Medicine and Surgery. Vote: 110/110 cum laude. Federico II University of Naples, Italy.<br>Thesis internship at the Unit of Hypertension Research Center, Department of Translational Medical Science, Federico II University of Naples aimed at defining the efficacy of two nutraceutical compositions in improving blood pressure control and lipid profile. |
| July 2005             | High school Diploma  |

## PERSONAL SKILLS

Mother tongue(s) Italian

Other language(s)

English

UNDERSTANDING		SPEAKING		WRITING
Listening	Reading	Spoken interaction	Spoken production	
C2	C2	C2	C1	C1

Levels: A1/A2: Basic user - B1/B2: Independent user - C1/C2 Proficient user  
[Common European Framework of Reference for Languages](#)

Organisational / managerial skills

Predisposition to work in a team of 5-6 persons by collaborating each other in a friendly manner developed during my Residency period.

Digital competence

Use of Word, graphical softwares such as Power Point, Publisher, Excel.

## ADDITIONAL INFORMATION

Membership Scientific Societies: Italian Society of Cardiology

- Certification in EACVI Adult Transesophageal Echocardiography Level 2
- Certification in EACVI Adult Transthoracic Echocardiography

## List of Publications

### BOOK CHAPTERS

- **Pagnano G**, Monaghan MJ. How to assess a patient with aortic disease? EACVI handbook of Echocardiography. *Manuscript in preparation*

-----

### PEER-REVIEWED MANUSCRIPTS AND ABSTRACTS

- “*Nutraceuticals for blood pressure control in patients with high-normal or grade 1 hypertension*”. Trimarco V, Cimmino CS, Santoro M, **Pagnano G**, Manzi MV, Piglia A, Giudice CA, De Luca N, Izzo R. High Blood Press Cardiovasc Prev. 2012 Sep 1;19(3):117-22.
- “*Lifestyle-related risk factors, smoking status and cardiovascular disease*”. Giudice R, Izzo R, Manzi MV, **Pagnano G**, Santoro M, Rao MA, Di Renzo G, De Luca N, Trimarco V. High Blood Press Cardiovasc Prev. 2012 Jun 1;19(2):85-92.
- “*Standardized Delineation of Endocardial Boundaries in Three-Dimensional Left Ventricular Echocardiograms*”. Papachristidis A, Galli E, Geleijnse ML, Heyde B, Alessandrini M, Barbosa D, Papitsas M, **Pagnano G**, Theodoropoulos KC, Zidros S, Donal E, Monaghan MJ, Bernard O, D'hooge J, Bosch JG. J Am Soc Echocardiogr. 2017 Nov;30(11):1059-1069. doi: 10.1016/j.echo.2017.06.027. Epub 2017 Sep 1.
- “*Mitral pseudostenosis due to a large left atrial myxoma*”. Theodoropoulos KC, Masoero G, **Pagnano G**, Walker N, Papachristidis A, Monaghan MJ. J Geriatr Cardiol. 2018 Mar;15(3):244-245.



- *“Clinical characteristics and prognosis of hospitalized COVID-19 patients with incident sustained tachyarrhythmias: A multicenter observational study”*. Russo V, Di Maio M, Mottola FF, **Pagnano G**, Attena E, Verde N, Di Micco P, Silverio A, Scudiero F, Nunziata L, Fele N, D'Andrea A, Parodi G, Albani S, Scacciatella P, Nigro G, Severino S. Eur J Clin Invest. 2020 Aug 19:e13387.
- *“Right ventricular-arterial uncoupling independently predicts survival in COVID-19 ARDS”*. D'Alto M, Marra A, Severino S, Salzano A, Romeo E, De Rosa RC, Stagnaro F, **Pagnano G**, Verde R, Murino P, Farro A, Ciccarelli G, Vargas M, Fiorentino G, Servillo G, Gentile I, Corcione A, Cittadini A, Naeije R, Golino P. Crit Care 2020 Nov 30;24(1):670.

### Abstracts

- *“Effect of Cigarette Smoking on Risk Profile of Patients with Optimally Controlled Hypertension”*. Giudice R, Izzo R, Casalnuovo G, Trimarco V, Hettiarachchige N, **Pagnano G**, Manzi Mv, Bassi A, de Simone G, Trimarco B. High Blood Press Cardiovasc Prev. 2011 Sep; 18(3):115-161.
- *“Statins Therapy and Incidence of Atrial Fibrillation in Hypertensive Patients”*. Trimarco V, de Simone G, De Marco M, Maglione F, **Pagnano G**, Santoro M, Manzi MV, De Luca N, Izzo R. High Blood Press Cardiovasc Prev. 2012 Sep; 19 (3): 143-195.

## **Acknowledgments**

There are probably too many people I should thank that have been with me during these last 3 years and I should apologize for not being able to write all their names here.

I want to sincerely thank Prof Mark Monaghan for welcoming me in a special team. I will always be grateful to him for teaching me everything I know about Echocardiography but also for being always available for help and advice. Thanks to all the great colleagues that I found in London, Dr Michael Papitsas first for the professional support and then for his unvaluable friendship during these years. Dr Amin-Youssef for believing in me and his support in everyday clinical practise. Dr Dimitris Papasaikas for sharing responsibilities and hobbies during my last year in London and all the Cardiology Fellows and Consultants that I had the pleasure to work with.

Thanks to Marilou, Carolina, Can and Hannah for all the good laugh we had together, Tiago, Pete, Sergio, Patricia and all the other fantastic sonographers that I worked with, coming from all over the world, for sharing with me their knowledge and skills and adding so much to my experience in the UK.

A sincere thanks to Prof Emanuele Barbato for making my experience abroad possible in the first place, for believing in me and for the constant support during the last 3 years.

A special thanks to Giuliana, my fiancée and soon wife, for always being there for me, supporting me and pushing me forward. Thanks to Marcello for his 24/7 support from Italy and to my family that never stopped sustaining me since everything started.